國立臺灣大學醫學院分子醫學研究所

博士論文

Graduate Institute of Molecular Medicine

College of Medicine

National Taiwan University

Doctoral Dissertation

調節型核醣核酸內切酶 REGNASE-1 對 M2a 巨噬細胞功能的影響及其與腫瘤生長的關聯性

The Impact of REGNASE-1 on M2a Macrophage Function and Its Relevance in Tumor Growth

馬佳宏

Jia-Hung Ma

指導教授：蔡欣祐 博士

Advisor: Hsin-Yue Tsai, Ph. D.

中華民國 113 年 8 月

Aug 2024

doi:10.6342/NTU202403029

口試委員會審定書

國立臺灣大學博士學位論文
口試委員會審定書
DOCTORAL DISSERTATION ACCEPTANCE CERTIFICATE
NATIONAL TAIWAN UNIVERSITY

調節型核糖核酸內切酶 Regnase-1 對 M2a 巨噬細胞功能的影響

及其與腫瘤生長的關聯性

The Impact of Regnase-1 on M2a Macrophage Function and Its

Relevance in Tumor Growth

本論文係 馬佳宏 (F05448013) 在國立臺灣大學 分子醫學研究所 完成之博士學位論文，於民國 113 年 7 月 3 日承下列考試委員審查通過及口試及格，特此證明。

The undersigned, appointed by the National Taiwan University Institute of Molecular Medicine on 3 July 2024 have examined a Doctoral Dissertation entitled above presented by Jia-Hung Ma (F05448013) candidate and hereby certify that it is worthy of acceptance.

口試委員 Oral examination committee:

蔡欣祐　　李建國　　楊鏡堅　　

（指導教授 Advisor）

徐元中　　譚婉玉　　詹世鵬　　林志生

系（所、學位學程）主管 Director: 潘俊良

doi:10.6342/NTU202403029

誌謝

光陰荏苒，轉眼八年已到了博士畢業的時刻。此時此刻，我衷心感謝這一路上幫助我完成此篇論文的老師們、學長姐以及同儕們。

首先，我要感謝我在博士生涯中重要的引路人蔡欣祐副教授，見證我從生疏的碩士生一路成長為能夠自主研究的研究人員。感謝徐立中教授、李建國教授、譚婉玉教授、楊鎧鍵教授、詹世鵬副教授與林志萱助理教授願意擔任我的口試委員並指導我完成此篇論文。感謝台大醫學院分子醫學所的老師們給予的教導。

感謝這一路上參與我研究旅途的學長姐和學弟妹們：庭婕、獻堂（小夸父）、伊婷、依婷、秋媛（小辣椒）、以新、冠霖、恬伊（馬來之光）、威羽、文婷、淑婷、柏緒、孟涵（台北水姑娘）、羽薇（支語警察）、佳祐（小精靈）、念祖（小精靈使用說明）、呈熙、佩妤。特別感謝依婷在我實驗過程中提供經驗和實驗方法的幫助，讓我能夠挑戰各種實驗上遇到的問題；那段日子與伊婷、以新、庭婕和獻堂一起闖關的密室逃脫和校園路跑；與獻堂、冠霖和威羽在實驗閒暇之餘與我一起打籃球；孟涵、佳祐以及羽薇一起打的羽球比賽；文婷、恬伊與我分享的實驗秘辛以及小八卦。忙碌的實驗少不了與生活的相互配合，認識你們豐富並充實了我的博士生生活。感謝你們對於我在實驗室或生活中的協助與包容。祝福大家未來能有更好的發展。

最後，感謝我的爸媽，馬建輝先生和劉芳君女士，感謝你們在我博士就學期間無數的支持與關心，讓我能在研究的路上無後顧之憂。這篇論文的完成，離不開上述各位以及更多人在方方面面對我的幫助，原諒我無法在此一一呈述，請各位接受我誠摯的感謝。

馬佳宏 謹誌

於台灣大學分子醫學所

一一三年 八月

doi:10.6342/NTU202403029

摘要

免疫網絡是一個複雜的系統，需要先天性免疫系統和適應性免疫系統之間的緊密配合，以在促發炎和抗發炎微環境中實現有效的反應。巨噬細胞透過啟動不同的極化狀態在先天免疫系統中發揮關鍵作用。它們大致分為 M1（促發炎）和 M2（抗發炎）巨噬細胞。在 M2 巨噬細胞中，M2a 亞型是研究最充分的亞型之一，並且透過 細胞介白素 4 (IL-4) 和/或 細胞介白素 13 (IL-13) 刺激而極化。調節型核糖核酸內切酶 REGNASE-1 具有核糖核酸酶和去泛素酶活性，已知在促發炎狀態下參與各種免疫細胞的免疫抑製作用。然而，其在 M2 巨噬細胞中的調節功能仍不清楚。於本論文中，我們透過分析 mRNA 定序數據中的差異表達基因來研究 REGNASE-1 在 M2a 巨噬細胞中的作用，並觀察到兩種 T 細胞趨化因子 CCL17 和 CCL22 的顯著減少。隨後的表徵表明，REGNASE-1 透過降解針對這些基因的 microRNA 來增強這些 mRNA 的穩定性。此外，在確認 REGNASE-1 吸引調節性 T 細胞 的能力後，我們觀察到，當將 Lewis 肺癌細胞植入巨噬細胞特異性 *Regnase-1* 敲除小鼠中時，腫瘤重量顯著減少。總的來說，我們的研究結果闡明了 REGNASE-1 在 M2a 中的作用及其對腫瘤生長的潛在影響。

關鍵詞：先天性免疫，替代極化巨噬細胞，小分子核糖核酸，調節型核糖核酸內切酶，第十七趨化因子，第二十二趨化因子。

doi:10.6342/NTU202403029

Abstracts

The immune network is a complex system requiring cohesive cross-talk between the innate and adaptive immune systems to achieve efficient responses in both pro-inflammatory and anti-inflammatory microenvironments. Macrophages play a key role in the innate immune system, initiating distinct polarization states. They are broadly classified into M1 (pro-inflammatory) and M2 (anti-inflammatory) macrophages. Among the M2 macrophages, the M2a subtype is one of the most well-studied and is polarized through IL-4 and/or IL-13 stimulation. REGNASE-1, which possesses both ribonuclease and deubiquitinase activities, is known to participate in immunosuppressive roles across various immune cells during pro-inflammatory states. However, its regulatory function in M2 macrophages remains unclear. Here, we investigate the role of REGNASE-1 in M2a macrophages by analyzing differentially expressed genes in mRNA sequencing data and observe significant reductions in two T cell-attractant chemokines, CCL17 and CCL22. Subsequent characterization reveals that REGNASE-1 enhances the stability of these mRNAs by degrading microRNAs targeting these genes. Furthermore, upon confirming the ability of REGNASE-1 to attract regulatory T cells (Tregs), we observed a marked reduction in tumor weight when Lewis lung carcinoma cells are implanted in macrophage-specific *Regnase-1* knockout mice. Collectively, our findings elucidate the role of REGNASE-1 in M2a and their potential impact on tumor growth.

doi:10.6342/NTU202403029

Keyword: Innate immune responses, alternative polarized macrophage, microRNA, REGNASE-1, CCL17, CCL22

doi:10.6342/NTU202403029

Contents

doi:10.6342/NTU202403029

doi:10.6342/NTU202403029

doi:10.6342/NTU202403029

List of Figures

doi:10.6342/NTU202403029

doi:10.6342/NTU202403029

doi:10.6342/NTU202403029

doi:10.6342/NTU202403029

List of Tables

doi:10.6342/NTU202403029

Chapter I: Introduction

Overview of Macrophage

Macrophage development

Macrophages, identified by Elie Metchnikoff for their phagocytic role against pathogens, are key components of the innate immune system [1]. They are broadly categorized into tissue-resident macrophages and bone marrow monocyte-derived macrophages (BMDM). The tissue-resident macrophages originated from EMP (erythroid-myeloid progenitor)-derived macrophage precursors localized in the yolk sac around embryonic day 7 (E7) and subsequently spread throughout the embryo, including to the fetal liver at E10.5 [2]. These macrophage precursors are further differentiated into tissue resident macrophages with self-renewal capability throughout adulthood. Due to the colonization of macrophage precursors is concurrently with organogenesis, thus, Lineage-determining factors (LDFs) are detected in tissue macrophage in different tissues. For instance, ID3 was found in Kupffer cells in liver, SALL1 was found in microglia [3], PPARgamma was found in alveolar macrophages.

These tissue-resident macrophage derived from embryonic progenitors demonstrate self-renewal capacity without requiring input from hematopoietic stem cells [4 5 6 7] . The persistence of tissue-resident macrophages into adulthood were contribute to embryonic

doi:10.6342/NTU202403029

derived macrophage self-renewal and/or replenished from circulating monocytes which initially stored in the bone marrow (BM) and spleen throughout life [8]. Unlike embryonic-derived macrophages, monocyte-derived macrophage has a limited lifespan and lack self-renewal ability [9]. Collectively, tissue-resident macrophages are primarily established during prenatal development but can also be replenished postnatally through the recruitment of circulating monocytes.

Bone marrow monocyte-derived macrophages (BMDMs) originate from hematopoietic stem cells (HSCs) in the bone marrow. These HSCs, fundamental precursors to all bone marrow-derived immune cells, emerge from hemogenic endothelial cells (HECs) via an endothelial-to-hematopoietic transition and then differentiate into HSCs. Coming into existence after EMP-derived macrophage precursors, HSCs first expand within the fetal liver before migrating to and settling in the bone marrow, where they continue to possess self-renewal capabilities [10]. Despite their relatively brief lifespan, BMDMs depend on circulating monocytes for replenishment and can experience substantial growth in response to challenges like infections.

Macrophage polarization

Macrophages are versatile immune cells that can adopt various polarization statuses in response to diverse environmental stimuli. Their functions are broadly classified into

doi:10.6342/NTU202403029

pro-inflammatory macrophages (M1-like or classically activated macrophage) and the anti-inflammatory macrophages (M2-like or alternatively activated macrophage) based on their functions [11]. The M1 and M2 macrophage classification was introduced in 2000 by Mills et al., named for their major T cell stimuli: M1 macrophages are activated by Th1 cells (IFN-gamma and/or LPS), and M2 macrophages respond to Th2 cells (IL-4/IL-13).

M1-like macrophages are pro-inflammatory and play crucial roles in defense against microbes, pathogen clearance and tumor suppression. M1-like macrophages are typically activated by the Th1-secreted cytokine, interferon-gamma (IFN-gamma) or microbes released pathogen-associated molecular patterns (PAMPs) with molecules is lipopolysaccharide (LPS) being one of most well-characterized PAMPs [12]. Upon detecting IFN-gamma through the interferon-gamma receptor (IFNGR), the Janus kinase (JAK)- signal transducer and transcription activator 1 (STAT1) cascade is activated, ultimately triggering the expression of downstream Interferon-stimulated genes (ISGs) such as IL-12 and IL-18 [13]. Moreover, microbes releasing LPS are detected by TLR-4, a pathogen recognition receptor (PRR), which promotes the activation of M1 macrophage activation. Upon binding to LPS, TLR-4 activates TIR-domain-containing adapter-inducing interferon-beta (TRIFbeta) and myeloid differentiation response 88 (MyD88)

doi:10.6342/NTU202403029

signaling pathways, leading to the production of type I interferon and pro-inflammatory cytokines and chemokines [12 14].

M2-like macrophages are referred to as anti-inflammatory macrophages and play roles in tissue repair, immune regulation and inflammation resolution. M2-like macrophages are subdivided into four distinct subtypes: M2a, M2b, M2c, M2d, each defined by distinct stimuli and unique transcriptomic and proteomic profiles [11 15 16]. M2a macrophages, also referred to as wound-healing macrophages, are the most extensively studied and were first identified in 1992. They are activated by Th2-secreted cytokines, interleukin-4 (IL-4) and/or iterleukin-13 (IL-13), which induce high expression of surface mannose receptors. [15]. IL-4-IL-4Ra engagement leads to Stat6 phosphorylation by IL-4Ra associated JAK proteins, with dimerized phosphorylated STAT6 entering the nucleus to initiate targeted gene expression. In addition to the predominant role of STAT6, other transcription factors also participate in M2-like macrophage polarization, including Krüppel-like factor 4 (KLF4), Interferon regulatory factor 4 (IRF4), and peroxisome proliferator-activated receptor gamma (PPARgamma), etc. Besides the predominant surface expressed C-type mannose receptor (Mrc1, also named CD206), M2a macrophages express distinctive markers such as *Arginase-1*, *Ym1*, and *Fizz1* along with chemokines, CCL17 and CCL22. Tissue remodeling is a hallmark of M2a macrophages. IL-4, released from damaged tissue, promotes M2a macrophage

doi:10.6342/NTU202403029

differentiation. The differentiated M2a macrophages produce various metabolites for extracellular matrix (ECM), fibronectin for wound repair and pro-fibrotic factors such as, Fibroblast growth factor 2 (FGF-beta), fibronectin, insulin-like growth factor (IGF), and transforming growth factor beta (TGF-beta). Although increasing single-cell sequencing (scRNA-seq) of transcriptomic data from tumor-associated macrophages (TAMs) indicates that the expression profiles of TAMs from various tumors have distinct patterns and differ from macrophages in normal tissues, studies on pulmonary metastasis from mammary carcinomas suggest that TAMs stimulated by IL-4, secreted by Th2 cells, are the primary drivers of increased pulmonary metastasis in the MMTV-PyMT mammary carcinoma mouse model.

M2b macrophages, also referred to as regulatory macrophages, are activated through binding of immune complex (IC) and TLR agonist or IL-1R agonist. Different from M2a macrophages, M2b macrophages express high levels of *Ccl1*, *TNF superfamily member 14 (TNFSF14)*, and *Il-10*, while showing low levels of *Il-12*. The widely accepted marker for M2b macrophages is the high IL-10/IL-12 ratio. Additionally, M2b macrophages secrete CCL-1, as well as TCA3, which acts as a chemoattractant for monocytes and natural killer cells (NK cells). This emergence of a specific marker distinguishes M2b macrophages from other subtypes [17].

doi:10.6342/NTU202403029

M2c macrophages, also known as deactivated macrophages, are activated with IL-10, glucocorticoids and transforming growth factor-beta (TGF-beta). Upon activation, M2c macrophage secreted IL-10 and TGF-beta and expressed surface markers such as CD163, CD16 (FcγRIIIa), and TLR1 [18]. In contrast, M2c do not express M2a transcription factors *Egr2* and *Irf4* but express *Hif-1alpha* and *Stat3* [19] [20]. M2d macrophages, also known as TAMs, are common present in tumor microenvironment. Despite the initial understanding that TAMs exhibit anti-tumor activity and can phagocytose cancer cells, subsequent studies have revealed that TAMs can also promote tumor progression [21]. Recent studies support the idea that TAMs undergo a shift in polarization stages during tumor progression and generally exhibit an M2-like phenotype, categorized as M2d macrophages [22]. The intricate and heterogeneous nature of TAMs, influenced by both the specific tumor type and its progression stage, poses a challenge in their characterization. Traditional classifications, solely based on M1-like or M2-like phenotypes or marker gene expressions, may oversimplify the diverse functions exhibited by TAMs within the tumor microenvironment. ScRNA-seqs are helping to define different TAM states. Currently, distinct TAMs can be further categorized into three groups based on clinical outcomes: those associated with favorable outcomes, those linked to unfavorable outcomes, and those not significantly associated with clinical outcomes [23].

doi:10.6342/NTU202403029

Signal transduction that modulating M2-like macrophage polarization

Recent decades have witnessed a growing understanding of the molecular mechanisms governing signaling pathways involved in the polarization of M2-like macrophages. Noteworthy signal transduction pathways encompass Janus kinase–signal transducer and activator of transcription (JAK-STAT) signaling and at least six different transcription factors; nuclear factor kappa-light-chain-enhancer of activated B cells (NF-kappaB), interferon regulatory factor 4 (IRF-4), CCAAT/enhancer-binding protein (C/EBP), peroxisome proliferator-activated receptor (PPAR), and Kruppel-like factor 4 (KLF4) [15]. Among them, JAK-STAT plays most crucial role in IL-4/IL-13 induced M2a macrophage polarization. Upon binding of IL-4 and IL-13 to IL-4R and IL-13R, JAK1/2/3 is recruited, leading to their phosphorylation. Phosphorylated JAK proteins, in turn, recruit and phosphorylate STAT6. Activated phosphorylated STAT6 forms dimers that translocate into the nucleus, promoting the expression of M2-related genes such as *Arginase-1, Ym1, Fizz-1, Ccl17, Ccl22* and mannose receptor [24 25 26 27]. NF-kappaB play an essential role in innate immunity and regulate proinflammatory gene expression under TLR signaling pathway. The NF-kappaB family comprises five members: NF-kappaB1 (p105/p50), NF-kappaB2 (p100/p52), RELA (p65), RELB, and c-REL. These members associate with each other to form various transcriptionally active homo- and heterodimeric complexes. Under normal conditions, NF-kappaB dimers remain in an

doi:10.6342/NTU202403029

inactive state by interacting with I-kappaB proteins. Upon stimulation, I kappaB proteins are phosphorylated by I-kappaB kinase, leading to the release of the NF-kappaB dimer. Subsequently, the released NF-kappaB dimer translocated into the nucleus and promotes gene expression [28]. In the Taenia crassiceps metacestode mice model, a prior study underscored the significance of p50 NF-kappaB1 in M2 polarization. Peritoneal macrophages from mice lacking p50 exhibited decreased expression of *Arginase-1, Ccl17, Ym1, and Fizz1* in comparison to the control group [29]. IRF-4, belonging to the IRF family, is a crucial transcriptional factor that not only controls Th2 cell differentiation [30] but also plays a regulatory role in M2 macrophage polarization. IRF-4 promotes M2 macrophage polarization through the histone demethylase Jumonji domain-containing-3 (JMJD-3)-IRF4 signaling axis. Activated JMJD-3 subsequently removes H3K4 and H3K27, contributing to the silencing of factors associated with M2 macrophage polarization [31]. Additionally, IRF-4 is required for mTORC2-mediated M2 macrophage polarization and metabolic reprogramming through the M-CSF-mTORC2-IRF-4 signaling axis. The associated metabolic reprogramming involves critical processes such as glycolysis, fatty acid oxidation (FAO), and oxidative phosphorylation (OXPHOS), all of which contribute to M2-like macrophage polarization [32]. The C/EBP family comprises six members named from C/EBPalpha to C/EBPzeta. Among these member, C/EBPalpha depletion impaired M2 gene expression, including *Arginase-1, Mrc1, Ym1, Mgl1 and Il-10* upon IL-4

doi:10.6342/NTU202403029

induction [33]. Otherwise, C/EBPbeta regulates Toll-like receptor (TLR)-induced M2 gene expression, including *Arginase-1*, *Il13ra1*, *Macrophage Scavenger Receptor 1* (MSR1), and *Il10* [34]. The peroxisome proliferator-activated receptor (PPAR) family comprises a group of nuclear receptors and function as transcription factors. This family consists of three subtypes: PPARalpha, PPARgamma and PPARdelta. PPARalpha expressed in peripheral tissue, plays a role in regulating fatty acid transport, esterification, and oxidative phosphorylation (OXPHOS). PPARdelta, also known as PPARbeta, is involved in fatty acid oxidation. hematopoietic deficiency of PPARdelta impairs alternative activation of Kupffer cells in obese mice, leading to reduction in oxidative metabolism and insulin sensitivity [35]. Conversely, PPARgamma, a pivotal transcription factor predominantly found in adipose tissue, colon, and macrophages, governs adipocyte differentiation and glucose metabolism [36]. Upon IL-4 induction, PPARgamma activation downstream of STAT6 [37] [38] regulates fatty acids contributing to the long-term maintenance of M2-like macrophage polarization [39] [40]. KLF4, one of four key factors required for inducing pluripotent stem cell (iPSCs) [41], has also been implicated in enhancing M2-like macrophage polarization. KLF4 promoting Regnase-1, leading to enhancing reactive oxygen species (ROS), endoplasmic reticulum (ER) stress and autophagy, all of which are required for achieving M2-like macrophage polarization [42].

doi:10.6342/NTU202403029

Role of macrophage in tumor microenvironment

Tumor microenvironment (TME) is the environment surrounding the tumor which is consist of blood vessels, immune cells, fibroblast, signal molecules and extracellular matrix (ECM). Macrophages within tumor microenvironment (TME) are termed tumor associated macrophages (TAMs), also referred to as M2d macrophages. TAMs are major component of immune cells within tumor that involving tumor progression including invasion, angiogenesis, metastasis and immune suppression. Despite TAMs rarely display bona fide M1 or M2 phenotypes [23] [43] , the prevailing view is that tumor-associated macrophages (TAMs) infiltrating tumors at an early stage primarily display an M1-like phenotype, exhibiting anti-tumor activity and bolstering host immunity. However, subsets of TAM populations tend to transition towards an M2-like phenotype, fostering tumor development, particularly under hypoxic conditions and as the tumor progresses [22].

In a clinical study from advanced renal cell carcinoma (RCC), specific subsets of tumor-associated macrophages (TAMs), namely $VSIR^+$ TAM, $GPNMB^+$ TAM and $FOLR2^+$ TAM transitioned towards an M1-like phenotype in patients. This transition was marked by heightened proteasome function and antigen presentation, in response to anti-PD-1 antibodies. however, these same subsets of TAM upregulated M2-associated genes to varying degrees [44]. In the context of the growing use of immune-checkpoint blockade (ICB) in cancer therapy, the interaction between T cells and TAMs has become a focal

doi:10.6342/NTU202403029

point. Analysis of scRNA-seq in breast cancer patients revealed that TAMs expressing PD-L1 and PD-L2 exhibited elevated expression in patients with clonotype expansion of T cells in biopsies before anti-PD1 treatment. Furthermore, in the same comparison, $LYVE^+$ TAMs demonstrated heightened expression of anti-inflammatory genes (MRC1, CD163, FOLR2, and STAB1), while $CX3CR1^+$ TAMs displayed increased gene expression of inflammatory genes (CCL3, CCL4, TNF). $SLC2A1^+$ TAM and $MT1G^+$ TAM demonstrated heightened expression of Hypoxia related genes (PGAM1, ENO1, LDHA) [45].

The role of Regnase-1 in immune response regulation

Phenotype characterization of REGNASE-1

REGNASE-1, also known as MCPIP1, is a 65.8-kDa protein encoded by Zinc finger CCCH-type containing 12A (*Zc3h12a*) gene. As a member of the CCCH zinc finger proteins, it encompasses a PilT N-terminus (PIN) domain-like RNase domain and a novel ubiquitin (Ub)-associated domain at its N-terminus [46]. Regnase-1 initially identified in human monocytes induced by monocyte chemoattractant protein 1 (MCP1), was originally named MCP1-induced protein 1 (MCPIP1) [47]. Subsequent investigations into Mcpip1 revealed its role in post-transcriptional posttranslational mRNA regulation, leading to its renaming as Regulatory RNase 1 (Regnase-1) based on its physiological

doi:10.6342/NTU202403029

function [48]. Complete knockout of Regnase-1 in mice leads to growth retardation, severe splenomegaly and lymphadenopathy, with most individuals succumbing within 12 weeks after birth. Hematological analysis, including complete blood count (CBC), reveals significantly reduced red blood cells, elevated white blood cells, and increased platelets in *Regnase-1*$^{-/-}$ mice. Additionally, these mice develop hyper-gammaglobulinemia across all immunoglobulin isotypes. Flow cytometry analysis revealed that about 70% of CD19^{+} B cells were IgM^{-} IgD^{-}, but immunoglobulin^{+}, indicating that most *Regnase-1*$^{-/-}$ B cells underwent a class switch in the spleen [49]. T cell-specific *Regnase-1*$^{-/-}$ mice driven by the CD4 promoter (CD4-Cre) display a phenotype similar to complete *Regnase-1*$^{-/-}$ mice, characterized by growth retardation, majority succumbing within 17 weeks, and severe splenomegaly and lymphadenopathy. Notably, T-cell development appears unaffected in *Regnase-1*$^{-/-}$ T cells; however, there is an observed increase in the gene expression of c-Rel, Ox40, and IL-2 mRNA following stimulation with PMA plus ionomycin [50].

In another study, myeloid-specific *Regnase-1*$^{-/-}$ mice (*M-Regnase-1*$^{-/-}$) were generated by crossing mice with floxed *zc3h12a* allele with the mice expressing Cre recombinase driven by the Lysozyme M promoter (LysM-Cre). *M-Regnase-1*$^{-/-}$ mice displayed a late-onset inflammatory syndrome, exhibiting phenotypes similar to those of *Regnase-1*$^{-/-}$ mice but at a much older age. Mortality in *M-Regnase-1*$^{-/-}$ mice commenced

doi:10.6342/NTU202403029

after 5 months, with 60% of these mice surviving at 7 months of age. *M-Regnase-1*$^{-/-}$ mice developed spontaneous splenomegaly and lymphadenopathy at 6 months of age [51].

Functional characterization of REGNASE-1

REGNASE-1 was initially recognized as a transcriptional factor associated with Monocyte chemoattractant protein-1 mediated inflammation in human peripheral blood monocytes, however the downstream regulatory still unclear [47]. The later study of complete *Regnase-1*$^{-/-}$ mice revealed that the primary function of REGNASE-1 is the post-transcriptional regulation of specific sets of mRNAs through the recognition of stem-loop (SL) structure within their 3' UTR regions. Regnase-1 directly targets *Il6* and *Il-12b* mRNAs in LPS-induced peritoneal macrophage [49], IL-2, c-Rel and Ox40 in T lymphocytes [52], ten-eleven translocation (TET) family proteins (Tet1/Tet2/Tet3) in neural progenitor cells [53], as well as IL-8 in HeLa cells [54]. Interestingly, upon LPS-TLR4 activation, Regnase-1 mRNA undergoes uridylation in the 3'UTR stem-loop region, leading to its degradation by exonucleases [55]. Reganse-1 also recognized itself mRNA through stem-loop structure in 3'-UTR [56].

However, the cleavage of SL structures by Regnase-1 also depends on the translation status of the targeted mRNA. Inhibition of targeted mRNA translation through treatments

doi:10.6342/NTU202403029

with cycloheximide or anisomycin eliminates the degradation of mRNA that is dependent on Regnase-1. Given that REGNASE-1 colocalizes with ribosomes on the endoplasmic reticulum (ER), it is believed that REGNASE-1 specifically targets mRNAs for cleavage during active translation, acting on SL structures within their 3'UTRs. Proteomics studies and in vitro activity assays have shown that REGNASE-1 physically associates with up-frameshift protein-1 (UPF1) by binding to SMG1-phosphorylated residue T28 in UPF1. UPF1 unwinds the stem loop structure of mRNA, enabling REGNASE-1 to degrade mRNAs [57] [58].

In addition to ribonuclease activity, purified REGNASE-1 has also been discovered to possess deubiquitinase activity. This activity, targeting both K48- and K63-linked ubiquitin chains, has been shown to negatively regulate NF-kappa-B and c-JUN N-terminal kinase (JNK) signaling pathway by deubiquitinating TNF receptor-associated factors (TRAF2/TRAF3/TRAF6) [59].

Role of REGNASE-1 in MicroRNA biogenesis

MicroRNAs (miRNAs), a group of 22-nucleotides non-coding RNAs, are known to regulate around half of all mammalian coding genes. They exert their influence by affecting the stability of targeted mRNAs and their translation efficiency, thereby impacting a wide range of biological processes. MiRNAs were initially identified in

doi:10.6342/NTU202403029

Caenorhabditis elegans [60], and their targeting specificity became apparent through molecular genetic studies in Drosophila [61]. The biogenesis of mature miRNA in most mammals begins with noncoding primary miRNA transcripts (pri-miRNA) transcribed by RNA polymerase II (Pol II). Pri-miRNAs are 5'-capped, spliced, and polyadenylated, composed of a long stem-loop structure flanked by single-stranded tails at both the 5’ and 3’ ends of the transcript.

Two subsequent steps trim the pri-miRNA transcript into mature miRNA, transitioning from the nucleus to the cytoplasm. In the nucleus, the pri-miRNA is cleaved into an approximately 70-nucleotide hairpin-structured precursor (pre-miRNA) by a multiprotein complex called the Microprocessor. The two core components of the Microprocessor are Drosha, an RNase III enzyme, and DGCR8/Pasha, a double-stranded RNA-binding domain (dsRBD) protein. The pre-miRNA is subsequently transported into the cytoplasm by Exportin-5. Once in the cytoplasm, the pre-miRNA undergoes further cleavage, resulting in the formation of an approximately 22-nucleotide miRNA duplex. This processing step is facilitated by Dicer, another RNase III enzyme. One strand of the miRNA duplex complexes with Argonaute to form the RNA-induced silencing complex (RISC)[62]. More than 100 miRNAs are expressed by immune system cells, playing crucial roles in their development and immune responses [63].

doi:10.6342/NTU202403029

Numerous studies have revealed that the abundance of miRNA is primarily regulated at their transcription level. For instance, STAT6 phosphorylation enhances miR-155 expression, while NF-kappa B activation boosts miR-146 expression. Additionally, post-transcriptional modifications play a significant role in controlling the abundance of mature miRNAs. Specifically, the level of mature miR-21, critical for TGF-beta or BMP signaling in the contractile phenotype of human vascular smooth muscle cells [64], is regulated by Receptor-specific SMAD (R-SMAD) proteins in response to TGF-beta or BMP-4 signaling. R-SMAD proteins contribute to the formation of pre-miR-21 by assembling an R-SMAD-microprocessor-pri-miR-21 complex, thereby facilitating an increase in mature miR-21 production. The abundance of mature mir-142 is also regulated post-transcriptionally. Mir-142, a miRNA expressed in cells of hematopoietic origin, is crucial for the normal development and function of dendritic cells, mast cells, and B cells [65]. It has been discovered that Adenosine Deaminases Acting on RNA (ADAR), which convert adenosine (A) to inosine (I), can catalyze this A-to-I conversion not only in messenger RNAs (mRNAs) but also in a specific subset of miRNAs, including miR-142. This conversion impedes the processing of primary miRNA (pri-miRNA) into precursor miRNA (pre-miRNA) by microprocessor complexes, thereby reducing the production of mature miRNA. Another example of regulating mature let-7 in post-transcription processes involves Terminal uridylyl transferases 4 (TUT-4). Let-7, a microRNA

doi:10.6342/NTU202403029

conserved from nematodes to humans, acts as a tumor suppressor and is predominantly expressed in differentiated cells. The abundance of mature let-7 is precisely controlled by LIN-28, an RNA-binding protein, and TUT-4 in embryonic stem cells. LIN-28 and TUT-4 specifically target let-7 due to its conserved GGAG motif in the loop region. The uridylation of pre-let-7 by TUT-4 via LIN-28 obstructs its recognition by Dicer, preventing the production of mature let-7 [66]. The discovery of REGNASE-1's role in microRNA regulation was made through a screening designed to identify immune response-related RNA-binding proteins that influence microRNA targeting capabilities, utilizing a miR-122 sensor. It was found that overexpressing REGNASE-1 affects mir-122 targeting due to inefficient mature mir-122 production [67].

Further studies revealed that REGNASE-1 cleaves pre-miRNAs without affecting primary or mature microRNAs, consistent with its predominant cytoplasmic localization. This cleavage activity relies on the PilT N-terminus (PIN) domain-like RNase domain, as previously described, with the identified cleavage sites on pre-miRNAs primarily located in the loop region. However, unlike the sequence-specific actions observed with LIN-28 and TUT-4, REGNASE-1 exhibits a broad spectrum of pre-miRNA cleavage in vitro. Observations have shown that the overexpression of miR-155, known for its suppression of IL-4 production in Th2 cells and consequent contribution to autoimmunity, can be counteracted in Jurkat T cells overexpressing REGNASE-1, effectively restoring IL-4

doi:10.6342/NTU202403029

production [67]. Further research into the role of REGNASE-1 in hypoxia-induced angiogenesis has demonstrated that miR-20b and miR-34a are degraded by REGNASE-1. This degradation leads to the derepression of HIF-1alpha and SIRT-1 expression, ultimately facilitating angiogenesis [68].

Pathological importance of CCL17 and CCL22

Overview of CCL17 and CCL22

CCL17, also known as Thymus and activation-regulated chemokine (TARC), was first identified in 1996 from phytohemagglutinin-stimulated peripheral blood mononuclear cells. Following the subsequent nomenclature system, TARC was reclassified as CC chemokine ligand 17 (CCL17), placing it within the CC chemokines family. Chemokines are categorized based on the number and arrangement of conserved cysteine residues in their N-terminal regions. These categories include cysteine (C), cysteine-cysteine (CC), cysteine-X-cysteine (CXC), and cysteine-X3-cysteine (CX3C) subsets. CCL17 is specifically identified by two adjacent cysteine residues in the conserved cysteine-rich N-terminal region, fitting the CC category. Among over 50 known endogenous chemokines [69], CCL17 shares the highest degree of homology (about 32%) with CCL22. Both CCL17 and CCL22 interact with the CCR4 receptor, which is prevalent in dendritic cells, NK cells, and T lymphocytes. Notably, within T lymphocyte

doi:10.6342/NTU202403029

population, CCR4 is predominantly expressed in Th2 and Treg cells. Additionally, murine CCL17 shares 66% identity with its human counterpart at the amino acid level. Elevated levels of CCL17 have been observed in various chronic allergic conditions, including cutaneous lupus erythematosus, asthma, and atopic dermatitis. The expression of endogenous CCL17 is primarily observed in dendritic cells (DC) across various lymphoid organs including the thymus, cutaneous lymph node, and Peyer's patch, albeit not in the spleen. This was determined through detecting GFP fluorescence of an N-terminus GFP tagging at the CCL17 locus and flow cytometry analysis [70]. However, the expression of CCL17 in spleen DC is found inducible by glycosphingolipid alpha-galactosylceramide (alpha-GC), a widely used model antigen for natural killer T cells [71], and plays a critical role in recruiting cytotoxic T cell for presenting extracellular antigens obtained in DCs. Expression of CCL17 can also be induced in macrophages derived from either mouse peritoneal or human peripheral blood mononuclear cells when stimulated with Th2 cell-secreted cytokines, such as IL-4 or IL-13 [72]. Additionally, STAT6, a crucial transcription factor for M2a macrophage activation, has been identified as pivotal in regulating *Ccl17* expression in response to IL-4/IL-13 stimulation [26]. Although CCL17 can attract cytotoxic T cells and Treg cells, recent studies on its depletion have demonstrated numerous beneficial effects. *Ccl17*$^{-/-}$ mice exhibited more youthful characteristics, increased motor function, anxiety-like behavior, and improved spatial

doi:10.6342/NTU202403029

working memory than WT littermates. Additionally, *Ccl17*$^{-/-}$ mice showed improved cardiac systolic dysfunction (ejection fraction [EF] and fractional shortening [FS]) and decreased fibrosis compared to WT aged littermates [73]. Depletion of CCL17 with a blocking antibody exhibited a protective effect, including decreased renal LN inflammation and a reduced number of infiltrated cells in the kidneys in a well-characterized systemic lupus erythematosus (SLE) mouse model. This observation emerged from comparing the survival of malaria-infected SLE mice, which was longer than that of non-infected controls, and was attributed to decreased CCL17 expression in DCs [74]. Besides, in a sodium hypochlorite-induced mouse model. Macrophages could switch to pro-fibrotic(M2-like) phenotype that activated peritoneal fibroblasts through CCL17. Blocking of CCL17 by antibody reduced peritoneal fibrosis and improved peritoneal function [75].

CCL22, also referred as Macrophage-derived chemokine (MDC), is another member of CC-chemokine family. Immunohistochemistry analysis has shown that under naïve status, Ccl22 is majority expressed in DC although it is also recognized as an inducible chemokine in various cell types. The protein levels of CCL22 can be induced by different stimuli: LPS in DCs, IL-4 or IL-13 in monocytes, monocyte-derived macrophages, B lymphocytes, and NK cells. Additionally, anti-CD3 and anti-CD28 in T lymphocytes can trigger CCL22 production. Apart from DCs, the highest levels of CCL22 are observed in

doi:10.6342/NTU202403029

macrophages upon IL-4 stimulation [76 77]. While CCL22 shows elevated concentrations in the plasma of SLE patients and the airway epithelial cells of asthmatic patients, akin to CCL17 [78], the *Ccl22* knockout mice do not manifest apparent phenotypical differences compared to wild-type mice. However, *Ccl22* knockout mice are more susceptible to dextran sodium sulfate (DSS). When subjected to a milder dose of DSS in a DSS-induced colitis model—insufficient to induce colitis in wild-type mice—they exhibit severe effects. A recent study in Chronic lymphoproliferative disorder of natural killer cells (CLPD-NK), *Ccl22* mutations were associated with dysregulated immune signaling with the hematopoietic microenvironment, resulting from altered G Protein coupled receptor (GPCR) signaling that facilitates NK cell expansion [79]. The CCR4 receptor is predominantly expressed by Th2, cutaneous lymphocyte antigen-positive skin-homing T cells, Treg, and other T cell subset including Th17 cells, Th22 cells, Tc2 cells, IL-2-activated natural killer (NK) cells, and $CD4^+$ NKT cells [80]. Similar to *Ccl17* and *Ccl22* knockout mice, CCR4 knockout mice exhibit no observable phenotype under stress-free conditions. Intriguingly, CCR4 knockout mice demonstrate enhanced tolerance when subjected to intraperitoneal injection of LPS. While wild-type mice typically succumb 2 to 4 days post-LPS injection, an impressive 14 out of 15 CCR4 knockout mice remain alive by day 6 [81]. Interestingly, through the comparison of mixed bone marrow from wild-type and CCR4 knockout mice, both combined with Treg deficient bone marrow, the

doi:10.6342/NTU202403029

critical role of CCR4 in Treg function is elucidated. Mice receiving Treg deficient bone marrow exhibit severe dermatitis, wasting, and survive for only 40 days, contrasting with the up to 300-day survival and maintenance of health when transferred with a mixture of half T-reg deficient and half wild-type bone marrow. However, when the transferred bone marrow contains a blend of half T-reg deficient and half CCR4 knockout cells, it leads to localized skin inflammation and a survival range of 50 to 150 days [82].These datas suggested that the absence of phenotype observed in CCR4 knockout mice likely results from their inability to attract both T helper and Treg cells.

The role of CCL17 & CCL22 in Tumor microenvironment

In order to evade immune elimination, tumors acquire anti-inflammatory characteristics from both the innate and adaptive immune systems. Among the notable components of the anti-inflammatory immune response are alternatively polarized macrophages and Treg cells, found in the innate and adaptive immune systems, respectively. Notably, elevated levels of CCL17 and CCL22, potent chemotactic factors for CCR4-containing cells, are implicated in attracting Treg cells to tumor sites. Ovarian carcinoma studies have demonstrated an accumulation of $CD4^+$ $CD25^+$ Treg cells as tumor stage advances. Inhibiting CCL22, but not CCL17, through CCL22-specific antibodies has been shown to impede the migration of $CD4^+$ $CD25^+$ T cells toward ascites

doi:10.6342/NTU202403029

in patients. Furthermore, a robust correlation between Treg cells and advanced tumor stages has also been observed in gastric cancer, where Treg cells are identified using $CD4^+$ $CD25^+$ $Foxp3^+$ markers. Notably, abundant levels of CCL17 and CCL22 are exclusively found in the gastric mucosa of tumor patients [83]. Consistently, Ccl22 knockout mice injected with Panc02-OVA tumor subcutaneously and subsequently vaccinated twice with OVA showed a significant reduction in tumor size and prolonged survival compared to wild-type mice. The production sources of CCL17 and CCL22, leading to tumor evasion from immune elimination, may stem from tumor cells, DCs, and TAMs.

The significance of CCL17 and CCL22 in attracting Treg to implanted Lewis lung carcinoma cells (3LL-R) or PyMT, a model for spontaneous breast adenocarcinoma development and progression, was demonstrated in a study examining the effects of an inhibitor of Liver X receptors alpha (LXRa), a transcription factor secreted by tumors that further contributes to immune escape [84]. Administering the LXR agonist T1317 to mice implanted with 3LL-R cells (expressing both LXRalpha and LXRbeta) resulted in a reduction of MHCIIhigh TAMs, with no significant impact on the frequency of other myeloid cell populations. Further examination of T lymphocytes revealed a specific downregulation of Treg in the tumor region but not in the spleen. Subsequent analysis of TAMs showed a no apparent changes in markers associated with alternatively polarized

doi:10.6342/NTU202403029

macrophages, such as *Arginase1*, *Mrc1*, and *Retnla*, while only *Ccl17* and *Ccl22* are specifically inhibited by the LXR agonist. These findings support the notion that reducing CCL17 and CCL22 in TAMs may sufficiently decrease Treg recruitment to the tumor site, leading to a reduction in tumor size.

doi:10.6342/NTU202403029

Chapter II: Materials and Methods

Plasmids

Plasmids that were used in expressing Regnase-1, either wild-type and various mutant derivatives, in RAW264.7 *Regnase-1*$^{-/-}$ were constructed into pWS4.1wPpuro-aOn vector (Tet-On Regnase-1) (RNAi core). The 3x-flag tag was fused to the N-terminus of Regnase-1 protein. Mutant constructs used in this study included those with defects in both ribonuclease (RNase) and deubiquitinase (DUB) activities, specifically Regnase-1(D141N); mutants with defects solely in RNase activity, denoted as Regnase-1(D225A, D226A); and mutants with defects only in DUB activity, designated as Regnase-1(C157A). All the mutations were generated through site-directed mutagenesis using Q5 Site-Directed Mutagenesis Kit (Cat#E0544S, NEB) with primer sequences listed in Table 1. Plasmids employed in the firefly luciferase reporter assay were sourced from pmirGLO Dual-Luciferase miRNA target expression vector (pmirGLO vector) containing either full-length or partial *Ccl17* and *Ccl22* 3' UTRs. Various lengths of the 3' UTR were employed, including *Ccl17* 3'UTR regions (100-181, 1-181) and *Ccl22* 3'UTR regions (1-304, 305-608, 1-608, 609-1072, 1072-1495, 1-1495) situated immediately downstream of the firefly luciferase gene (luc2). Plasmids that were used in expressing Regnase-1 D141N mutant in RAW264.7 for RNA-IP experiment was constructed into pcDNA3 vector. 3x-flag tag was fused to Regnase-1 cDNA at its N-terminus. Mutant construct combinations; D141N (RNase-, DUB-) were generated through site-directed mutagenesis

doi:10.6342/NTU202403029

using Q5 Site-Directed Mutagenesis Kit (Cat#E0544S, NEB). All plasmids underwent validation through DNA sequencing. Detailed primer sequences for plasmid construction can be found in Table1.

Mice

Both Regnase-1 total knockout (*Regnase-1*$^{-/-}$) and conditional knockout (*Regnase-1*$^{Cre+\ f/f}$) mouse models were generated via Clustered Regularly Interspaced Short Palindromic Repeats (CRISPR)/ Cas9-mediated genomic editing at the Transgenic Mouse Models Core Facility of the National Core Facility Program for Biotechnology. *Regnase-1*$^{-/-}$ mice were generated by targeting a single guide RNA (sgRNA), to a region immediately upstream of the translation start site, and supplemented with a recombination sequence: nde1_Zc3h12a_HAtag. Primer sequences to identify the variation between *Regnase-1*$^{-/-}$, *Regnase-1*$^{f/f}$ and *Regnase-1*$^{Cre+\ f/f}$ was provided in Table 1. Complete blood counts (CBCs) of *Regnase-1*$^{-/-}$ and WT are listed in Table 5. CBCs of Regnase-1$^{Cre+\ f/f}$ and Regnase-1$^{f/f}$ are listed in Table 6.

Dual luciferase reporter assay

The Tet-On Regnase-1 constructs, encompassing wild-type (WT) or specific genetic variants (D141N, D225A, D226A, C157A), were stably expressed in *Regnase-1*$^{-/-}$ RAW264.7 cells. Subsequently, RAW264.7 cells harboring Tet-On Regnase-1 variants

doi:10.6342/NTU202403029

were seeded into 12-well plates at a density of 2 x 10^5 cells per well and transfected with the designated pmirGLO vector for 24 hours. Following transfection, cells were treated with either doxycycline (5μg/ml, Cat#24390-14-5, Sigma) or DMSO, in addition to IL-4 (20ng/ml) (Cat#Z02996, Genscript) stimulation, for an additional 24 hours. Total RNA was then collected for RT-qPCR analysis to determine the luc2/Rlc ratio between the doxycycline and DMSO groups.

For the analysis of firefly and Renilla luciferase activities, cells were seeded at a density of 2 x 10^5 cells per 100μl RPMI in a 96-well plate. After transfection and induction with doxycycline (5μg/ml, Cat#24390-14-5, Sigma) or DMSO, along with IL-4 (20ng/ml), the Dual-Luciferase Reporter Assay kit (Cat#E1960, Promega) was employed following the manufacturer's protocol. Briefly, 100μl of Luciferase Assay buffer II (containing substrate) was added to each well, followed by a 5-minute incubation at room temperature. Firefly luciferase activity was measured using a luminescent monitor (Spark® Multimode Microplate Reader). Subsequently, Renilla luciferase activity was assessed by adding 100μl of Stop&Glo buffer (containing substrate) to each well and incubating for 5 minutes at room temperature before measuring luminescence using the same instrument.

Regulatory T cell migration assay

doi:10.6342/NTU202403029

The Trans-well assay was performed to assess Treg cell migration. Pan T cells were isolated from lymph nodes by digestion with collagenase IV (Cat# 17104019, Gibco) and DNase I (Cat#M610A, PROMEGA). The resulting cell suspension was passed through the 70-μm Cell Strainer ((Cat#352350, Corning)) to obtain a single-cell suspension. Pan T cells were then purified using the Pan T Cell Isolation Kit II, mouse (Miltenyi Biotec). For in vitro Treg differentiation, 1 million Pan T cells were seeded in 24-well plates pre-coated with 0.5 mg/mL anti-CD3. The cells were cultured in RPMI1640 medium (Gibco) supplemented with 10% FBS (Gibco), 1 x penicillin/Streptomycin (Gibco), 20 ng/mL hIL2 (Biolegend), 5 ng/mL TGF-beta (Cat# Z03431, Genscript), 1 mg/mL anti-CD28 (Biolegend), 1 mg/mL anti-IL4 (Biolegend), and 1 mg/mL anti-IFNγ (Biolegend) for a period of five days to induce Treg differentiation. After differentiation, the Treg cells were seeded onto upper chamber of Trans-well inserts with a permeable membrane, while the conditional medium from IL4-treated *Regnase-1*$^{-/-}$ or WT macrophages were placed in the lower chamber. Following a 4-hour incubation period, the cells that migrated through the membrane were counted using hemocytometer.

Preparation of Bone Marrow-derived macrophages (BMDMs)

BMDMs were prepared following the protocol established by Professor Li-Chung Hsu's lab. Bone marrows (BMs) in femurs and tibia bones from 6-8 weeks mice were flushed with PBS containing 2% FBS using 25-gauge syringe. The BMs were repeatedly

doi:10.6342/NTU202403029

resuspended (generally 20-25 times) until single cell were separated. The cells were then treated with I ml RBC lysis buffer (Cat#R7757, SIGMA) for 3 mins and washed twice with PBS containing 2% FBS. The BM progenitor cells were seeded onto petri dish cultured in DMEM containing 10%FBS, 1% penicillin/streptomycin and 20% L929 conditional medium for 7 days. Adherent BMDMs were collected and cultured in DMEM containing M-CSF (10 ng/ml, Cat#Z03275-50, GenScript) for subsequent experiments.

Preparation of L929 conditional medium

Seeding thawed L929 cells on 9cm culture dish with DMEM containing 10%FBS, 1% penicillin/streptomycin. When cells grow to 70%~80% Confluency, seed 2 x 10^6 L929 cells on T75 culture flask with 20ml DMEM containing 10%FBS, 1% penicillin/ streptomycin. Adding additional 20ml DMEM (10%FBS, 1% penicillin/streptomycin) after 7 days, then collected the conditional medium(CM) after another 7 days. The L929 cell culture medium was collected and centrifuged at 800g for 5 minutes at RT to remove cells and debris. Stored the conditional medium in -80°C.

Immunoblotting

The treated BMDM were collected in IP buffer (50mM Tris-Cl pH7.4, 100mM NaCl, 1%NP-40, 0.1% SDS, 0.5% sodium deoxycholate) and subjected to sonication (20 cycles of 1 sec on/1 sec off) on ice. Supernatants were harvested after centrifugation of sonicated cell lysates at 10000g/ for 30 minutes at 4°C. Protein concentrations were assessed using

doi:10.6342/NTU202403029

the Bradford assay (Cat#APL-1013-1, Apolo) assay according to the manufacturer's instructions. Prior to loading in SDS-PAGE, protein samples were boiled at 95°C for 10 minutes in SDS loading dye (50mM Tris-Cl pH6.8, 6% Glycerol, 2% SDS, 0.004% Bromophenol blue, 20mM Dithiothreitol DTT) and heated at 95 degree for 10 minutes. Protein samples that were separated by SDS-PAGE were transferred to the PVDF membranes using the wet-electrophoretic transfer method (100 V, 300 mA, 90 minutes). The PVDF membranes were blocked with 5% non-fat milk in PBST (1x PBS, 0.05% tween 20) for 1 hour. Primary antibody is added after blocking with fast blocking buffer after two washes by PBST, and then incubated in a hybridization bag at 4°C overnight. HRP-conjugated secondary antibody is added after another two washes by PBST. The chemiluminescence with detected by using ECL.

RNA extraction & Real-time quantitative PCR (RT-qPCR)

Total cell RNA was extracted using NucleoZol (#740404.200, MACHEREY-NAGEL) following the manufacturer's instructions. The cDNA was obtained by reverse transcribing the total RNA with M-MuLV reverse transcriptase (#PT-MMLV, Protech) with random hexamer primer (Cat#SO142, Thermo Scientific). 1 μg total RNA was used to synthesize cDNA in 10μl reaction. The targeted cDNAs were determined by quantitative PCR using 2x SYBR Green/Fluorescein qPCR Master Mix (Cat#PB20.11, PCRBIOSYSTEMS) with 200nM primers each. All targeted genes were first normalized

doi:10.6342/NTU202403029

to cDNA derived from 18S ribosomal RNA transcript as an internal control and then relative wild-type control. All experiments were carried out in triplicate. The primer sequences used in RT-qPCR are listed in Table 1.

RNA-immunoprecipitation (RNA-IP)

Total cell lysates of RAW264.7 stable expressed Tet_ON_Regnase-1(D141N) with or without doxycycline (5μg /ml) treatment was collected in IP buffer (50mM Tris-Cl pH7.4, 100mM NaCl, 1%NP-40, 0.1% SDS, 0.5% sodium deoxycholate, 5U/ml RNase inhibitor, 1x protease inhibitor) and subjected to sonication (20 cycles of 1sec on /1sec off) on ice. Supernatants of cell lysates were collected through centrifugation at 10000g for 30 minutes at 4°C. Anti-flag M2 affinity Gel (Cat#A2220, sigma) beads were wash with IP buffer for three times. The immunoprecipitation was performed using 2 to 5mg/ml cleared cell lysates incubated with 30μl of pre-equilibrated Anti-flag M2 affinity Gel for 24 hours at 4°C with rotation. Immunocomplexes containing RNA on beads were pelleted by centrifuge at 500g at 4°C for 5 minutes. The pelleted beads were washed for three times with IP buffer. The pelleted beads containing RNA were collected by TRIzol™ (Cat#15596018, Invitrogen) extraction. The total RNA is reverse transcribed with M-MuLV reverse transcriptase (#PT-MMLV, Protech). The targeted genes were quantified by RT-qPCR.

doi:10.6342/NTU202403029

Flow cytometry of tumor infiltrating lymphocytes

LLC tumor tissues were sliced into small pieces with sterile dissecting scissors. The sliced tumor tissue was resuspended in a digestion solution (DMEM containing 2% FBS, Collagenase IV (Cat# C4-28-100MG, Sigma) for 30 minutes at 37°C.The digested tissue suspensions were passed through 70 μm nylon mesh filters (Cat#352350, Corning). Cells suspensions were pelleted with 400g for 5 minutes and resuspended in 100 μl FACS buffer (PBS containing 2% FBS). The suspension was first blocked with 0.1 mg/mL purified rat anti–mouse CD16/CD32 (BD Biosciences) for 15 minutes at 4°C. Staining Zombie NIR™ Fixable Viability Kit (Cat# 423105, BioLegend) was used to stain viable cells in FBS-free PBS for 30 minutes at 4°C. Subsequently, cells were then washed twice with FACS buffer and incubated with the respect antibody at a concentration (Antibody panel) suitable for 2x 10^6 cells in 100ul FACS buffer, followed by a 30-minutes incubation period (Antibody panel). The stained cells were washed with FACS buffer two times prior to being analyzed in Cytek® Aurora (Cytek), a full spectrum flow cytometry.

Antibody panel

CD25-Bv421 (clone 30-F11; 1:100; Invitrogen), CD11c-APC/Cy7 (clone HL3; 1:100; BD Biosciences), CD3-APC-Cy7(1:500; BioLegend), CD4-Bv711 (1:100; BD

doi:10.6342/NTU202403029

Biosciences), CD8-PE-Cy7 (1:500; BD Biosciences), Foxp3 APC (1:50; BioLegend), F4/80-AF488 (1:500; BioLegend), CD11b-PE (1:500; BioLegend), CD206 (1:100; BioLegend) L/D Zombie NIR (1:3000, BioLegend).

Measuring mRNA stability in BMDM

Wild-type and *Regnase-1*$^{-/-}$ were induced with 20 ng/ml IL-4 for 24 hours, followed by treatment with actinomycin D (5 μg/ml) for the indicated times. Total cellular RNAs were purified and the amount of the mRNA of interests were quantified using RT-qPCR with 18S ribosomal RNA served as internal control.

Cytokines array

The culture medium or cell lysates from *Regnase-1* $^{-/-}$, or wild-type BMDM were collected after treating with IL-4 (20ng/ml) for 24 hours. The protein expression level of 40 different cytokines were detect by using Proteome Profiler Mouse Cytokine Array Kit, Panel A (Cat#ARY006, R&D) kit. Briefly,

Enzyme-linked immunosorbent Assay (ELISA)

The culture medium from *Regnase-1*$^{-/-}$, or wild-type BMDM was collected after treatment with IL-4 (20ng/ml) for the indicated time point. The concentration of CCL22 chemokine

doi:10.6342/NTU202403029

in supernatants was detected using the Mouse CCL22/MDC DuoSet ELISA kit (Cat#DY439, R&D) following the manufacturer's instructions. Briefly, 100µl of diluted CCL22 capture antibody diluted (1:200 in PBS) is pre-coated in the VICTOR X4 Multilabel Plate Reader (Cat#6005640, PerkinElmer) overnight at room temperature on day 0. The coated plate was first washed three times with 400µl of PBST and followed by Blocking plate with 300µl Reagent Diluent (1% BSA in PBS) for 1 hour. Two times 400µl of PBST washed were prior to addition of 100µl of sample or standards in Reagent Diluent for 4 °C overnight. 2 hours RT incubation with 100µl Detection Antibody (1:200 in diluent) followed by 20mins RT of 100µl Streptavidin-HRP was applied. Each well was washed two times with PBST for two times between each steps above. The amount of CCL22 was quantity by adding 100µl of Substrate solution (Cat#01016-1, Clinical) was added for 20 minutes at RT (avoid light) followed by adding 50µl of Stop solution (2N H_2SO_4). The 450nm absorbance was detected using TECAN SPARK 10 M Hibrid microplate reader (TECAN).

Beads-based ELISA

The culture medium from both wild-type and *Regnase-1*$^{-/-}$ BMDM, which were induced with 20 ng/ml IL-4 for 0, 24, 48, 72 hours, were collected. LEGENDplex™ Multi-Analyte Flow Assay Kits recognize CCL2, CCL17 and CCL22 was used to detect the

doi:10.6342/NTU202403029

presence of these three chemokines. The procedure to use the LEGENDplex assay kit was following the manufacturer's instructions. In brief, the filter plate was pre-wet the by adding 100 μl of Wash Buffer to each well for 1 minute at RT followed by applying vacuum to remove the wash buffer. Twenty-five μl of the sample or standard with equal Assay buffer and 25 μl Mixed beads were mixed in a well in a sealed the plate shaking at 500rpm for 2 hours at RT and washed twice with 200μl Wash buffer by vacuum filtration. Twenty-five μl of Detection Antibodies was added and place on shaker at 500rpm for 1 hours at RT followed by adding 25 μl of SA-PE to each well and shaking at 500rpm for 30 minutes at RT. Samples prepared for analyzing were washed twice with 200 μl wash buffer by vacuum filtration and resuspended the beads with 150 μl Wash buffer. The PE signal of each capture bead is measured using Cytek® Aurora (Cytek).

Preparation of mRNA amplification library

Total cell RNA is extracted using NucleoZol (Cat#740404.200, MACHEREY-NAGEL) following the manufacturer's instructions. To remove enrich mRNA population, the NEBNext® Poly(A) mRNA Magnetic Isolation Module (Cat# E7490S, NEB) was utilized following the manufacturer's instructions. The mRNA library was constructed using the KAPA mRNA Capture Kit (Cat#KK8440, Roche). Briefly, 1-100ng of poly(A)-enriched mRNA was concentrated by RNA Clean & Concentrator^{TM}-5 (Cat#R1016,

doi:10.6342/NTU202403029

ZYMO research) following the manufacturer's instructions and then resuspended in 10μl RNase-free water. mRNA is fragmented into desired size (300-400nt) by incubating at 85°C for 6 minutes followed by 1st stand synthesis, 2nd stand synthesis, A- tailing and Adapter ligation. The cDNA library was amplified by PCR following the indicated amplification cycles (for 50ng-100ng started mRNA, 6-8 cycles are recommended). After cleaning up with KAPA pure beads, the cDNA library from each sample was quantified by qPCR, and equal amounts were mixed into a library mixture. cDNA library was sequencing using Hiseq x-ten (Genomics) 2x150bp. The quality and quantity of RNA were analyzed using a bioanalyzer (Agilent 2100 Chip-1). Total of 6.32-22.3 million unique reads were obtained from each sample from mRNA sequencing of Fastq files.

mRNA-seq analysis

mRNA-seq analysis was conducted on the raw Fastq file using the online NGS analysis tool “Galaxy” (v22.1). Reads were trimmed using “Cutadapt” to remove 3’adapter sequences and filter out reads that were shorter than 20 bp or below the quality cut-off. Trimmed reads were mapped to the mouse reference genome (mm10/GRC38) using “HISAT2”. Reads mapping to the genome were quantified using "FeatureCounts" for gene-level analysis. Differential expressed genes (DEGs) analysis between samples was normalized with Trimmed Mean of M-values (TMM) normalization and conducted using

doi:10.6342/NTU202403029

"limma-voom" including: MD plot, Volncano plot, PCA analysis and DEGs analysis. The DEGs are listed in Table2 (*Regnase-1*$^{-/-}$ versus WT without IL-4 induction), Table3 (*Regnase-1*$^{-/-}$ versus WT with IL-4 induction for 4 hour) and Table4 (Regnase-1$^{-/-}$ versus WT with IL-4 induction for 24 hour).

In vivo murine allograft tumor models

LLC cells at their exponential phase were collected and resuspended at 2.5 x10^6 cells/ml. The cell suspension was mixed at a 3:2 volume with Matrigel Matrix (Cat#354234, Corning®). Subsequently, 200μl of the LLC cells mixture (3 x10^5 cells) was injected subcutaneously into the lower abdominal cavity of 6- to 7-weeks-old mice, either *Regnase-1*$^{f/f}$ or *Regnase-1*$^{Cre+\ f/f}$. Tumor size and mice weight were recorded every two or three days until the tumor size exceeded 2000mm^3 or the tumor radius exceeded 20mm or the observation period exceeded a month. Tumor sizes were measured using microCT with the formula V=1/2 [(length)^2 × width]. Tumor tissue for additional analysis, such as IHC and FACS were collected in mice sacrificed on the 13th day post-inoculation.

Mouse experiments were carried out in accordance with animal welfare guidelines and were approved by the Institutional Animal Care and Use Committee (IACUC) of the College of Medicine, National Taiwan University (no. 20220077).

doi:10.6342/NTU202403029

Transfection of siRNA

Regnase-1 knockdown experiments are using siRNA-mediated knockdown. BMDM subcultured in 2 x 10^5 per 6-well plate are transfect with siCtrl (D-001810-10-05, Horizon Discovery) or *siRegnase-1* (L-052076-01, Horizon Discovery, On-TARGETplus SMARTpool siRNA including four sequences target *Regnase-1*: 5'-AGUACUGGUCUGAGCCGUA-3', 5'-CGAGAAGGCUCACCGCAGA-3', 5'-UGGACAACUUCCUUCGUAA -3', 5'-GGAAACGCUUCAUCGAGGA-3') by using RNAiMAX transfection reagent (Cat# 13778150, Life Technologies).

Statistical analysis

The graph and statistical analysis were performed using GraphPad Prism version 9.4.1 (San Diego, CA). To determine significance between groups, Student's t tests or one-way ANOVA tests were performed. Data are presented as mean ± SEM. Significant differences are indicated by *p <0.0332, ** p <0.0021, *** p <0.0002.

doi:10.6342/NTU202403029

Chapter III: Results

Regnase-1 expression is induced by IL-4 in BMDM and RAW264.7 macrophages

Despite extensive studies on the role of Regnase-1 in pro-inflammatory macrophages, its specific involvement in alternative polarization remains uncertain. To address this, we investigated Regnase-1's function in the well-characterized M2a macrophage subtype induced by IL-4 or IL-13. Both the mouse macrophage cell line, RAW 264.7, and bone marrow-derived macrophages (BMDM) were stimulated with IL-4, and changes in mRNA and protein levels were monitored. Notably, while Regnase-1's up-regulation in macrophages is typically associated with exposure to LPS, a proinflammatory ligand, its expression was also induced in IL-4-treated macrophages, indicative of an anti-inflammatory milieu. Regnase-1 mRNA peaked at 2 hours and 4 hours post-IL-4 stimulation in RAW264.7 and BMDM, respectively.

Furthermore, REGNASE-1 protein expression exhibited a gradual increase within the initial 4 and 24 hours following IL-4 induction in RAW264.7 and BMDM, respectively. The expression of *Regnase-1* in IL-4 induced alternative polarization differs from its rapid response to most TLR stimulation, as previously reported by Akira's group. Here, REGNASE-1 exhibits a steady increase and persist for at least 48 hours (Figure 1).

Generating *Regnase-1* deficient RAW264.7 cells and Regnase-1 total knockout

doi:10.6342/NTU202403029

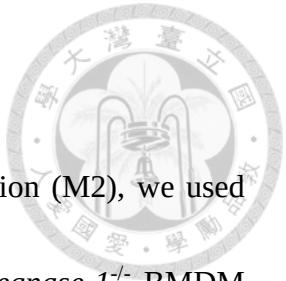

Mouse models

To assess the role of Regnase-1 in M2a macrophage polarization (M2), we used CRISPR to generate *Regnase-1*$^{-/-}$ RAW264.7 cells and obtained *Regnase-1*$^{-/-}$ BMDM from newly generated *Regnase-1* deleted (*Regnase-1*$^{-/-}$) transgenic mice (Figure 2). The *Regnase-1*$^{-/-}$ RAW264.7 cell line harbors a 155-nucleotide deletion from the 14th position from the translational start site, which resulted in only three amino acids at the N terminus being preserved in endogenous Regnase-1 (Figure 3). The newly generated *Regnase-1*$^{-/-}$ mice contain a 196-nucleotide insertion before the translational start site, further resulting in the skipping of the ATG-containing exon (Figure 4). Both the *Regnase-1*$^{-/-}$ RAW264.7 cell line and the *Regnase-1*$^{-/-}$ mice were by-products while we attempted to obtain *HA:Regnase-1* transgenic RAW264.7 cells and mice.

The phenotypes of *Regnase-1*$^{-/-}$ mice were closely aligned with previously reported findings in the literature. These mutant mice displayed growth retardation, along with enlarged spleens, pale organs, and a mortality rate of approximately 50% within eight weeks. Complete blood counts (CBCs) analysis further revealed manifestations of anemia, evidenced by decreased hemoglobin and red blood cell counts, alongside elevated white blood cell and platelet counts in our *Regnase-1*$^{-/-}$ mice (Figure 4, Table 5).

REGNASE-1 Does Not Affect M2a Macrophage Polarization

doi:10.6342/NTU202403029

To understand the impact of *Regnase-1* deletion on M2a-polarized macrophages following IL-4 stimulation, we examined marker genes including *Arginase-1*, *YM1*, and *Fizz1* in both RAW264.7 and BMDM. To monitor changes in these marker genes, we quantified mRNA changes at 0, 2, 4, 6, and 24 hours post IL-4 stimulation. While wild-type BMDM demonstrated a gradual and noteworthy increase in these marker mRNAs upon IL-4 stimulation, no significant differences were observed between wild-type and Regnase-1 mutant cells in both RAW264.7 and BMDM following IL-4 stimulation. Additionally, no significant variances in YM1 protein levels were observed in BMDM between wild-type and Regnase-1 mutant mice following 24-hour IL-4 induction. (Figure 5). These findings were unexpected, considering previous reports indicating the involvement of Mcpip1 (an alternative name for Regnase-1) in macrophage M2 polarization in response to IL-4. Thus, despite our data suggesting that Regnase-1 does not participate in M2a macrophage polarization, whether it is involved in the function of M2a-polarized macrophages remains unclear.

REGNASE-1 regulates a subset of macrophage alternative polarization genes

To elucidate whether Regnase-1 plays a role in M2a polarized macrophages, we conducted a comprehensive analysis of global mRNA expression profiles in IL-4

doi:10.6342/NTU202403029

stimulated BMDM from WT and *Regnase-1*$^{-/-}$ mice, both with and without IL-4 induction for 4 or 24 hours. Principal component analysis (PCA) revealed a well clustered among all three replicates and distinct polarization states following IL-4 induction (Figure 6A). As expected, significant differences were found between naïve and IL-4 polarized groups. However, only minor differences were found between wild-type and *Regnase-1*$^{-/-}$ BMDM with IL-4 stimulation (Figure 6B). The global differences in PCA also reflect in differential expressed genes (DEGs). A total of 1072 and 1,542 genes are differentially expressed by comparing 4 or 24hrs IL-4 stimulated WT BMDMs to their naïve status, respectively. However, only 58, 93 or 76 differentially expressed genes were observed when comparing *Ragnase-1*$^{-/-}$ to wild-type BMDM at 0, 4, 24 hours, respectively, upon IL-4 treatment. The GO term analysis of the DEGs between *Ragnase-1*$^{-/-}$ to wild-type BMDM reveal that the "Immune system response" was found in all three time points (0, 4, 24 hours) (Figure 7). Unexpectedly, the major DEGs in the "immune system response" gene sets are re-arranged immunoglobulin. Though this observation was also found in peritoneal macrophage (personal communications), the reason behind IgG rearrangement take place in macrophage remain unclear.

To narrow down to the genes that participate in alternative polarized macrophage, we specifically examined the overlapped DEGs between IL-4 treatment v.s. naiive and wild-type v.s. *Regnase-1*$^{-/-}$ after IL-4 treatment. Notably, 24 DEGs were found in

doi:10.6342/NTU202403029

Ragnase-1$^{-/-}$ compared to wild-type after IL-4 treatment for 24 hour, including the M2a macrophages -produced chemokines *Ccl17*, and *Ccl22* (supplementary figure 1). Despite no significant differences were found in M2a marker genes between *Regnase-1*$^{-/-}$ and WT BMDMs at both 4 and 24 hours post IL-4 stimulation, consistent with prior findings. Given the crucial role of Ccl17 and Ccl22 secreted from tumor-associated macrophages (TAMs) in Treg recruitment across various tumor models and their importance in peritoneal fibrosis, we shifted our focus to understanding how Regnase-1 modulates Ccl17 and Ccl22 mRNA expression.

REEGNASE-1 regulates *Ccl17* and *Ccl22* production in M2a polarized macrophages

To conclusively verify that the alterations in *Ccl17* and *Ccl22* mRNA levels observed in M2a-polarized BMDMs from *Regnase-1*$^{-/-}$ mice are directly attributable to the absence of Regnase-1, we performed Regnase-1 knockdown in BMDMs using siRNA. The siRNA-mediated Regnase-1 knockdown resulted in approximately a 50% decrease in mRNA levels, and significant reductions in Regnase-1 protein levels were evident as well (see Figure 9). Encouragingly, we observed significant decreases in Ccl17 and Ccl22 mRNA levels in IL-4 stimulated BMDMs following Regnase-1 knockdown by siRNA (Figure 8, 9).

doi:10.6342/NTU202403029

To further investigate whether the reduction in Ccl17 and Ccl22 mRNA levels in *Regnase-1*$^{-/-}$ M2a-polarized BMDM leads to decreased CCL17 and CCL22 chemokine production, we measured the secretion levels of CCL17 and CCL22 at 0, 24, 48 and 72 hours post IL-4 treatment using a customized LEGEND^{plex} mouse M2 macrophage panel. Encouragingly, while both CCL17 and CCL22 chemokines were detected in the culture medium from IL-4-treated wild-type BMDM, only minimal amounts were observed in *Regnase-1*$^{-/-}$ BMDMs (Figure 10). Specifically, under wild-type conditions, less than 1pg/ml and 2.408 pg/ml of CCL17 were detected after 48 and 72 hours of IL-4 treatment, respectively, whereas the most significant increase in CCL22 production was observed at 24 (7.59 pg/ml) and 48 (432.7 pg/ml) hours post IL-4 treatment. Interestingly, although the decreases in mRNA expression of both Ccl17 and Ccl22 in IL-4-treated *Regnase-1*$^{-/-}$ BMDM were within six fold, no detectable CCL17 chemokine present in the culture medium of IL-4-treated *Regnase-1*$^{-/-}$ and CCL22 chemokine levels were reduced by 10.7- and 50.6-fold compared to IL-4-treated wild-type BMDMs. Notably, CCL22 chemokine production in the culture medium of *Regnase-1*$^{-/-}$ BMDMs was up-regulated after 72 hours, though still around 10-fold less than the culture medium from IL-4-treated wild-type BMDMs at the same time point.

To broaden our understanding of additional cytokines affected in *Regnase-1*$^{-/-}$ BMDMs following IL-4 stimulation, we conducted a quick screening using a mouse

doi:10.6342/NTU202403029

cytokine array featuring 40 different mouse cytokines. Intriguingly, we observed significant increases in CXCL10, CCL12, CCL3, and CCL4, while IL16, CCL2, and TIMP-1 exhibited marked decreases in the medium derived from *Regnase-1*$^{-/-}$ BMDMs compared to wild-type BMDMs post IL-4 stimulation (Figure 11). However, none of their mRNA level in our mRNA-seq data exhibited significant changes when comparing *Regnase-1*$^{-/-}$ BMDMs to wild-type BMDMs post 24-hours IL-4 stimulation. Since CCL2 mRNA was the only one upregulated in IL-4-treated BMDMs, suggesting its potential function in M2a macrophage, we further investigated CCL2 using LEGEND^{plex}. Unfortunately, there were no statistically significant differences in CCL2 protein levels in the medium derived from IL4-treated BMDMs between *Regnase-1*$^{-/-}$ and wild-type (Figure 10). In summary, our findings indicate that while Regnase-1 does not influence M2a macrophage polarization, its presence is crucial for the expression of Ccl17 and Ccl22, at both mRNA and protein levels, in M2a-polarized macrophages.

REGNASE-1 does not affect the phosphorylation of STAT6

To understand how Regnase-1 regulates the mRNA expression level of Ccl17 and Ccl22, we first analyze the major transcription factor STAT6, known for its key role in Ccl17 and Ccl22 mRNA production as well as M2a macrophage polarization. Both the total and phosphorylated forms of STAT6 were detected in BMDMs treated with IL-4 for

doi:10.6342/NTU202403029

4 and 24 hours, from both wild-type and *Regnase-1*$^{-/-}$ mice, with no discernible differences observed. Phosphorylated STAT6 is significantly up-regulated in both wild-type and *Regnase-1*$^{-/-}$ BMDM following 4-hour and 24-hour IL-4 induction. However, the proportion of phosphorylated STAT6 gradually decreased after 4 hours of IL-4 treatment (Figure 12). The same amount of Phospho-STAT6 expression between wild-type and *Regnase-1*$^{-/-}$ is consistent with our previous finding that no significant difference was found in the mRNA levels of *Arg-1, Fizz-1,* and *Ym-1* between IL-4-stimulated BMDM from both genotypes. Therefore, it is reasonable to conclude that the differences in *Ccl17* and *Ccl22* mRNA are less likely due to variations in the major transcription factor for *Ccl17* and *Ccl22*.

Examination the potential REGNASE-1 targets found in mRNA-seq using RNA immunoprecipitation (RNA-IP).

To identify the potential Regnase-1 RNA targets, we performed enhanced crosslinking and immunoprecipitation (eCLIP) and RNA IP by immunoprecipitating Regnase-1 catalytically defective mutant, Regnase-1(DN). Several candidates from two groups of genes have been tested, including (1) Up-regulated genes found in Regnase-1mt/mt M2(IL4) BMDM mRNA-seq (Prps1, Gm4951, Batf2, Pou2f2). 2) Enriched RNA fragments found in IL-4 treated Regnase-1(DN) eCLIP sample (*Nfkbiz, Tnf, Arhgef18,*

doi:10.6342/NTU202403029

Arhgef5, Dnmt1, Inpp4b, Smad3, Naa15, Zc3h7a, Malat1, Ppm1e, and Neat1). Regnase-1 mRNA is a known targeting its own mRNA, therefore the Regnase-1 mRNA serves as positive control for our Regnase-1(DN) RNA IP. Among 16 Regnase-1 candidate targets, we found *Nfkbiz, Neat1* and *Batf2* show enrichments in IL4-treated RAW264.7 Regnase-1 (DN) RNA-IP (Figure 13). We identified BATF2, a transcription factor that plays a crucial role in the IFN-γ and LPS-activated inflammatory response in BMDMs [85]. Besides, BATF2 inhibits PD-L1 expression through inhibits the PI3K-AKT pathway [86]. However, Whether BATF2 is the intermediate regulator that promotes Ccl17 & Ccl22 mRNA degradation in the Ribonuclease defective Regnase-1 will be further validated.

The ribonuclease activity of REGNASE-1 is crucial for stabilizing *Ccl17* and *Ccl22* mRNA via their 3'UTR.

To investigate how *Ccl17* and *Ccl22* mRNAs are regulated by *Regnase-1*$^{-/-}$ BMDMs upon IL4 treatment, we assessed the mRNA decay rate of both transcripts in IL4-stimulated BMDM from either wild-type or *Regnase-1*$^{-/-}$ mice. Following Actinomycin D treatment, we observed a significant decrease in both *Ccl17* and *Ccl22* mRNA levels within the first half hour in 24-hour IL-4-stimulated BMDMs from *Regnase-1*$^{-/-}$ mice. In contrast, in 24-hour IL-4-treated wild-type BMDMs, *Ccl22* mRNA exhibited a gradual decrease, while *Ccl17* mRNA displayed rapid decay after an hour (Figure 14). Our results

doi:10.6342/NTU202403029

suggest that the decrease in *Ccl17* and *Ccl22* mRNA in *Regnase-1*$^{-/-}$ BMDM relative to wild-type BMDM is, at least in part, attributable to decreases in their mRNA stability.

To gain a better understanding of the regions on *Ccl17* and *Ccl22* mRNAs that contribute to their stability, we shifted our experiment to another manipulable macrophage cell line, RAW264.7. Initially, we investigated whether the destabilization of *Ccl17* and *Ccl22* mRNA could also be observed in a previously generated *Regnase-1*$^{-/-}$ RAW264.7 cell line. While only *Ccl22* mRNA was induced in RAW264.7 following 24 hours of IL-4 treatment, the absence of Regnase-1 also resulted in a significant decrease in *Ccl22* mRNA levels, akin to observations in BMDMs (Figure 15). This data suggests that although only *Ccl22* mRNA showed induction in RAW264.7, the Regnase-1-dependent destabilizing machinery for *Ccl22* mRNA remains intact in RAW264.7 cells.

Since regulatory elements in mRNAs are primarily localized in their 3' UTRs, we clone the 3'UTR from both *Ccl17* and *Ccl22* into the pmirGLO-dual luciferase vector and expressed them in *Regnase-1*$^{-/-}$ RAW264.7 cells containing doxycycline-inducible wild-type Regnase-1. Encouragingly, upon induction of wild-type REGNASE-1 by doxycycline, a substantial increase in luciferase mRNA was observed, averaging at 2.7- and 3.8- fold for luciferase constructs containing *Ccl17* and *Ccl22* 3'UTRs, respectively (Figure 16). Our results confirm the destabilization elements within the 3' UTRs of *Ccl17* and *Ccl22* mRNAs following IL-4 stimulation. Additionally, our results unveil the

doi:10.6342/NTU202403029

retention of REGNASE-1 dependent regulatory elements for *Ccl17* within RAW264.7 cells, even in the absence of IL-4-mediated *Ccl17* induction.

To examine if the ribonuclease activity contributes to the increase in mRNA stability of *Ccl17* and *Ccl22* 3'UTRs, luciferase reporters bearing these two 3' UTRs were transfected into two *Regnase-1*$^{-/-}$ RAW264.7 cell lines. These cell lines had been engineered to express doxycycline-inducible, ribonuclease-defective *Regnase-1* mutants, including both REGNASE-1(D141N) and REGNASE-1(DDAA). Both of the ribonuclease-defective mutants of Regnase-1 failed to induce an elevation in luciferase mRNA levels with either *Ccl17* and *Ccl22* 3'UTRs. Our results suggest that the ribonuclease activity of REGNASE-1 is critical for increasing the mRNA stability containing *Ccl17* and *Ccl22* 3'UTRs.

REGNASE-1 destabilizes microRNAs targeting *Ccl17* and *Ccl22*.

We further aimed to investigate the destabilizing regions of *Ccl17* and *Ccl22* 3'UTRs that are controlled by REGNASE-1. We designed various truncation forms of *Ccl17* and *Ccl22* 3'UTRs (Figure 17A). While full-length Ccl17 3'UTR$_{1\text{-}181FL}$ shows significant enhanced luciferase mRNA expression in wild-type relative to ribonuclease defective Regnase-1(DDAA), the enhancement was abolished in *Ccl17* 3'UTR$_{1\text{-}100}$. Whereas the enhancement of luciferase mRNA expression in wild-type relative to

doi:10.6342/NTU202403029

ribonuclease defective Regnase-1 was preserved in *Ccl22* 3'UTR within the first 608 nucleotides. Further analysis of these 608 nucleotides revealed that the destabilizing elements are located within the *Ccl22* 3'UTR$_{304\text{-}608}$ region (Figure 17B).

Given that REGNASE-1 has previously been shown to antagonize DICER in microRNA production, we conducted a systematic screening to identify potential microRNA target sites within the previously identified regulatory region of *CCL17* and *CCL22* 3'UTR. To manage the abundance of microRNAs predicted in both UTRs, our selection process involved two key strategies: 1) Utilizing TargetScan to identify a manageable subset of microRNAs. 2) Employing the miRDB scoring system to pinpoint the highest-scoring microRNAs meeting our criteria when the number exceeded manageability (Figure 18). Through TargetScan analysis, five microRNAs (miR-138-5p, miR-130-3p, miR-301-3p, miR-142-3p.1, and miR-129-5p) were identified in *Ccl17* 3'UTR with the category 'broadly conserved among vertebrates'. Among the top 20 microRNAs with the highest targeting scores, only four microRNAs (miR-7667-3p, miR-7062-5p, miR-5120, and miR-764-3p) were specifically targeted to the *Ccl22* 3'UTR$_{304\text{-}608}$ region. Additionally, miR-337 was included due to its targeting of both *Ccl17* and *Ccl22* 3' UTRs. To assess the potential influence of REGNASE-1 on the stability of these microRNA candidates under IL-4 stimulation, we utilized Taqman assays to quantify microRNA abundance. We scored for significant increases in microRNA levels within

doi:10.6342/NTU202403029

the IL-4-stimulated *Regnase-1*$^{-/-}$ RAW264.7 cell compared to IL-4-stimulated wild-type RAW264.7 cell (Figure 19).

Additionally, among the top-scored miRNAs targeting the *Ccl22* 3'UTR304-608 region, only miR-764-3p showed significantly up-regulation in IL-4-treated *Regnase-1*$^{-/-}$ RAW 264.7 cells relative to wild-type counterparts. Interestingly, despite of no significant, the tested miRNAs targeting the *Ccl17* 3'UTR, miR-130a-3p and miR-301a-3p exhibited higher expression in IL-4-treated *Regnase-1*$^{-/-}$ RAW 264.7 cells compared to their wild-type counterparts.

Next, we investigate the miRNA binding site in the *Ccl22* 3'UTR304-608 and *Ccl17* 3'UTR101-181 using miRDB and TargetScan, which are the online miRNA prediction tools can predict miRNA-mRNA interactions with a higher probability. Additionally, among the top-scored miRNAs targeting the *Ccl22* 3'UTR304-608 region, only miR-764-3p showed significantly up-regulation in IL-4-treated *Regnase-1*$^{-/-}$ RAW264.7 cells relative to wild-type counterparts. Additionally, among the top-scored miRNAs targeting the *Ccl22* 3'UTR304-608 region, only miR-764-3p showed specific up-regulation in IL-4-treated *Regnase-1*$^{-/-}$ RAW264.7 cells relative to wild-type counterparts.

To confirm whether the upregulation of microRNAs dependent on both IL-4 and Regnase-1 indeed leads to downregulation of their predicted targets, *Ccl17* and *Ccl22*, we introduced mutations in the seed regions targeted by these microRNAs in the

doi:10.6342/NTU202403029

luciferase reporter assay. We then compared luciferase mRNA levels in IL-4-treated *Regnase-1*$^{-/-}$ RAW264.7 cells relative to wild-type counterparts. Interestingly, miR-130a-3p and miR-301a-3p share an identical seed region and potentially target the *Ccl17* 3'UTR117-138, while potentially miR-764-3p targets the *Ccl22* 3'UTR488-512. Remarkably, the significant differences in luciferase mRNA levels observed in IL-4-treated *Regnase-1*$^{-/-}$ RAW264.7 cells compared to wild-type counterparts were no longer present when mutations were introduced between positions 117-138 and 488-512 in the 3'UTRs of *Ccl17* and *Ccl22*, respectively (Figure 20).

Our findings indicate that the Regnase-1-dependent enhancement of *Ccl17* and *Ccl22* expression in M2a macrophages is attributed to the upregulation of *Regnase-1*, leading to the decreased expression of miR-130a-3p, miR-301a-3p, and miR-764-3p. This reduction in microRNA levels alleviates the suppression exerted on *Ccl17* and *Ccl22* mRNAs, ultimately resulting in the upregulated expression of *Ccl17* and *Ccl22* in M2a-polarized macrophages.

Generate myeloid-specific *Regnase-1* knockout mice.

Previous studies have highlighted the pivotal role of Treg cells in skin inflammation, with their recruitment heavily reliant on CCR4 receptors. Additionally, Treg cells recruited to tumors have been associated with promoting tumor growth. To examine

doi:10.6342/NTU202403029

whether Treg recruitment is compromised in mice with *Regnase-1* deficiency in macrophages under physiological conditions, we aimed to determine if fewer Tregs were recruited to tumors implanted in mice with macrophage-specific *Regnase-1* knockout. To facilitate this investigation, we established a mouse model featuring two loxp sites inserted at the second intron and after the 3' UTR of the *Regnase-1* gene. Subsequently, we crossed the newly generated Regnase-1 flanked with loxp mice (*Regnase-1*$^{f/f}$) with transgenic mice containing LysM-driven Cre recombinase, a common model for macrophage-specific knockout. The myeloid-specific deletion via Cre recombinase driven by the LysM promoter results in the removal of Regnase-1's original termination sequence for transcription, along with the stop codon. Consequently, if protein production occurs, only the first 147 residues (out of the full-length 596 residues) are translated, lacking the intact ribonuclease domain. The success of generating *Regnase-1* deficiency in BMDM was further confirmed by detecting REGNASE-1 protein using western blot analysis (Figure 21).

Similar to the phenotypes described in the literature, older *LysM:Cre; Regnase-1*$^{f/f}$ mice display apathy, decreased sensitivity to handling, and enlarged spleen (Figure 21). Moreover, the seven-week-old *LysM:Cre; Regnase-1*$^{f/f}$ mice exhibit milder anemia compared to *Regnase-1*$^{-/-}$ mice, with 77% hemoglobin remaining in *LysM:Cre; Regnase-1*$^{f/f}$ mice compared to only 28% in *Regnase-1*$^{-/-}$ mice. Additionally, the increase in white

doi:10.6342/NTU202403029

blood cells is 1.4-fold in *LysM:Cre; Regnase-1*$^{f/f}$ mice relative to 2.9-fold in Regnase-1$^{-/-}$ mice (Table 6).

Besides, we confirmed the mRNA expression and cytokine secretion of *Ccl17* and *Ccl22* in BMDMs from *LysM:Cre; Regnase-1*$^{f/f}$ mice. Consistent with total *Regnase-1*$^{-/-}$ BMDMs, the mRNA expression levels of *Ccl17* and *Ccl22* were 3.97-fold and 7.854-fold lower, respectively, in *LysM:Cre; Regnase-1*$^{f/f}$ BMDMs compared to controls after treatment with IL-4 for 24 hours. The expression level of CCL22 cytokines tested by ELISA (R&D) also showed significantly lower expression in *LysM:Cre; Regnase-1*$^{f/f}$ BMDMs at 24, 48, and 72 hours, with fold changes of 10.55, 41.03, and 12.34, respectively (Figure 22).

Macrophage REGNASE-1 enhances Treg cell recruitment by M2a macrophage.

We further investigated whether *Regnase-1* deficiency affects the recruitment of CCR4-abundant Treg cells. Initially, we assessed the presence of CCR4 on isolated T cells from the spleen and lymph nodes of wild-type mice, as previous reports indicate the CCR4 receptor is present in $CD3^+$ pan T cells. Subsequently, we differentiated pan T cells into Treg cells by treating them with IL-2, TGF-beta, and anti-IL-4 antibodies for 3 days. The success of Treg differentiation was confirmed using flow cytometry to verify the

doi:10.6342/NTU202403029

percentage of $CD4^+CD25^+foxp3^+$ Tregs (Figure 23A-C). Following this, we conducted migration assays using trans-well chambers to observe whether the conditioned medium from IL-4-treated BMDM from wild-type or *Regnase-1*$^{-/-}$ mice resulted in differences in the migration of differentiated Treg cells. Consistent with previous observations, we noted a significant increase in Treg migration in the cultured medium obtained from IL-4-treated BMDM compared to naive BMDM from wild-type mice. However, this notable increase in migrated Treg cells was abolished when using culture medium from *Regnase-1*$^{-/-}$ BMDM (Figure 23 D, E).

Decreased LLC tumor growth in macrophage-specific *Regnase-1* deleted mice compared to wild-type mice.

To investigate the role of REGNASE-1 in macrophages in tumor development, LLc cancer cells were implanted into the lower abdominal cavity of 7-week-old *Regnase-1*$^{f/f}$ and *LysM:Cre; Regnase-1*$^{f/f}$ transgenic mice, and tumor weights were recorded over a 29-day period. Remarkably, a significant reduction in tumor size was observed after 13 days of implantation, with notable differences becoming more pronounced thereafter. By the 29th day, the disparity in tumor volume had reached a two-fold difference (Figure 24).

doi:10.6342/NTU202403029

To understand the cellular contributors to the decreased tumor size observed in *LysM:Cre; Regnase-1*$^{f/f}$ transgenic mice, we conducted immunohistochemistry (IHC) and flow cytometry analyses of tumors harvested at day 13. Our investigations revealed a significant increase in infiltrated macrophages ($CD68^+$) and helper T cells ($CD4^+$) within the tumors derived from *LysM:Cre; Regnase-1*$^{f/f}$ transgenic mice compared to those from *Regnase-1*$^{f/f}$ transgenic mice (Figure 25). Further analysis of the T cell population within the tumors via flow cytometry unveiled the most notable differences in $CD4^+CD25^+$ Treg cells (Figure 26). Consistent with our prior findings, *Regnase-1* deletion specifically in macrophages resulted in decreased recruitment of Tregs.

Chapter VI: Discussion

Alternative macrophage polarization is important for innate immunity regulation to resolved inflammation over activation. However, the alternative macrophage polarization of macrophage would be utilized by virus or tumor cell to escape host defense mechanism. Thus, the underlying mechanism that important for processing alternative macrophage polarization need to elucidate. In this thesis, we demonstrate that Regnase-1 participated in cytokines production regulation during IL-4-treated macrophage alternative polarization, specifically to *Ccl17* and *Ccl22* (Figure 27).

doi:10.6342/NTU202403029

Differential contributions of REGNASE-1 to M2a macrophage polarization between this study and previous research

REGNASE-1's involvement in macrophage IL-4-stimulated alternative polarization was initially reported by the Kolattukudy group in 2015. However, our study did not directly observe Regnase-1's involvement in macrophage polarization. Here, we outline several experimental variations that could explain these disparities. Firstly, the types of macrophages isolated from Regnase-1 deletion mice differed. In this thesis, we utilized RAW264.7 cells, a macrophage cell line, and bone marrow-derived macrophages (BMDM) to generate IL-4-stimulated M2a polarized macrophages, while Kapoor et al. used peritoneal macrophages (pMAC) from Regnase-1 knockout mice in their study. Previous research comparing the response of pMAC and BMDM to external stimuli such as IL-4 and IL-13 revealed significant differences. Notably, the expression of the alpha chain of the IL-4 receptor, CD124, was lower in pMAC compared to BMDM, and arginase-1 mRNA expression was approximately 100 times lower in pMAC than in BMDM. Thus, while both pMAC and BMDM were derived from *Regnase-1* defective mice, their distinct responses to external stimuli, such as IL-4, could account for variations in the importance of REGNASE-1 in M2a macrophage polarization. Secondly, we observed sustained upregulation of all M2a marker mRNAs, including *Arginase-1*,

doi:10.6342/NTU202403029

Ym1, and *Fizz1*, for up to 24 hours following IL-4 stimulation, whereas Kapoor et al. monitored changes in these marker genes only within a four-hour timeframe. Differences in the duration of monitoring M2a marker gene changes could also contribute to the discrepancies in our conclusions regarding the importance of REGNASE-1 in M2a macrophage polarization.

Detection of rearranged Immunoglobulin mRNAs in *Regnase-1*$^{-/-}$ BMDM mRNA-seq Analysis

Our mRNA sequencing analysis has unveiled subtle yet significant differences in differentially expressed genes (DEGs) between wild-type (WT) and *Regnase-1*$^{-/-}$ BMDM. Specifically, we identified 58, 94, and 77 DEGs among IL-4 treated samples for 0, 4, and 24 hours, respectively. Among these DEGs, 31 genes consistently exhibited alterations across all conditions, predominantly featuring recombinant immunoglobulin DNA sequences, despite their relatively low read counts. This finding is intriguing, as macrophages were not previously known to undergo DNA rearrangement. The presence of DNA rearrangements in IgG was further confirmed by PCR (Supplementary figure 1). Given the well-established role of RAG1 and RAG2 in DNA rearrangements of IgG in T cells, we investigated mRNA expression changes in BMDM derived from wild-type and total *Regnase-1* knockout mice using our mRNA sequencing data. As anticipated, we

doi:10.6342/NTU202403029

observed low expression levels of both *Rag1* and *Rag2* in BMDM, regardless of genotype or IL-4 treatment, with fold changes within 1.3 and no statistically significant differences between wild-type and *Regnase-1*$^{-/-}$ BMDM. This observation suggests that the increased recombinant IgG sequences may originate from contaminating T or B cells in the bone marrow. Notably, REGNASE-1 has been reported as crucial for maintaining homeostasis in hematopoietic stem and progenitor cells (HSPCs) from the bone marrow. Lack of REGNASE-1 in HSPCs leads to a significant increase in T cell differentiation from the bone marrow, a phenomenon rarely observed. This expansion of bone marrow-derived T cells may contribute to the observed increase in recombinant immunoglobulin sequences, despite their limited numbers.

The Impact of REGNASE-1 in tumor pathology

In this thesis, we identified reduced tumor weight and volume in macrophage-specific *Regnase-1* knockout mice. Additionally, we observed increased infiltration of $CD4^{+}CD25^{+}$ T cells in wild-type mice compared to *Regnase-1*$^{Cre+\ f/f}$ mice. Despite the absence of the major transcriptional factor FOXP3 in tumor-infiltrating lymphocytes (TILs) within LLC allografts, due to the low infiltration of total T cells, we have shifted our focus to other cancer types with higher T cell infiltration, such as B16 (melanoma)

doi:10.6342/NTU202403029

cells and MC-38 (colon adenocarcinoma) cells. Preliminary experiments of MC-38 allograft exhibited similar result to LLC in reduced tumor development.

According to "THE HUMAN PROTEIN ATLAS," *Regnase-1* mRNA is mainly expressed in the respiratory system and bone marrow and lymphoid tissue, indicating its important role in the immune system. REGNASE-1 protein levels show moderate to strong cytoplasmic and/or nuclear staining in more than half of patients with various tumors, including testis cancer, melanoma, thyroid cancer, head and neck cancer, ovarian cancer, glioma, and colorectal cancer. However, REGNASE-1 is rarely expressed in skin cancer, breast cancer, liver cancer, and prostate cancer. Our latest data show that MC-38 cell allografts exhibit reduced tumor development in *Regnase-1*$^{Cre+\ f/f}$ mice, similar to LLC cell allografts (Supplementary figure 3). This suggests that REGNASE-1 regulates tumor progression across at least two types of cancer.

REGNASE-1 regulate M2a cytokines secretion

Currently, understanding of alternative macrophages is largely limited to marker gene expression in mouse models. However, marker genes alone do not fully capture the function of alternative macrophages. Cytokine expression and secretion are crucial for M2 macrophage function and for regulating the local microenvironment to support host immunity. Our cytokine array revealed at least fourteen cytokines secreted by M2a

doi:10.6342/NTU202403029

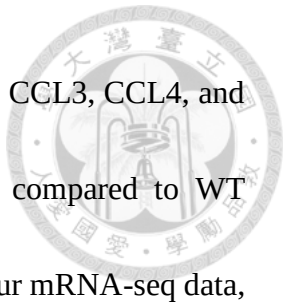

macrophages after IL-4 induction. Among these cytokines, CXCL11, CCL3, CCL4, and CCL12 were expressed at higher levels in *Regnase-1*$^{-/-}$ BMDMs compared to WT BMDMs. We checked the mRNA expression of these candidates in our mRNA-seq data, but no significant differences were observed between *Regnase-1*$^{-/-}$ and WT BMDMs. This result for mRNA expression of *Ccl12* was also confirmed by RT-qPCR (data not shown), suggesting that REGNASE-1's regulatory effect on these cytokines occurs post-translationally. CXCL11 is a chemoattractant that binds to the CXCR3 receptor on effector T cells. CCL3 and CCL4 bind to CCR1, CCR4, and CCR5, which are expressed on polymorphonuclear leukocytes. CCL12 attracts eosinophils, monocytes, and lymphocytes through binding to CCR2.

doi:10.6342/NTU202403029

Figures

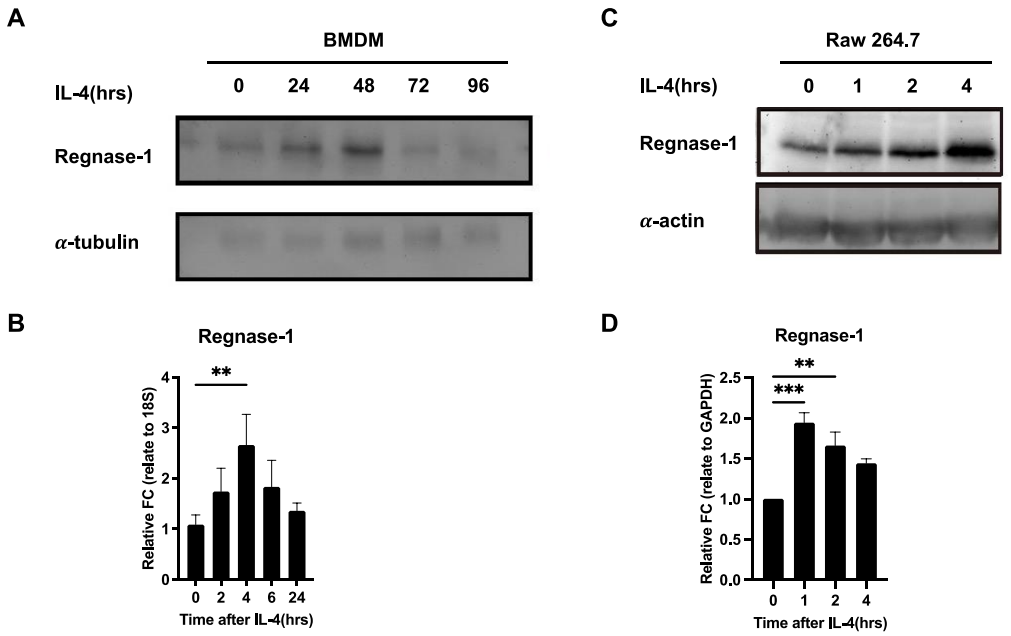

Figure 1. Dynamic regulation of Regnase-1 expression upon IL-4 stimulation.

Regnase-1 expression levels exhibit a steady increase upon IL-4 induction in both Bone Marrow-Derived Macrophages (BMDM) and RAW264.7 cells. Cells were challenged with 20 ng/ml IL-4 for the indicated durations. Protein and mRNA expression levels of *Regnase-1* are assessed via immunoblotting and RT-qPCR, respectively. (A) Western blot depicting REGNASE-1 protein levels in BMDM treated with IL-4 (20 ng/ml) for 0, 4, 24, 48, 72, and 96 hours. (B) Relative fold change (FC) in mRNA expression levels of *Regnase-1* in BMDM treated with IL-4 (20 ng/ml) for 0, 2, 4, 6, and 24 hours. (C) Western blot showing REGNASE-1 protein levels in RAW264.7 cells. (D) Relative fold change (FC) in mRNA expression levels of *Regnase-1* in RAW264.7 cells treated with IL-4 (20

doi:10.6342/NTU202403029

ng/ml) for 0, 1, 2, and 4 hours. These findings represent data from three independent experiments conducted in triplicate. Error bars represent standard error of the mean (SEM). Statistical significance is denoted as *p < 0.0332, **p < 0.0021, ***p < 0.0002.

doi:10.6342/NTU202403029

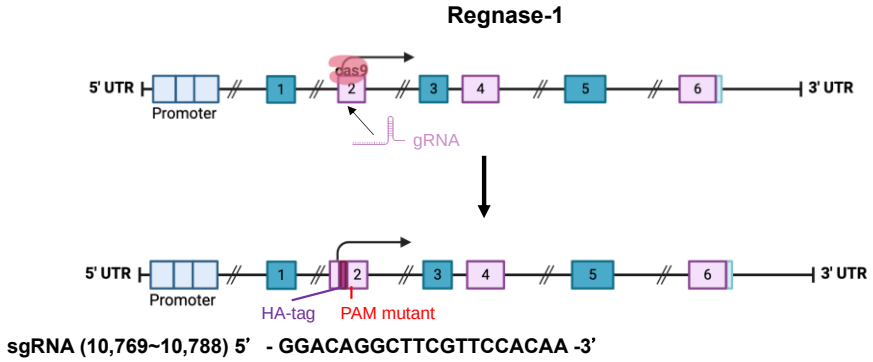

sgRNA (10,769~10,788) 5' - GGACAGGCTTCGTTCCACAA -3'

Template: nde1_Zc3h12a_HAtag DNA (197bp, 10,677~10,837)

5' - CCTATATTGGGCATTGCTTGCCCTTAACCCTGTGGTCTGGTCAATAGGAGCTGTGATG
GACACATTCCAAGAATGTGAAATatggcttacccatatgatgtgccagattatgcctccATGAGTGAt
CCTTGTGGAACGAAGCCTGTCCAAGAATCCAACCCCACCATGAGTCTGTGGAGTCTTGA GGACAGACACAG -3'
gRNA

HA-tag knock-in site (10,757)

HA-tag: atggcttacc**catatg**atgtgccagattatgcctcc

NdeI: CATATG

Figure 2. Schematic representation of *HA-Regnase-1* knock-in in RAW264.7 cells via CRISPR/Cas9.

A schematic diagram illustrates the design for achieving *HA-Regnase-1* knock-in in RAW264.7 cells using CRISPR/Cas9 technology. The diagram depicts the targeted *Regnase-1* allele downstream of the translation start site, indicating the gene structure with exons labeled and numbered within boxes. A purple line represents the guide RNA (gRNA) utilized to induce Cas9-mediated cleavage in the *Regnase-1* gene. The sequence of the gRNA and the repaired template are depicted, with regions of deviation from the original Regnase-1 gene sequence highlighted in red.

doi:10.6342/NTU202403029

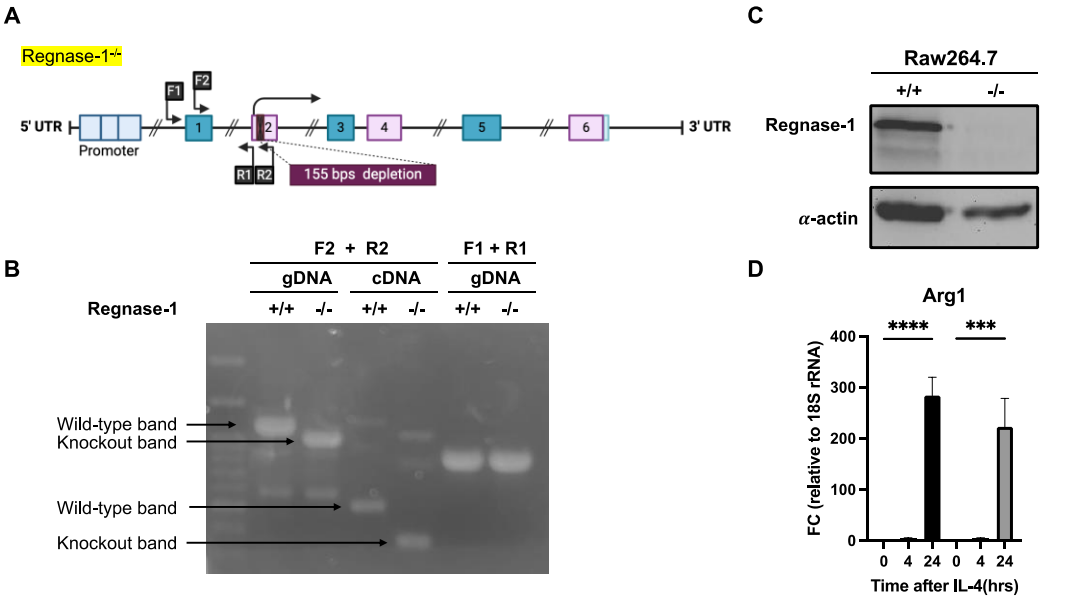

Figure 3. Impact of *Regnase-1* deficiency on macrophage alternative polarization marker genes in response to IL-4 in RAW264.7 Cells.

(A) Schematic representation of the mouse *Regnase-1* gene structure, displaying individual exons numbered. The 155bp deletion created via CRISPR is highlighted in dark purple and labeled as "155bp deletion". Primers (F1, F2, R1, and R2) used for *Regnase-1* deletion genotyping are indicated. (B) Genotyping of the *Regnase-1* allele by PCR using genomic DNA isolated from mouse toes. The 1195bp (WT) or 1040bp *(Regnase-1$^{-/-}$)* of PCR products corresponding to each genotype are labeled on the left. (C) Analysis of REGNASE-1 protein expression via immunoblotting. (D) Quantification of *Arginase (Arg1)* mRNA levels using RT-qPCR from total RNA harvested after treatment with 20 ng/ml IL-4 for the specified durations. These findings represent three

doi:10.6342/NTU202403029

independent experiments conducted in triplicate. Error bars represent SEM. Statistical significance is denoted as *p < 0.0332, **p < 0.0021, ***p < 0.0002."

doi:10.6342/NTU202403029

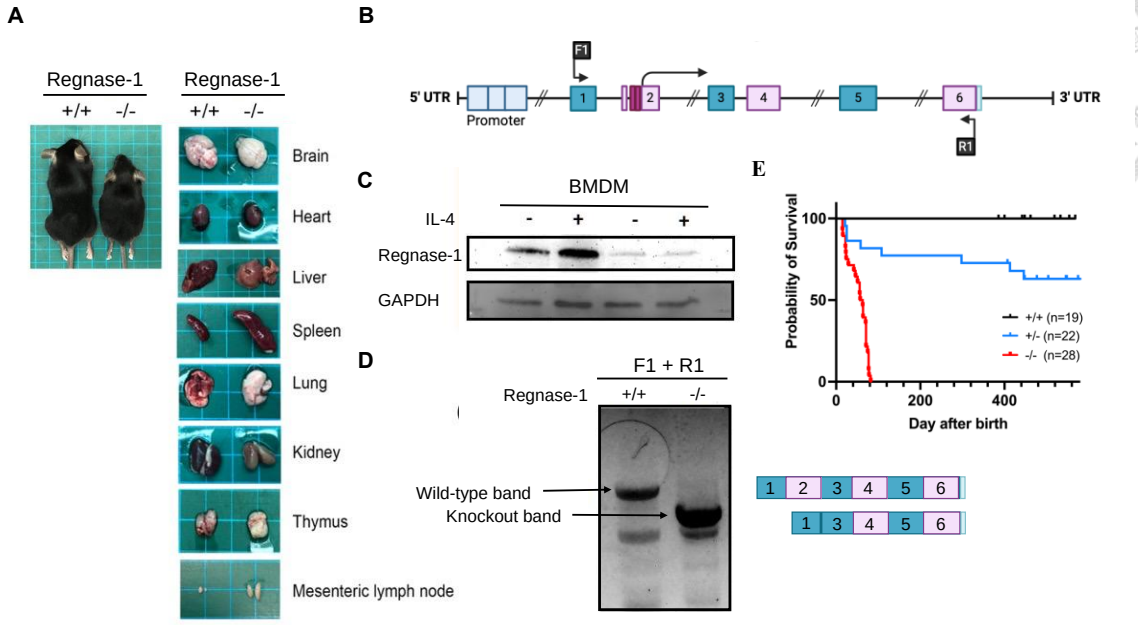

Figure 4. Generation of *Regnase-1* deletion mice.

(A) Gross appearance of 7-week-old mice (left) and their organs (right) from wild-type and *Regnase-1*$^{-/-}$ mice. (B) Schematic diagram illustrating the *Regnase-1* allele with a 196-nucleotide insertion before the translational start site, marked in dark purple. Arrows labeled with F1 and R1 indicate the positions of two primer sets used for cDNA analysis. (C) Confirmation of REGNASE-1 protein expression levels in IL-4 treated and untreated BMDM from wild-type and *Regnase-1*$^{-/-}$ mice via western blot. (D) PCR products generated from wild-type and *Regnase-1*$^{-/-}$ cDNA, with the PCR product corresponding to the sequence of Regnase-1 cDNA shown on the right. (E) Survival curves of wild-type (*Regnase-1*$^{+/+}$), *Regnase-1*$^{+/-}$, and *Regnase-1*$^{-/-}$ mice. Median survival times are indicated for wild-type (WT) mice (n=19), *Regnase-1*$^{+/-}$ mice (n=22), and *Regnase-1*$^{-/-}$ mice (n=28).

doi:10.6342/NTU202403029

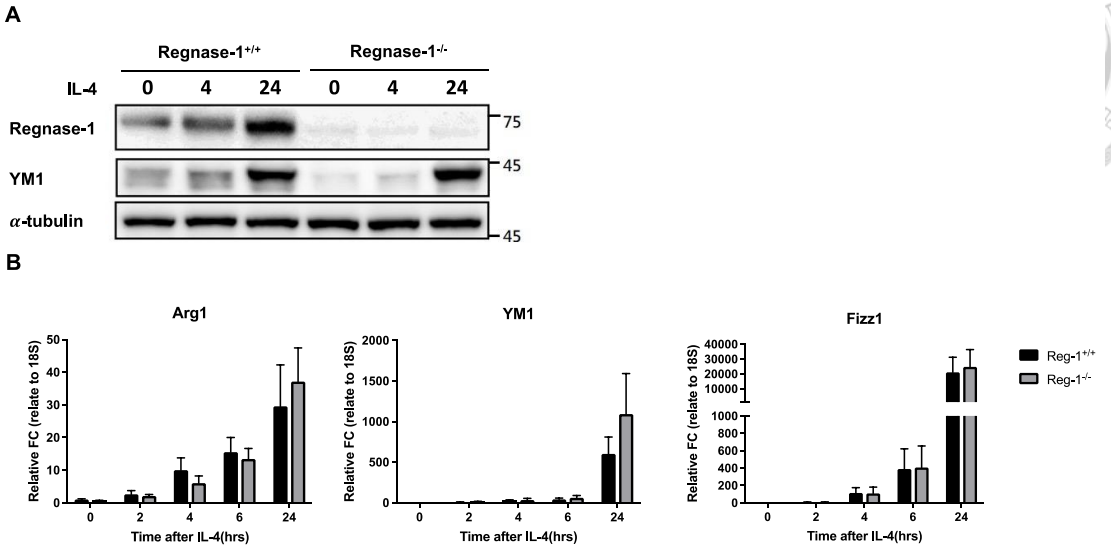

Figure 5. REGNASE-1 doesn't affect M2a macrophage marker genes in response to IL-4 in BMDMs.

(A) Immunoblot analysis of REGNASE-1 and YM-1 expression in IL-4-stimulated BMDMs derived from wild-type and *Regnase-1*$^{-/-}$ (*Reg-1*$^{-/-}$) mice. (B) Quantification of relative fold change (FC) in mRNA expression levels of three marker genes over time following treatment with 20 ng/ml IL-4. The mRNA levels were measured using quantitative PCR, normalized first to 18S RNA and then to the baseline expression level observed in wild-type cells at 0 hours post IL-4 treatment. All experiments were conducted in triplicate, and error bars represent the standard deviation. Error bars denote SEM. Statistical significance is indicated as *p < 0.0332, **p < 0.0021, ***p < 0.0002."

doi:10.6342/NTU202403029

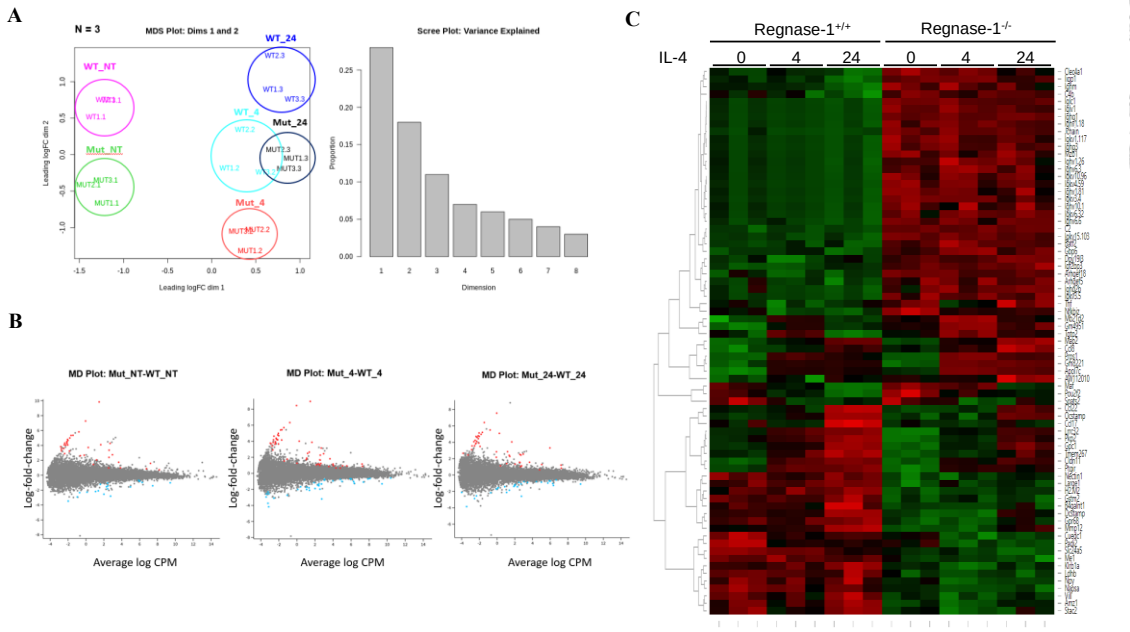

Figure 6. The mRNA-seq analysis of IL-4 treated BMDM from WT and *Regnase-1* deletion mice.

(A) Principal Component Analysis (PCA) plot illustrating the mRNA-seq data from all samples, comprising triplicates of BMDM sourced from either *Regnase-1*$^{-/-}$ (Mut) or WT mice, and treated with IL-4 for 0 hours (NT), 4 hours, and 24 hours. (B) Manhattan Plot (MD) displaying the comparison between *Regnase-1*$^{-/-}$(Mut) Heatmap illustrating the differential expression of genes in BMDM treated with IL-4 for 24 hours, comparing *Regnase-1*$^{-/-}$(Mut) with WT samples. Each row represents a gene, with the gene name indicated on the right. Each column represents a sample. The color intensity denotes the expression level, with red indicating higher expression, green indicating lower expression, and black representing mean expression. In the plot, significant up-regulated genes are highlighted in red, while significant down-regulated genes are depicted in blue. CPM

doi:10.6342/NTU202403029

stands for counts per million total reads (C) Heatmap illustrating the differential expression of genes in BMDM treated with IL-4 for 24 hours, comparing *Regnase-1*$^{-/-}$ with WT samples. Each row represents a gene, with the gene name indicated on the right. Each column represents a sample. The color intensity denotes the expression level, with red indicating higher expression, green indicating lower expression, and black representing mean expression.

doi:10.6342/NTU202403029

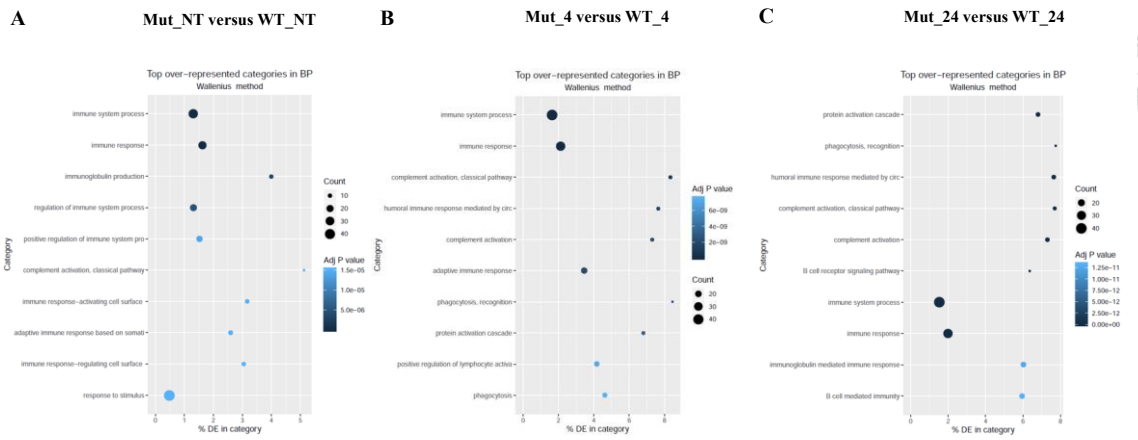

Figure 7. GO term enrichment analysis for biological process for up- and down-regulated genes between *Regnase-1*$^{-/-}$ and WT BMDM.

The top 10 ranked GO terms were performed for differentially expressed genes (DEGs) based on the comparisons of *Regnase-1*$^{-/-}$ versus WT BMDM in three conditions: (A) non-treated group, (B) IL-4 for 4 hours group, and (C) IL-4 for 24 hours group. Bubble plots were generated to display the 25 most significant GO terms identified in each analysis based on FDR significance, with all terms shown being significant at an FDR < 0.05.

doi:10.6342/NTU202403029

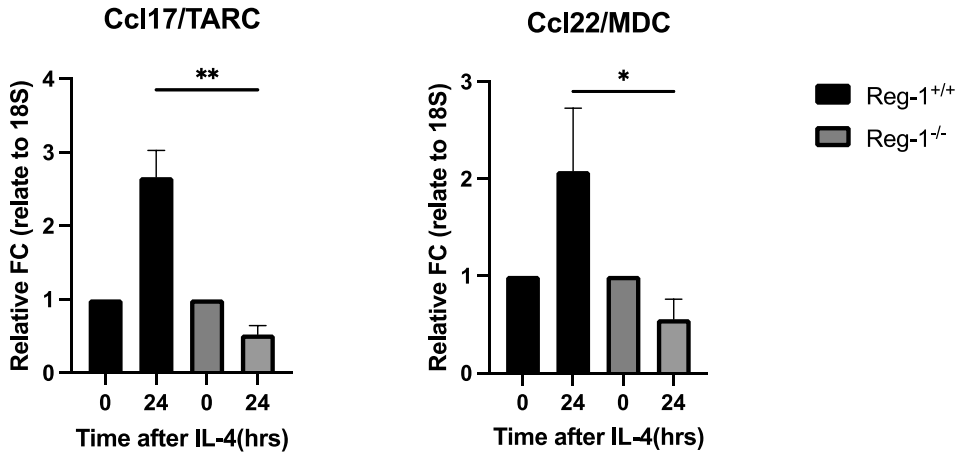

Figure 8. REGNASE-1 affects the RNA expression level of *Ccl17* and *Ccl22* in response to IL-4 in BMDM.

Comparison of *Ccl17* and *Ccl22* mRNA expression in BMDM derived from *Regnase-1* deleted (*Reg-1*$^{-/-}$) and wild-type (*Reg-1*$^{+/+}$) mice following 0 and 24 hours of IL-4 treatment. All quantitative PCR results were first normalized to 18S ribosomal RNA and further normalized to the untreated group. Error bars, SEM. *p <0.0332, ** p <0.0021, *** p <0.0002.

doi:10.6342/NTU202403029

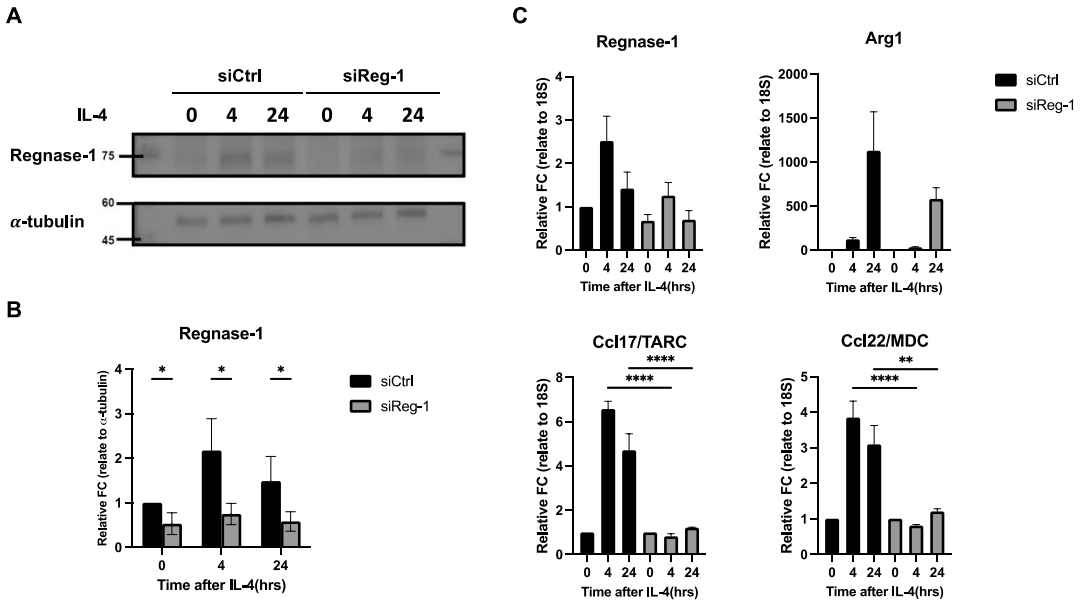

Figure 9. Knockdown of REGNASE-1 modulates *Ccl17* and *Ccl22* mRNA expression in IL-4 stimulated BMDMs.

Protein and RNA expression levels were assessed in siRNA-mediated knockdown of *Regnase-1* (*siReg-1*) or control (*siCtrl*) BMDMs following IL-4 induction. BMDMs isolated from C57BL/6 WT mice were treated with IL-4 after transfection with siCtrl or *siReg-1*, as indicated. (A) Western blot analysis depicts the protein levels of REGNASE-1 in BMDMs treated with IL-4 at specified timepoints, comparing cells with *Regnase-1* knockdown (*siReg-1*) to control (siCtrl) BMDMs. (B) Quantification of REGNASE-1 protein levels from (A) using ImageJ. (C) RT-qPCR analysis of *Regnase-1*, *Arg1*, *Ccl17*, and *Ccl22* mRNA expression in BMDMs transfected with siCtrl or siReg-1. Statistical analyses were conducted using one-way ANOVA with Tukey's multiple comparison test.

doi:10.6342/NTU202403029

Error bars represent standard error of the mean (SEM). Significance levels are denoted as

*p < 0.0332, **p < 0.0021, ***p < 0.0002.

doi:10.6342/NTU202403029

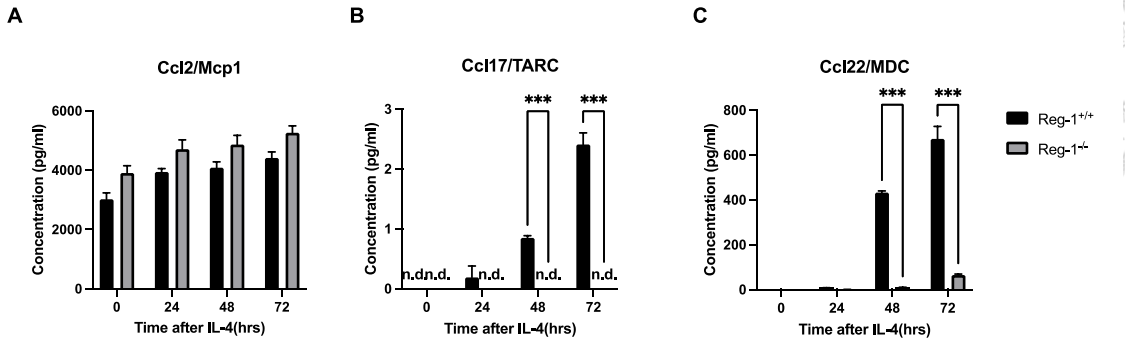

Figure 10. REGNASE-1 affects the protein expression level of CCL17 and CCL22 in response to IL-4 in BMDMs.

(A-C) LEGENDplex™ multi-analyte flow array kits are utilized to assess the protein levels of CCL2(A), CCL17(B), and CCL22(C) in the cultured medium from IL-4 treated wild-type (*Reg-1*$^{+/+}$) and *Regnase-1* deleted (*Reg-1*$^{-/-}$) BMDM at 0, 24, 48, and 72 hours. Statistical analyses were performed by using two-way ANOVA with Sidaks multiple comparison test. Data are expressed as mean ± SEM (n = 3, *p <0.0332, ** p <0.0021, *** p <0.0002, represent comparisons made between groups).

doi:10.6342/NTU202403029

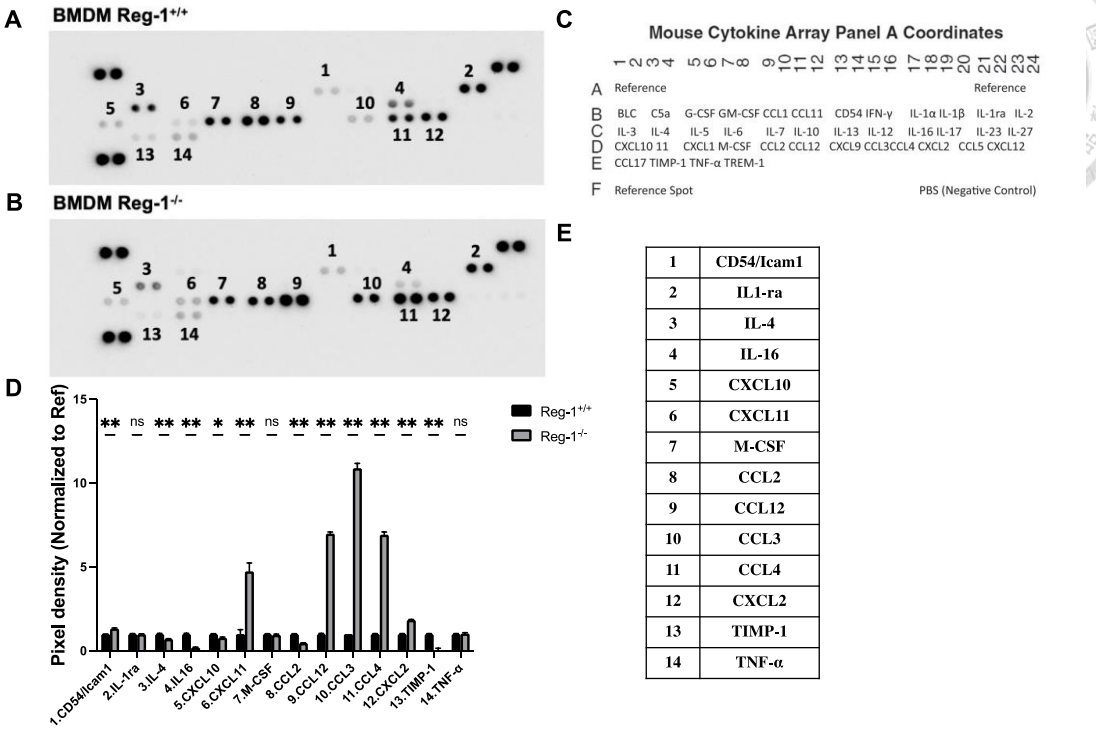

1	CD54/Icam1
2	IL1-ra
3	IL-4
4	IL-16
5	CXCL10
6	CXCL11
7	M-CSF
8	CCL2
9	CCL12
10	CCL3
11	CCL4
12	CXCL2
13	TIMP-1
14	TNF-α

Figure 11. REGNASE-1 affects the pro-inflammatory cytokines secretion in response to IL-4 in BMDM.

(A, B) Cytokine array blots probed with total protein lysate derived from IL-4-treated Wild-Type (*Reg-1*$^{+/+}$) (A) and *Regnase-1* knockout (*Reg-1*$^{-/-}$) (B) BMDM. (C) The corresponding antigen antibody was labeled. (D) Mean integrated pixel density of each protein spot from the blot is normalized to Reference spot and to *Regnase-1*$^{+/+}$ BMDM, the signals are quantified using ImageJ. (E) Fourteen most expressed cytokines were labeled as list.

doi:10.6342/NTU202403029

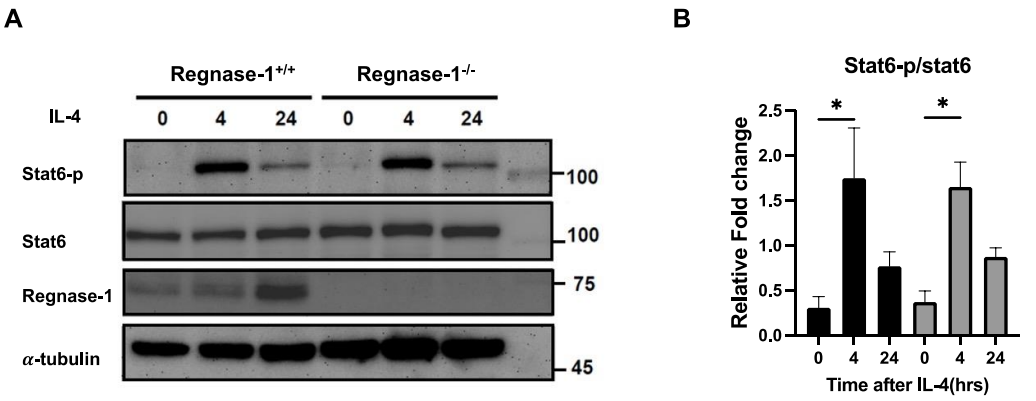

Figure 12. Regnase-1 doesn't affect STAT6 activation.

(A) Western blot depicting phosphorylated STAT6, total STAT6, and REGNASE-1 in Wild-Type and *Regnase-1*$^{-/-}$ BMDM treated with IL-4 (20ng/ml) for 0, 4, or 24 hours. (B) Quantification of the ratio of phosphorylated STAT6 (Stat6-p) to total STAT6 using ImageJ.

doi:10.6342/NTU202403029

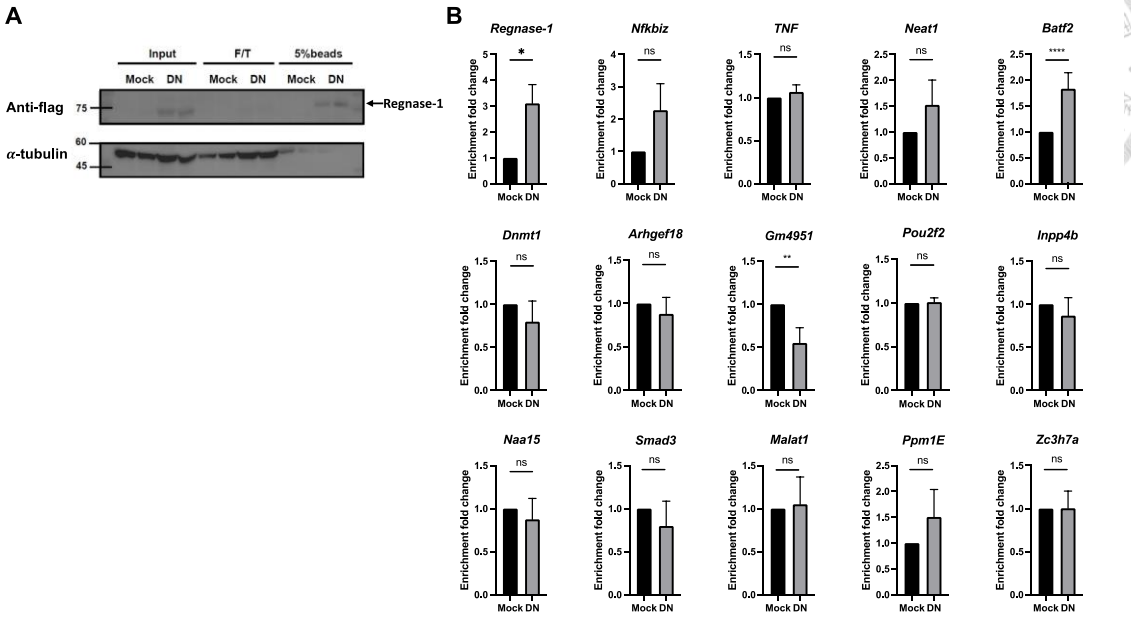

Figure 13. Identification of REGNASE-1 targeted mRNAs using RNA-IP followed by RT-qPCR.

(A) Western blot analysis of FLAG immunoprecipitation from RAW264.7 cells stably expressing PCDNA3_Three x FLAG REGNASE-1 mutant (D141N) or Mock control. (B) The mRNA molecules co-precipitated with Three x FLAG REGNASE-1 mutant (D141N) were subjected to analysis by RT-qPCR. Statistical analyses were performed by using two-way ANOVA with Sidaks multiple comparison test. Data are expressed as mean ± SEM (n = 3, *p <0.0332, ** p <0.0021, *** p <0.0002, represent comparisons made between groups)

doi:10.6342/NTU202403029

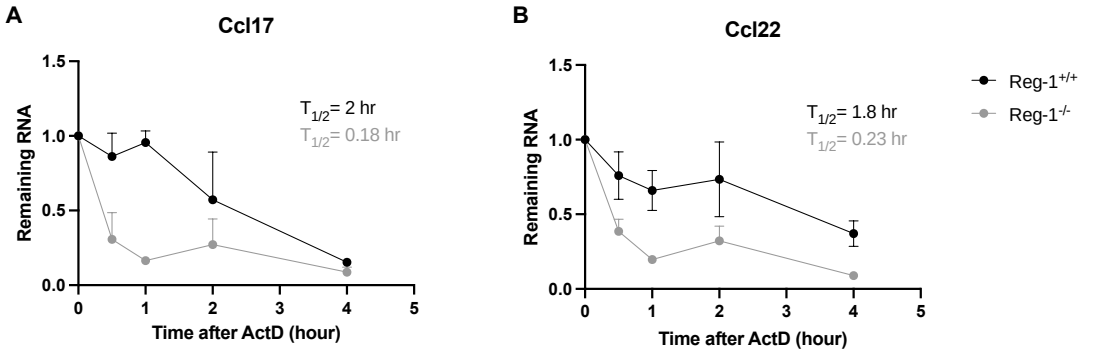

Figure 14. REGNASE-1 regulates mRNA stability of *Ccl17* and *Ccl22* in IL-4-Induced BMDM.

Quantification of (A) *Ccl17* mRNA and (B) *Ccl22* mRNA using quantitative PCR after 24 hours of IL-4 treatment in wild-type and *Reg-1*$^{-/-}$ BMDM, followed by actinomycin D treatment for the indicated time points. The half-life was determined using Prism. Three independent repeats were performed, with error bars representing the standard deviation.

doi:10.6342/NTU202403029

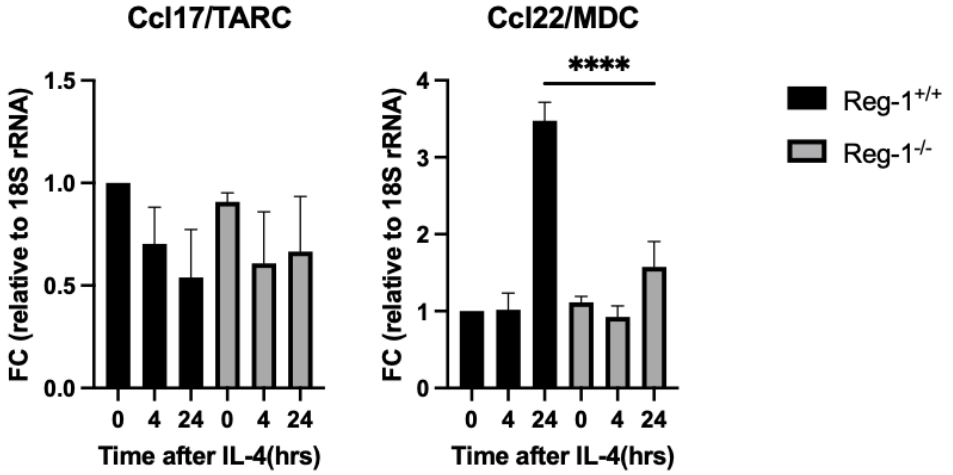

Figure 15. REGNASE-1 affects the RNA expression of Ccl17 and Ccl22 in response to IL-4 in RWA264.7 cell.

Total RNA was harvested after IL-4 treatment for indicated time points, and mRNA expression of the indicated genes were analyzed by RT-qPCR. These results are representative of three independent experiments performed in triplicate. Statistical analyses were performed by using two-way ANOVA with Sidaks multiple comparison test. Data are expressed as mean ± SEM (n = 3, *p <0.0332, ** p <0.0021, *** p <0.0002, represent comparisons made between groups)

doi:10.6342/NTU202403029

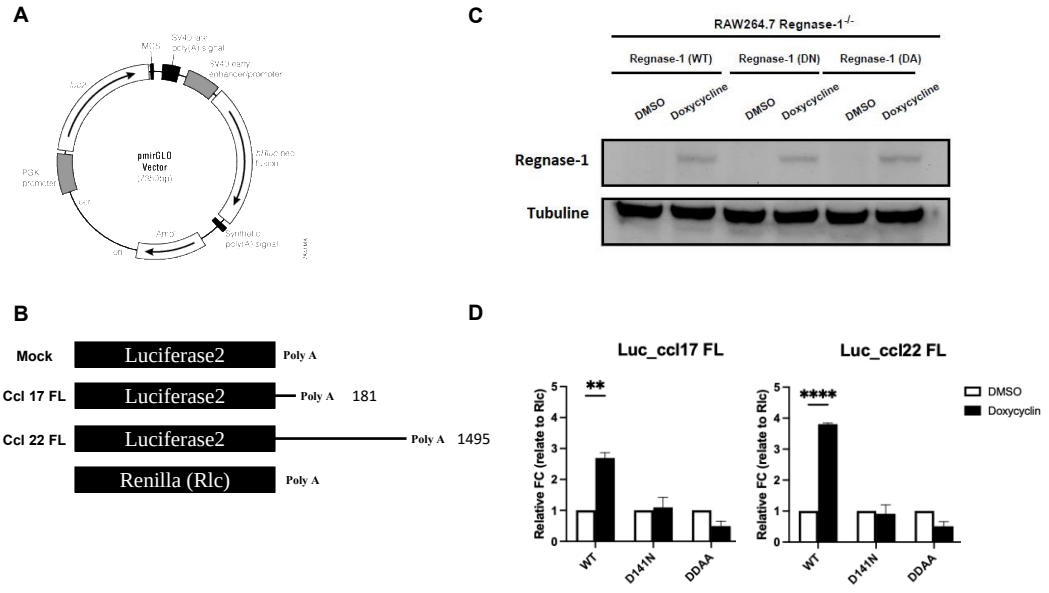

Figure 16. REGNASE-1 regulates *Ccl17* and *Ccl22* mRNA stability through its ribonuclease activity via their 3'-UTR in response to IL-4 in RAW 264.7 cells.

(A) The map of pmirGLO vector that was used for this study, the figure is adopted from pmirGLO Dual-Luciferase miRNA Target Expression Vector Protocol. (B) schematic diagram illustrates the dual-luciferase reporter constructs containing full-length (FL) mouse *Ccl17* and *Ccl22* 3'-UTRs after Luciferase2 and the internal control luciferase Renilla. (C) Western Blot analysis of *Regnase-1*$^{-/-}$ RAW264.7 cell stable expressed doxycycline-inducible three x flag wild-type Regnase-1 with wild-type sequence (WT) or D141N mutation (DN) or D225AD226A mutation (DDAA) constructs in the presence of DMSO or doxycycline (5μg/ml). (D) The mRNA expression levels of Firefly luciferase relative to Renilla upon IL-4 treatment, normalized to DMSO, were analyzed in doxycycline-inducible Regnase-1 stable lines in *Regnase-1*$^{-/-}$ RAW264.7 cells. Statistical

doi:10.6342/NTU202403029

analyses were performed by using two-way ANOVA with Sidaks multiple comparison test. Data are expressed as mean ± SEM (n = 3, *p <0.0332, ** p <0.0021, *** p <0.0002, represent comparisons made between groups).

doi:10.6342/NTU202403029

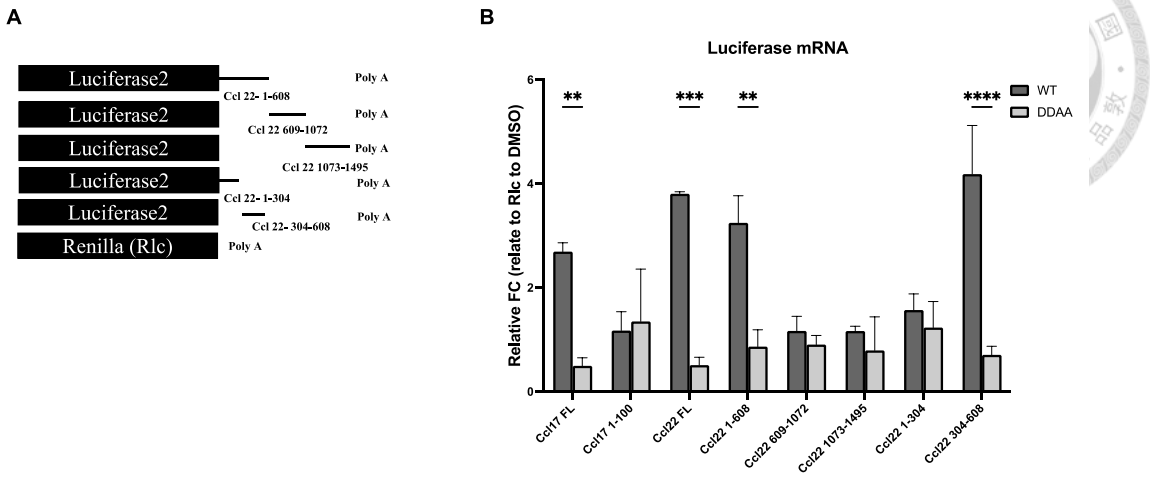

Figure 17. Identification of REGNASE-1-mediated regulatory regions in *Ccl17* and *Ccl22* via 3'UTR regions.

(A) Schematic diagram illustrating dual-luciferase reporter constructs containing various truncated forms of mouse *Ccl17* and *Ccl22* 3'-UTRs. The range of numbers indicates the starting and ending nucleotides of the truncated 3'UTRs, counted after the stop codon of either *Ccl17* or *Ccl22*. (B) mRNA expression levels of Firefly luciferase relative to Renilla following IL-4 treatment, normalized to DMSO, were analyzed in doxycycline-inducible wild-type REGNASE-1(WT) and REGNASE-1(D225AD226A) mutant (DDAA) stable lines in *Regnase-1*$^{-/-}$ RAW264.7 cells. Statistical analyses were performed by using two-way ANOVA with Sidaks multiple comparison test. Data are expressed as mean ± SEM (n = 3, *p <0.0332, ** p <0.0021, *** p <0.0002, represent comparisons made between groups).

doi:10.6342/NTU202403029

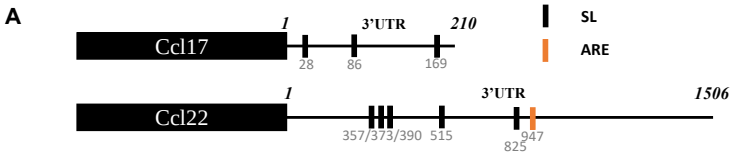

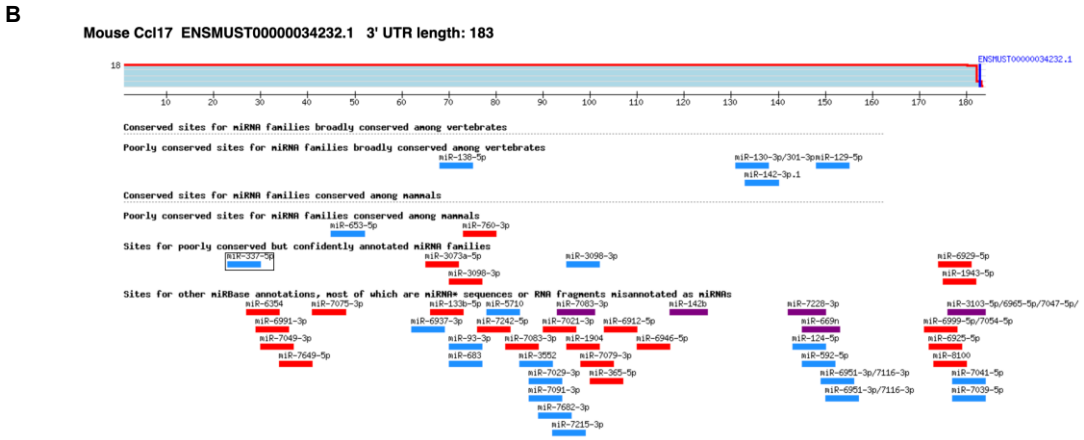

C

Gene Symbol	Target Rank	Target Score	miRNA Name	Seed Location
Ccl17	1	93	mmu-miR-142b	117-124
	2	71	mmu-miR-7083-3p	82-99
	3	62	mmu-miR-6929-5p	174-180
	4	60	mmu-miR-7228-3p	142-149
	5	51	mmu-miR-6946-5p	110-116

Gene Symbol	Target Rank	Target Score	miRNA Name	Seed Location
Ccl22	1	96	mmu-miR-6930-3p	568-575, 975-982, 1124-1131
	2	90	mmu-miR-7679-5p	215-221, 1345-1452
	3	89	mmu-miR-12189-3p	212-218, 568-575, 976-982, 1125-1131
	4	88	mmu-miR-6384	953-960
	5	87	mmu-miR-6414	1086-1101
	6	87	mmu-miR-6970-5p	1086-1101
	7	86	mmu-miR-148b-5p	1093-1100
	8	86	mmu-miR-7058-5p	147-164, 805-811
	9	86	mmu-miR-7034-3p	568-575, 975-982, 1124-1131
	14	79	mmu-miR-7667-3p	458-466*
	15	79	mmu-miR-369-3p	925-932
	16	79	mmu-miR-6954-5p	843-849
	17	78	mmu-miR-7062-5p	504-511*
	21	76	mmu-miR-5120	482-489*
	24	74	mmu-miR-764-3p	504-511*

Figure 18. Predicted structure and potential microRNA binding sites in *Ccl17* and *Ccl22* 3' UTRs.

(A) Schematic diagram illustrating the predicted stem-loop (SL) structure and adenosine-uridine-rich element (ARE) in mouse *Ccl17* and *Ccl22* mRNA 3' UTRs. (B) Prediction of microRNA (miRNA) targets on Mouse *Ccl17* 3' UTR using TargetScan. (C) Prediction of miRNA targets on Mouse *Ccl17* and *Ccl22* 3' UTRs using miRDB. An asterisk (*)

doi:10.6342/NTU202403029

denotes the indicated miRNA that closely targets the *Ccl22* 3’ UTR region spanning nucleotides 304-608.

doi:10.6342/NTU202403029

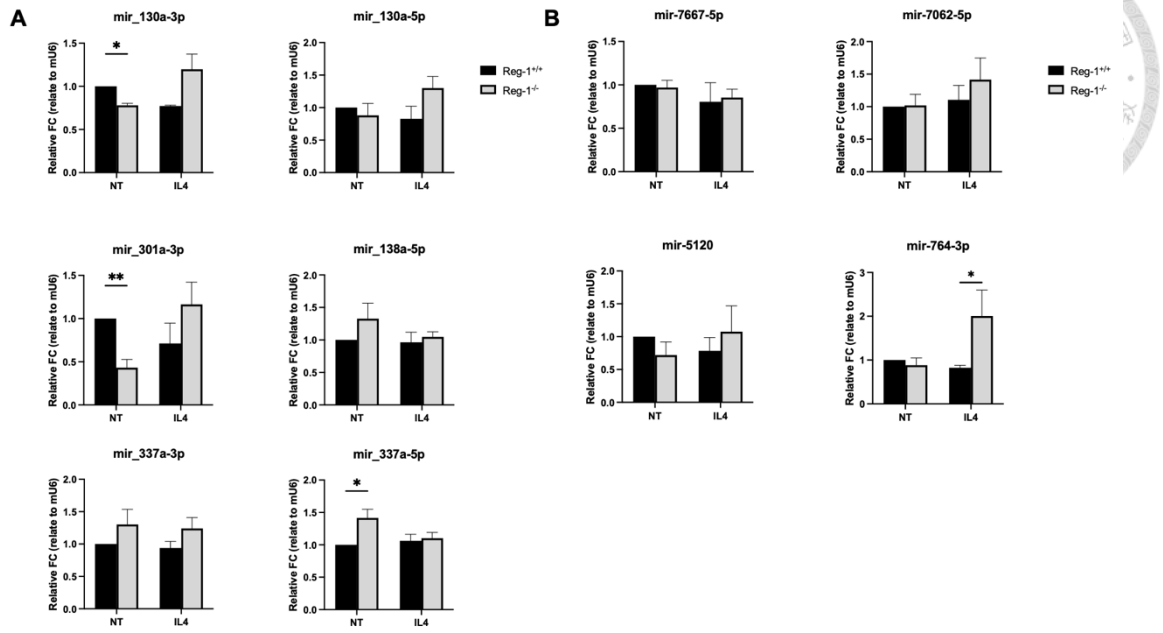

Figure 19. Exploration of candidate microRNAs targeting the 3'UTRs of Ccl17 and Ccl22 regulated by REGNASE-1.

The levels of microRNAs in Wild-Type and *Regnase-1*$^{-/-}$ RAW264.7 cell, treated with 0 (NT) or 24 hours (IL4) IL-4, were quantified using TaqMan assay. Micro RNA expression of prediction candidates of *Ccl17*(A) and *Ccl22*(B) were analyzed by TaqMan assay. These results are representative of three independent experiments performed in triplicate. Error bars, SEM. *p <0.0332, ** p <0.0021, *** p <0.0002.

doi:10.6342/NTU202403029

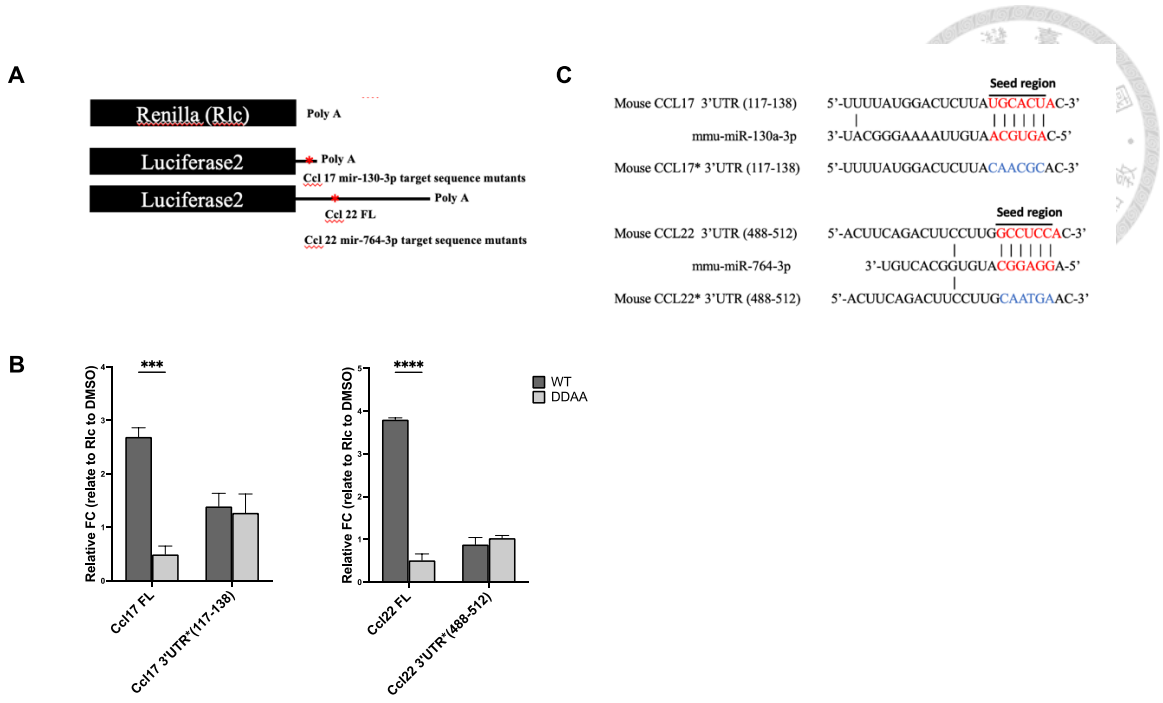

Figure 20. Regulation of *Ccl17* and *Ccl22* mRNA stability by REGNASE-1 via their 3'-UTRs through miR-130a-3p and miR-764, respectively.

(A) Schematic diagram illustrating dual-luciferase reporter constructs containing full-length (FL) mouse *Ccl17* and *Ccl22* 3'-UTRs with predicted miR-130a-3p or miR-764-3p target sites indicated. (B) Potential targeted positions of the *Ccl17* 3'-UTR by miR-130a-3p and *Ccl22* 3'-UTR by miR-764-3p are highlighted in red. Mutations introduced to the 3' UTRs of *Ccl17* and *Ccl22* are denoted as *Ccl17** and *Ccl22**, respectively, and labeled in blue. (C) mRNA expression levels of Firefly luciferase relative to Renilla following IL-4 treatment, normalized to DMSO, were analyzed in doxycycline-inducible wild-type REGNASE-1 (WT) and REGNASE-1 (D225AD226A) mutant (DDAA) stable lines in *Regnase-1*$^{-/-}$ RAW264.7 cells. Both full-length *Ccl17* and *Ccl22* 3'UTRs, along with mutations at potential microRNA targeted regions (*Ccl17** or *Ccl22**), transfected

doi:10.6342/NTU202403029

cells were quantified using RT-qPCR relative to Rlc mRNA levels and normalized to DMSO-treated control. Statistical analyses were performed by using two-way ANOVA with Sidaks multiple comparison test. Data are expressed as mean ± SEM (n = 3, *p <0.0332, ** p <0.0021, *** p <0.0002, represent comparisons made between groups)

doi:10.6342/NTU202403029

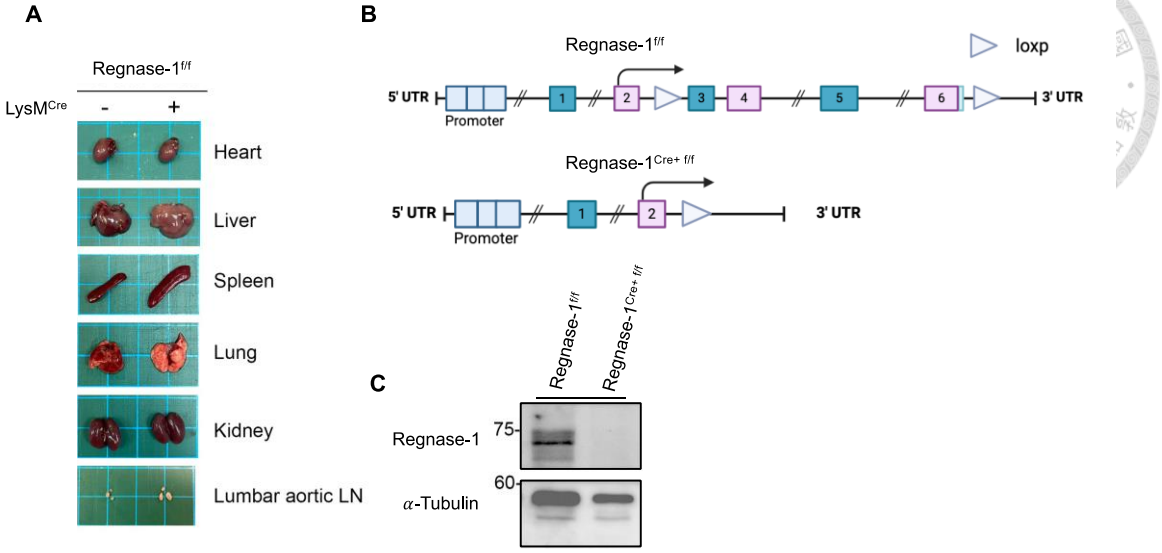

Figure 21. Phenotypic analysis of 6-week-old myeloid-specific *Regnase-1* deleted mice.

(A) Morphological comparison of organs between Wild-type and Myeloid-Specific Deletion of *Regnase-1* mice. (B) Schematic representation of the mouse *Regnase-1*$^{f/f}$ (top) and *Regnase-1*$^{Cre+\ f/f}$ gene structures, displaying individual exons numbered. The loxP regions are indicated with triangles. (C) Confirmation of REGNASE-1 protein expression in BMDM using immunoblotting.

doi:10.6342/NTU202403029

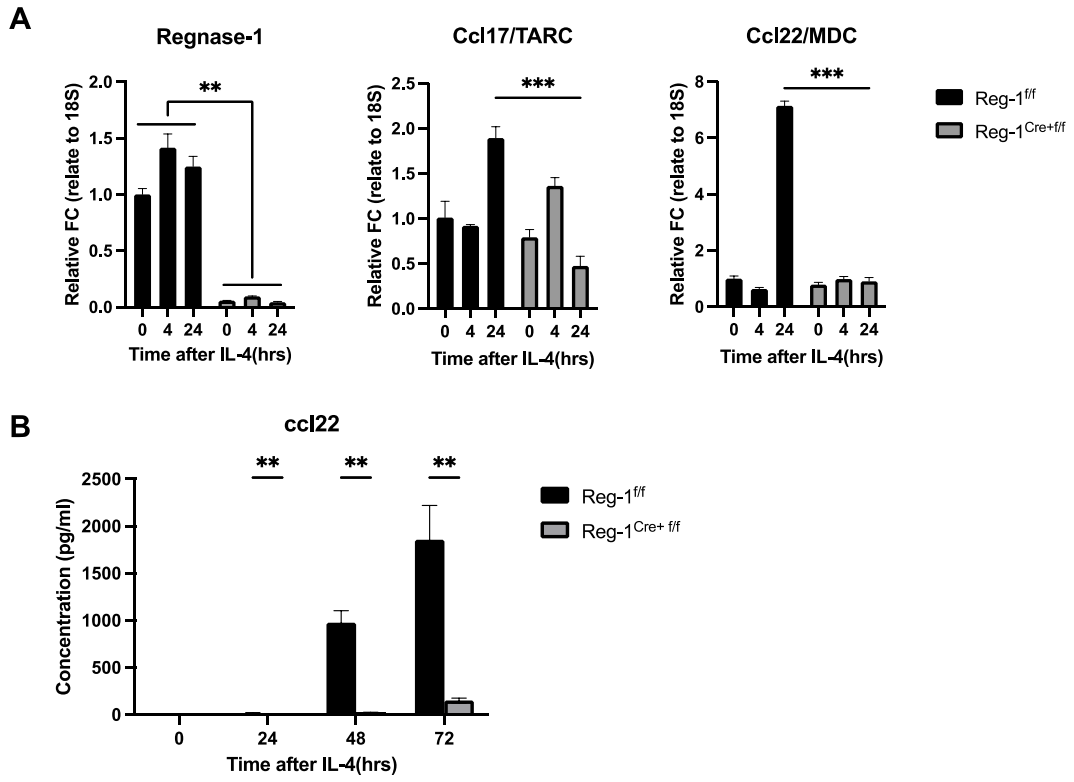

Figure 22. Decreased expression of *Ccl17* and *Ccl22* in *Regnase-1*$^{Cre+\ f/f}$ BMDMs compared to *Regnase-1*$^{f/f}$ BMDMs under IL-4 stimulation.

(A) Total mRNA levels of *Regnase-1*, *Ccl17*, and *Ccl22* harvested from IL-4-treated BMDMs at indicated time points were quantified by RT-qPCR. All datasets were initially normalized to 18S RNA and further normalized to wild-type (*Regnase-1*$^{f/f}$) BMDMs with 0-hour IL-4 treatment. (B) Comparison of the changes in CCL22 protein secretion from IL-4-treated BMDMs derived from wild-type (*Regnase-1*$^{f/f}$) and myeloid-specific *Regnase-1* knockout (*Regnase-1*$^{Cre+\ f/f}$) mice. Statistical analyses were conducted using two-way ANOVA with Sidak's multiple comparison test. Data are expressed as mean ±

doi:10.6342/NTU202403029

SEM (n = 3, *p < 0.033, **p < 0.002, and ***p < 0.001, representing comparisons made between groups).

doi:10.6342/NTU202403029

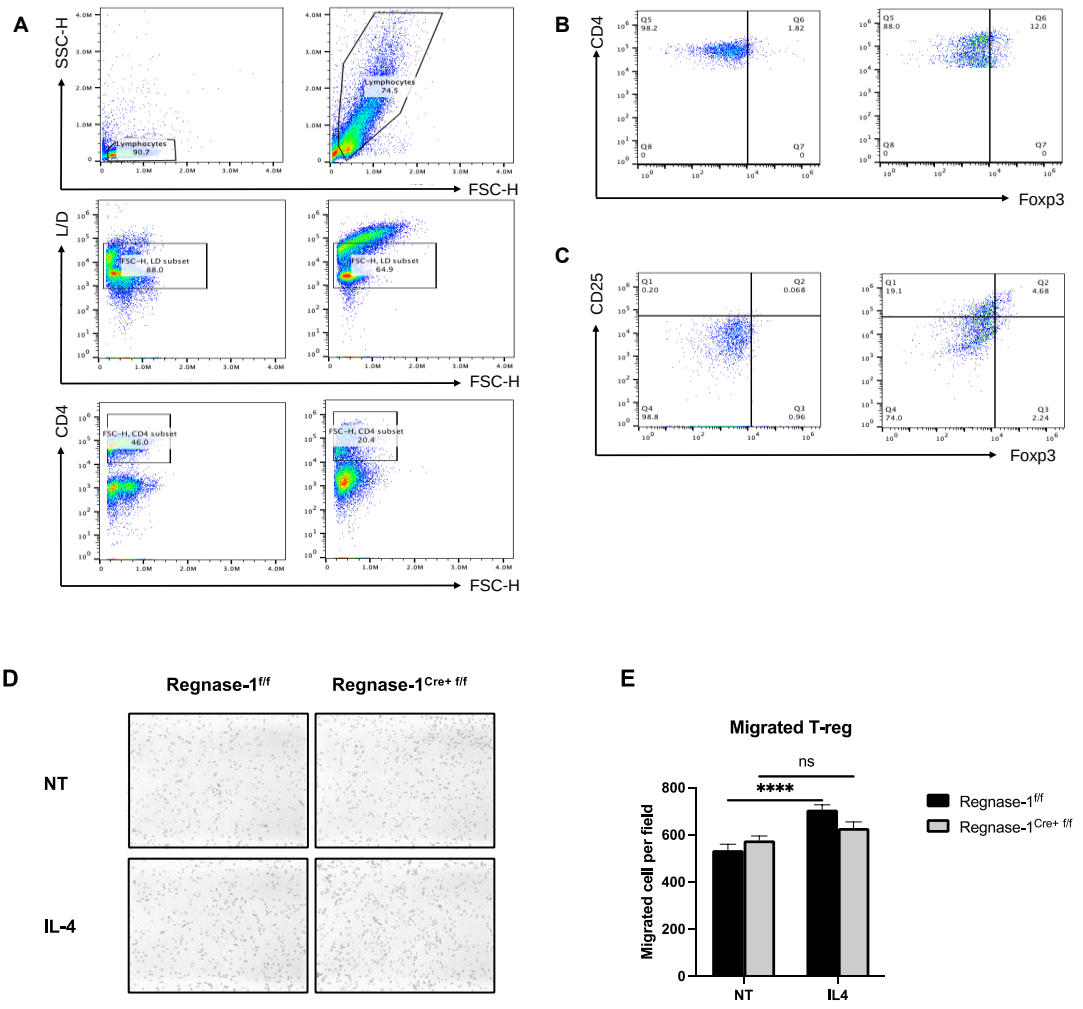

Figure 23. REGNASE-1 affects in vitro differentiated Treg upon IL-4 treated condition.

(A-C) Gating strategy to identify the percentage of in vitro differentiated regulatory T cells from Pan T cells. (A) Initially, cells presenting lower SSC-FSC profiles were discriminated. Only viable cells with lower zombie ZIR L/D staining were selected. $CD4^+$ positive helper T cells were then distinguished, and regulatory T cells were identified as $CD4^+Foxp3^+$ (B) or $CD4^+CD25^+Foxp3^+$ (C). (D) A representative image displaying migrated cells in unstimulated (NT) or IL-4 (IL4)-stimulated BMDM derived from Wild-

doi:10.6342/NTU202403029

Type (*Regnase-1*$^{f/f}$) or *Regnase-1* knockout (*Regnase-1*$^{Cre+f/f}$) mice. (E) Quantification of the number of migrated cells per field (Average of 12 picture fields at 100x total magnification). Statistical analyses were conducted using two-way ANOVA with Sidak's multiple comparison test. Data are expressed as mean ± SEM (n = 3, *p < 0.033, **p < 0.002, and ***p < 0.001, representing comparisons made between groups).

doi:10.6342/NTU202403029

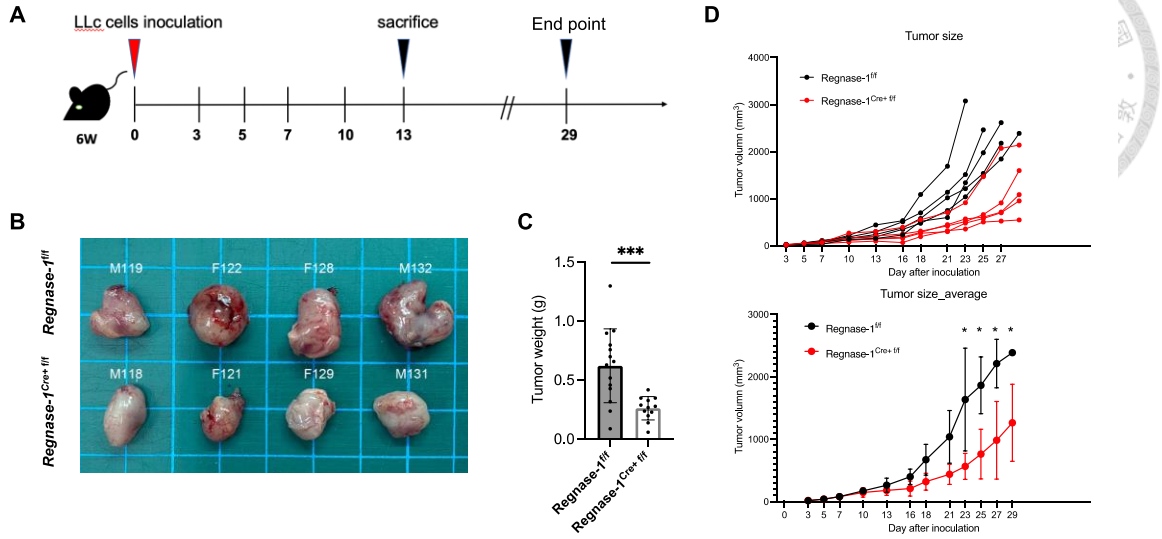

Figure 24. Myeloid-specific *Regnase-1* knockout mice reduce LLC tumor development.

(A) Schematic representation of the experimental design for monitoring tumor size. Briefly, 2.5 x 10^6 LLC tumor cells were inoculated into the inguinal region of 6-week-old wild-type (*Regnase-1*$^{f/f}$) and myeloid-specific *Regnase-1* knockout (*Regnase-1*$^{Cre+\ f/f}$) mice. Some mice were sacrificed on the 13th day to verify the size of tumor and for the rest, Tumor volume was evaluated every 2 or 3 days till the size of tumor reaches the maximum size (roughly around the 29th day) defined by the animal care center.

(B) Surgically removed tumor tissues from *Regnase-1*$^{f/f}$ and *Regnase-1*$^{Cre+\ f/f}$ mice at 13 days post-inoculation. (C) Average tumor weights from (B). (D) Tumor volume was assessed at different time-points after inoculation, and the endpoint was determined upon reaching a volume of 2000 mm^3. Statistical analyses were conducted using two-way ANOVA with Sidak's multiple comparison test. Data are expressed as mean ± SEM (n =

doi:10.6342/NTU202403029

3, *p < 0.033, **p < 0.002, and ***p < 0.001, representing comparisons made between groups).

doi:10.6342/NTU202403029

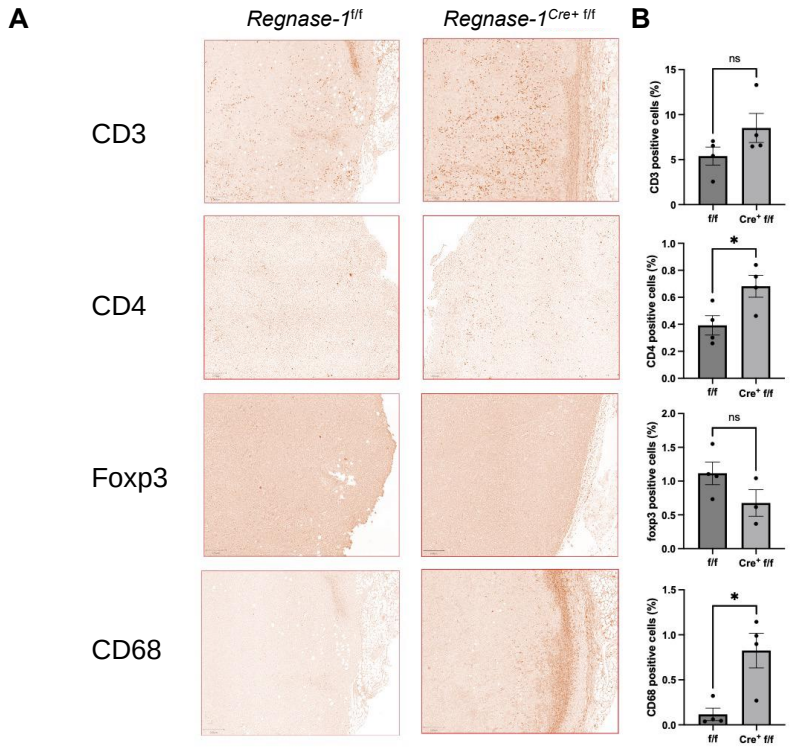

Figure 25. Myeloid-specific *Regnase-1* deleted mice exhibited enhanced immune cell infiltration in LLC tumors.

(A) IHC staining of CD3, CD4, CD68 and Foxp3 in LLC tumor sections dissected from wild-type and myeloid-specific *Regnase-1* deleted mice. (B) Quantification of positive cells for each indicated antibody in LLC tumor sections was performed using QuPath. Statistical analyses were conducted using Student's t-test. Data are expressed as mean ± SEM (n = 3, *p < 0.033, **p < 0.002, and ***p < 0.001, representing comparisons made between groups).

doi:10.6342/NTU202403029

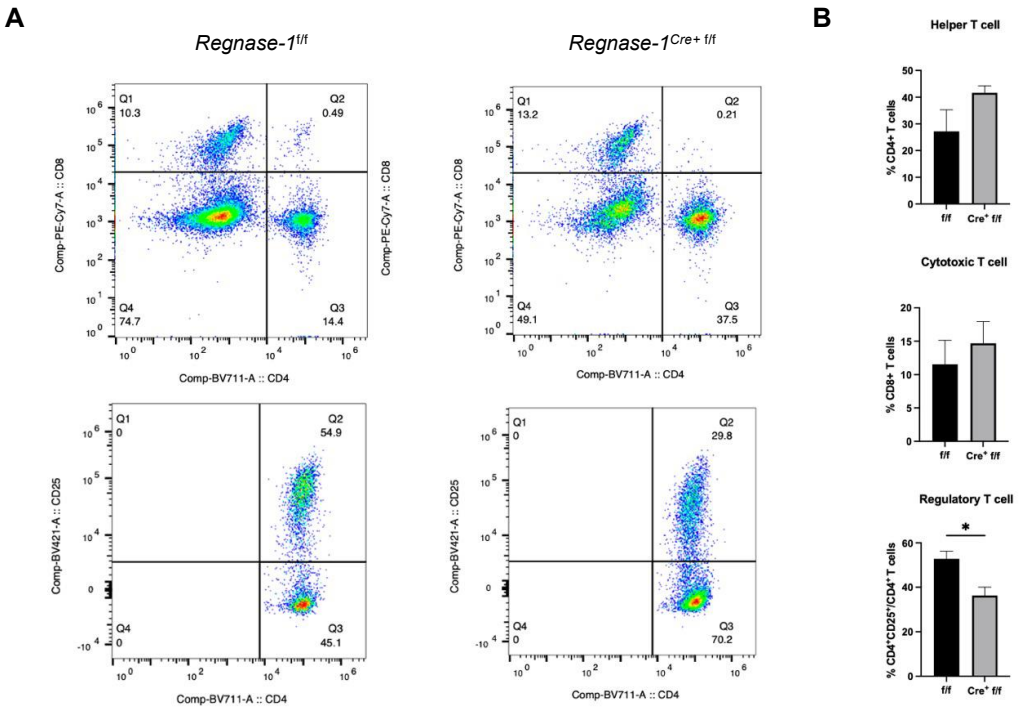

Figure 26. Myeloid-specific *Regnase-1* deleted mice exhibited reduced $CD4^+CD25^+$ T cell in LLC tumor.

(A) Cells dissociated from the tumor were stained with CD4 and CD8 antibodies to determine the relative populations of helper T cells ($CD4^+$) and cytotoxic T cells ($CD8^+$) within the tumor. Additionally, staining for $CD4^+$ and $CD25^+$ T cells was conducted to identify potential regulatory T cells within the tumor. (B) Frequencies quantification of three replicates is shown. Statistical analyses were performed using the Student's t-test. Data are expressed as mean ± SEM (n = 4, *p < 0.033, **p < 0.002, and ***p < 0.001, representing comparisons made between groups).

doi:10.6342/NTU202403029

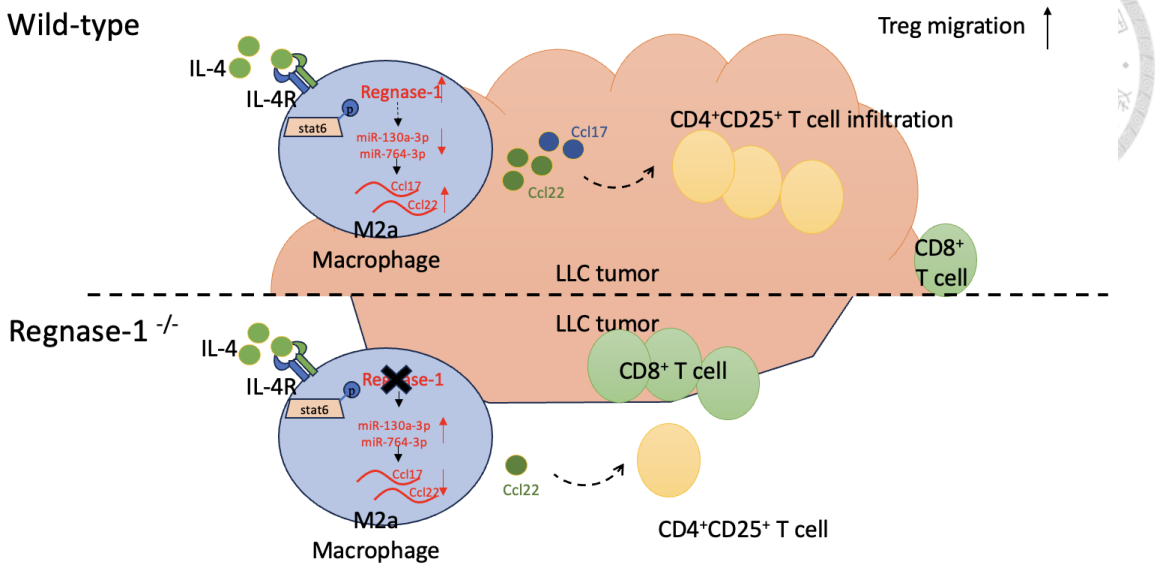

Figure 27. A proposed model of REGNASE-1 regulating CCL17 and CCL22 in macrophages.

Upon IL-4 activation, JAK1/3 phosphorylates STAT6, leading to STAT6 dimerization and translocation into the nucleus, where it activates the expression of alternative polarization genes, including *Regnase-1*, *Ccl17*, and *Ccl22*. REGNASE-1 down-regulates precursor microRNAs pre-mir-130a-3p and pre-mir-764-3p, along with their mature microRNAs. miR-130a-3p and miR-764-3p target Ccl17 and Ccl22 mRNA, respectively, leading to mRNA decay. When *Regnase-1* is deleted, miR-130a-3p and miR-764-3p are up-regulated, resulting in the down-regulation of *Ccl17* and *Ccl22* mRNA and protein expression. *Regnase-1* deletion in macrophages reduces Treg migration. In mice, macrophage-specific *Regnase-1* deletion leads to reduced LLC tumor development and decreased infiltration of $CD4^+$ $CD25^+$ T cells in tumor tissue.

doi:10.6342/NTU202403029

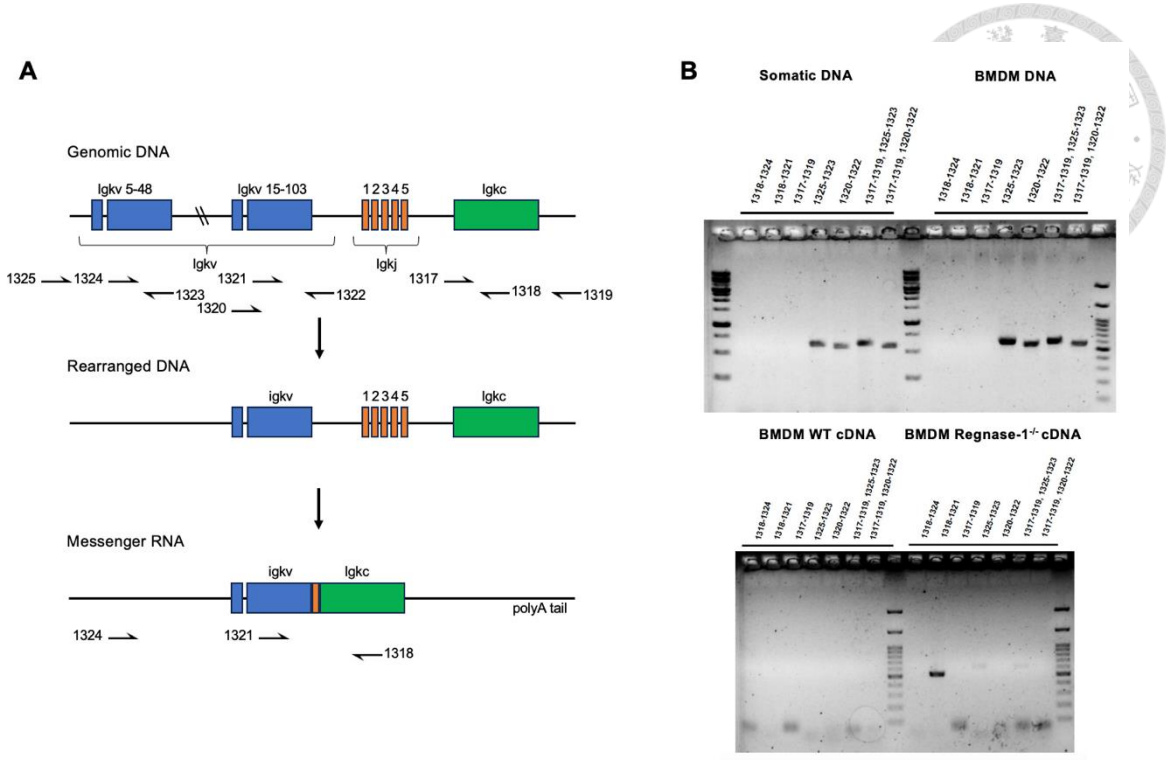

Supplementary figure 1. Detection of rearranged Immunoglobulin mRNA in *Regnase-1*$^{-/-}$ BMDM.

(A)Schematic representation of the mouse *Igkv5-48 and igkv15-103 rearrangement*, Primers (1317-1325) used for *igkv or igkc* DNA and cDNA are indicated. (B) The somatic DNA, BMDM DNA or BMDM cDNA from *Regnase-1*$^{-/-}$ and WT are examined by indicated primer.

doi:10.6342/NTU202403029

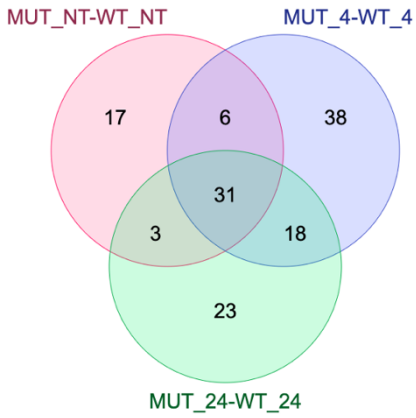

MUT_NT-WT_NT – (MUT_4-WT_4 ∪ MUT_24-WT_24) (17):

Siglec15	F10	Kif18a	Ddias
Gm5424	Slc39a4	Slco2a1	Gatm
Spata13	Il18bp	Cd276	
Lrrc4	Igkv8-30	Serp1	
Itgax	Pde1c	Fpr1	

MUT_24-WT_24 – (MUT_NT-WT_NT ∪ MUT_4-WT_4) (23):

Ccl17	C4b	Vill	Tnf	Pou2f2
Ccl22	Ocstamp	Gem	Ldhb	B4galnt1
Map2	Ccl8	Ighv10-1	Arhgef5	Stac2
Tgtp2	Ighm	Spats2l	Tmem267	
Ptgir	Gstm2	Gipc3	Ramp3	

MUT_NT-WT_NT ∩ MUT_4-WT_4 ∩ MUT_24-WT_24 (31):

Amz1	Gbp6	Ighg1	Igkv1-117	Iglc1	Mb21d2
Apol7c	Gm4951	Ighg3	Igkv15-103	Iglv1	
C2	Gpr68	Ighv1-18	Igkv3-4	Iigp1	
Clec4a1	H2-M2	Ighv1-81	Igkv3-5	Jchain	
Dcstamp	Igf2bp3	Ighv6-6	Igkv4-59	Lrrc32	

Supplementary figure 2. Multiple list comparator of DEGs from *Regnase-1*$^{-/-}$ versus WT BMDM in mRNA-seq.

(A)Venn plots of DEGs from *Regnase-1*$^{-/-}$ versus WT BMDM mRNA-seq (B)Members of list restricted in *Regnase-1*$^{-/-}$ versus WT BMDM non-treated group (MUT_NT-WT_NT) and IL-4 for 24 hours group (MUT_24-WT_24) or (C) Members overlapping within all three categories.

doi:10.6342/NTU202403029

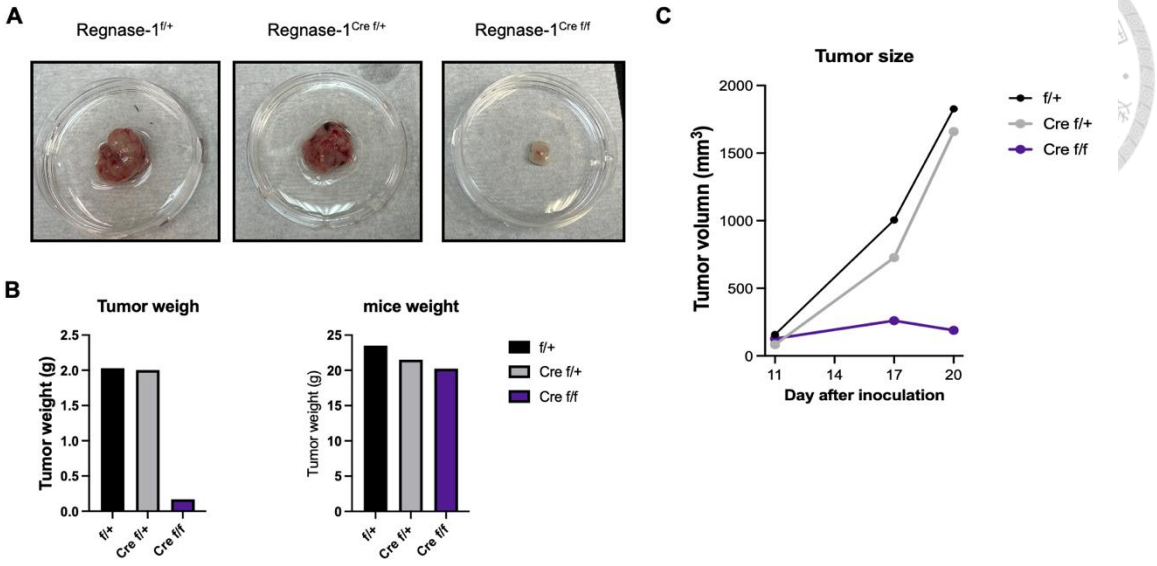

Supplementary figure 3. Myeloid-specific *Regnase-1* deleted mice reduce MC-38 tumor development.

(A)MC-38 tumor allograft isolated from *Regnase-1*$^{Cre+\ f/f}$ of *Regnase-1*$^{f/f}$ mice at 20th days after inoculation. (B) Average tumor weights from (A). (C) Tumor volume was assessed at different time-points after inoculation, and the endpoint was determined upon reaching a volume of 2000 mm^3.

doi:10.6342/NTU202403029

Tables

Table 1. Primer list

Primers for qPCR

m18S ribosomal_F	GCTTAATTTGACTCAACACGGGA
m18S ribosomal_R	AGCTATCAATCTGTCAATCCTGT
mRegnase-1_F	TCATCGACGGAAGCAATGTG
mRegnase-1_R	ATGTGCTGGTCTGTGATAGG
mTNFa_R	TCCACTTGGTGGTTTGCTACG
mTNFa_F	GTCTACTGAACTTCGGGGTGATC
mIL6_R	ATTGGAAATTGGGGTAGGAAG
mIL6_F	ACAAGAAAGACAAAGCCAGAGTC
mIL10_F	TGGGTTGCCAAGCCTTATCGG
mIL10_R	ACCTGCTCCACTGCCTTGCTC
mFIZZ1_F	CCAATCCAGCTAACTATCCCTCC
mFIZZ1_R	ACCCAGTAGCAGTCATCCCA
mYM1_F	AGAAGGGAGTTTCAAACCTGGT
mYM1_R	CTCTTGCTGATGTGTGTAAGTGA
mArginase1_F	GAAAGGAAAGTTCCCAGATGTACC
mArginase1_R	GGTAGCTGAAGGTCTCTTCC
mCCL17_F	TCC TGG CTG CTC TGC TTC TG
mCCL17_R	GAATGGCCCCTTTGAAGTAA
mCCL22_F	TAC ATC CGT CAC CCT CTG CC
mCCL22_R	GGA GTA GCT TCT TCA CCC AGA CCT

Firefly_luc2_F	GCCCTTCTTCGAGGCTAAGG
Firefly_luc2_R	CCCAGTGTCTTACCGGTGTC
Renilla_F	TCCAGATTGTCCGCAACTAC
Renilla_R	CTTCTTAGCTCCCTCGACAATAG

Primers for construct

mRegnase-1 (D141N) mutant_f	GCCACATTGCTTCCGTTGATGACCACAGGTCTC

doi:10.6342/NTU202403029

mRegnase-1 (D141N) mutant_r	GAGACCTGTGGTCATCAACGGAAGCAATGTGGC
mRegnase-1 (D225,226A) mutant_f	GCTATGCTGCCCGCTTCATTGTGAAGCTGGCC
mRegnase-1 (D225,226A) mutant_r	AGCGGGCAGCATAGCACACCACGCGCTTGC
pmirGLO_ccl17_F	tagttgtttaaacgagctcgCCTTCCCGCTGAGGCATTTG
pmirGLO_ccl17_R	ggtcgactctagactcgaggTGAGGGAGGAAGGCTTTATTCC
pmirGLO_ccl22_F	tagttgtttaaacgagctcgGGAGGAGGACCTGATGAC
pmirGLO_ccl22_R	ggtcgactctagactcgaggTTTTTATTATTGGCGAGCATTTATTTTC
pmirGLO_ccl17(1-100)_F	tagttgtttaaacgagctcgCCTTCCCGCTGAGGCATTTG
pmirGLO_ccl17(1-100)_R	ggtcgactctagactcgaggTCTGCTCTGTGGCTGCTC
pmirGLO_ccl17(101-182)_F	tagttgtttaaacgagctcgAGTCCCTGTTCCCTTTTTTATG
pmirGLO_ccl17(101-182)_R	ggtcgactctagactcgaggGAGGGAGGAAGGCTTTATTC
pmirGLO_ccl22(1-608)_F	tagttgtttaaacgagctcgGGAGGAGGACCTGATGAC
pmirGLO_ccl22(1-608)_R	ggtcgactctagactcgaggAGACCAAGAAACAGGAGG
pmirGLO_ccl22(609-1071)_F	tagttgtttaaacgagctcgGCAGCACGGGGCAGGGAG
pmirGLO_ccl22(609-1071)_R	ggtcgactctagactcgaggCAGCAGCTCCCACAACCATCTATTTTCTG
pmirGLO_ccl22(1072-1495)_F	tagttgtttaaacgagctcgCCAGTGGCAGAGTTAACTTAAAG
pmirGLO_ccl22(1072-1495)_R	ggtcgactctagactcgaggGGCGAGCATTTATTTTCC

Primers for miRNA qPCR

mmu-mir-21a-5p_RT	GTC GTA TCC AGT GCA GGG TCC GAG GTA TTC GCA CTG GAT ACG ACtcaacatcagt
mmu-mir-21a-5p_f	gccgccgcTAGCTTATCAGAC
mmu-mir-130a-3p_RT	GTC GTA TCC AGT GCA GGG TCC GAG GTA TTC GCA CTG GAT ACG ACatgccctttta
mmu-mir-130a-3p_f	ccgcggCAGTGCAATGTTA

doi:10.6342/NTU202403029

mmu-mir-301a-3p_RT	GTC GTA TCC AGT GCA GGG TCC GAG GTA TTC GCA CTG GAT ACG ACgctttgacaat
mmu-mir-301a-3p_f	accgcggCAGTGCAATAGT
U6 small nuclear RNA_RT_r	CGCTTCACGAATTTGCGTGTCAT
U6 small nuclear RNA_f	*GCTTCGGCAGCACATATACTAAAAT*
Universal Reverse Primer	CCAGTGCAGGGTCCGAGGTA
mmu-mir-337-5p_RT	GTC GTA TCC AGT GCA GGG TCC GAG GTA TTC GCA CTG GAT ACG ACaatcaactcct
mmu-mir-337-5p_f	cacgaaCGGCGTCATGCA
mmu-mir-337-3p_RT	GTCGTATCCAGTGCAGGGTCCGAGGTATTCGCACTGGATACGACaaaggcatcat
mmu-mir-337-3p_f	accgcggTCAGCTCCTATA
mmu-mir-138-5p_RT	GTCGTATCCAGTGCAGGGTCCGAGGTATTCGCACTGGATACGAcggcctgattc
mmu-mir-138-5p_f	cacggcGCTGGTGTTGTG
mmu-mir-7083-3p_RT	GTCGTATCCAGTGCAGGGTCCGAGGTATTCGCACTGGATACGAcctggggtccag
mmu-mir-7083-3p_f	cacggcCTCTGCTCTCCT
mmu-mir-23a-3p_RT	GTCGTATCCAGTGCAGGGTCCGAGGTATTCGCACTGGATACGAcggaaatccctg
mmu-mir-23a-3p_f	ccacggcATCACATTGCCA
mmu-mir-130a-5p_RT	GTCGTATCCAGTGCAGGGTCCGAGGTATTCGCACTGGATACGAcagtagcacaat
mmu-mir-130a-5p_f	ccacggcGCTCTTTTCACA
mmu-mir-34a-5p_RT	GTCGTATCCAGTGCAGGGTCCGAGGTATTCGCACTGGATACGAcacaaccagcta
mmu-mir-34a-5p_f	cacgccGGCAGTGTCTTA
mmu-mir-7667-5p_RT	GTCGTATCCAGTGCAGGGTCCGAGGTATTCGCACTGGATACGActcagggctag
mmu-mir-7667-5p_f	cacggcGAGCCATCTCTC
mmu-mir-7062-5p_RT	GTCGTATCCAGTGCAGGGTCCGAGGTATTCGCACTGGATACGAcagacactccaca
mmu-mir-7062-5p_f	cacgacTGGAGGCCAGCT
mmu-mir-5120_RT	GTCGTATCCAGTGCAGGGTCCGAGGTATTCGCACTGGATACGAcgctggtggcacc
mmu-mir-5120_f	cacggcTTTGGGGCTGTG

doi:10.6342/NTU202403029

mmu-mir-764-3p_RT	GTCGTATCCAGTGCAGGGTCCGAGGTATTCGCACTGGATACGAcacagttgccac
mmu-mir-764-3p_f	accgcgAGGAGGCCATAG

Primers for genotyping of Regnase-1 depletion RAW264.7 or Tg mice

Regnase-1_TKO_f	AAAAATCAGCATTTTCAACAAA
TKO_WT_r	TTGGATTTTAGTCCCCTATCTGA
TKO_*Regnase-1*$^{-/-}$_r	GTTTATTTACCGCCGTGTGTG
Regnase-1_lysM_f	CCCAGAAATGCCAGATTACG
Regnase-1_lysM_r	CTTGGGCTGCCAGAATTTCTC
Regnase-1_cDNA_f	TGGACACCTTACAGACGACG
Regnase-1_cDNA_r	CATGGCCACATTGCTTCC

Table 2. DEGs between *Regnase-1*$^{-/-}$ versus wilt-type without IL-4 induction.

SYMBOL	GENENAME	logFC	P.Value
Ighg1	immunoglobulin heavy constant i 1 (G1m marker)	5.355681	3.72E-10
Igkv3-4	immunoglobulin kappa variable 3-4	4.795978	2.08E-09
Iglc1	immunoglobulin lambda constant 1	4.663104	2.24E-09
C2	complement component 2 (within H-2S)	4.094282	1.27E-08
Igkv15-103	immunoglobulin kappa chain variable 15-103	5.815101	1.29E-08
Nfkbiz	nuclear factor of kappa light polypeptide gene enhancer in B cells inhibitor, zeta	2.741717	7.55E-08
Iglv1	immunoglobulin lambda variable 1	4.996886	1.07E-07
Ighv1-18	immunoglobulin heavy variable V1-18	4.365214	1.13E-07
Slc24a5	solute carrier family 24, member 5	-1.55298	3.87E-07
Igf2bp3	insulin-like growth factor 2 mRNA binding protein 3	1.738559	3.99E-07
Clec4a1	C-type lectin domain family 4, member a1	1.590276	4.02E-07
Ighg3	Immunoglobulin heavy constant gamma 3	4.507603	4.80E-07
Igkv1-117	immunoglobulin kappa variable 1-117	4.30651	6.39E-07
Iigp1	interferon inducible GTPase 1	3.723026	7.57E-07
Apol7c	apolipoprotein L 7c	4.273548	7.78E-07
Dcstamp	dendrocyte expressed seven transmembrane protein	-2.81086	8.33E-07

doi:10.6342/NTU202403029

Mmp12	matrix metallopeptidase 12	-1.0178	1.34E-06
Shisa9	shisa family member 9	-1.82792	3.51E-06
Siglec15	sialic acid binding Ig-like lectin 15	-3.47591	5.37E-06
Gm5424	argininosuccinate synthase pseudogene	-2.34133	5.67E-06
Ighv6-6	immunoglobulin heavy variable 6-6	4.066198	6.49E-06
Spata13	spermatogenesis associated 13	-1.22078	6.50E-06
Igkv3-5	immunoglobulin kappa chain variable 3-5	4.037727	9.08E-06
Mb21d2	Mab-21 domain containing 2	2.394476	9.10E-06
Padi2	peptidyl arginine deiminase, type II	-0.78992	9.38E-06
Nectin1	nectin cell adhesion molecule 1	-2.27401	1.06E-05
Gm4951	predicted gene 4951	3.357739	1.13E-05
Ighv1-81	immunoglobulin heavy variable 1-81	4.077374	1.82E-05
Napsa	napsin A aspartic peptidase	-0.96568	2.04E-05
Igkv4-59	immunoglobulin kappa variable 4-59	5.336197	2.41E-05
Lrrc4	leucine rich repeat containing 4	3.234462	2.66E-05
Ptgfrn	prostaglandin F2 receptor negative regulator	-1.43642	2.70E-05
Itgax	integrin alpha X	-1.4193	2.71E-05
Large1	LARGE xylosyl- and glucuronyltransferase 1	-0.82011	2.74E-05
Jchain	immunoglobulin joining chain	7.270821	3.10E-05
F10	coagulation factor X	-1.57069	3.31E-05
Slc39a4	solute carrier family 39 (zinc transporter), member 4	1.443759	4.15E-05
Mzb1	marginal zone B and B1 cell-specific protein 1	3.592737	4.16E-05
Slco3a1	solute carrier organic anion transporter family, member 3a1	0.979347	4.39E-05
Il18bp	interleukin 18 binding protein	0.987209	4.66E-05
H2-M2	histocompatibility 2, M region locus 2	-2.18797	4.80E-05
Igkc	immunoglobulin kappa constant	9.833133	5.00E-05
Igkv10-94	immunoglobulin kappa variable 10-94	3.272055	5.16E-05
Gbp6	guanylate binding protein 6	2.044443	5.53E-05
Igkv14-111	immunoglobulin kappa variable 14-111	4.280899	5.86E-05
Igkv8-30	immunoglobulin kappa chain variable 8-30	3.528894	6.13E-05
Pde1c	phosphodiesterase 1C	-2.91604	6.16E-05
Kif18a	kinesin family member 18A	2.616378	6.29E-05
Lrrc32	leucine rich repeat containing 32	-2.54719	6.33E-05
Slco2a1	solute carrier organic anion transporter family, member 2a1	2.897821	7.87E-05
Cd276	CD276 antigen	-1.06666	7.99E-05
Serp1	stress-associated endoplasmic reticulum protein 1	0.73088	8.18E-05
Fpr1	formyl peptide receptor 1	3.831077	8.41E-05

doi:10.6342/NTU202403029

Amz1	archaelysin family metallopeptidase 1	-0.70506	8.73E-05
Gpr68	G protein-coupled receptor 68	-2.09256	8.74E-05
Ddias	DNA damage-induced apoptosis suppressor	2.683304	0.000101
Gatm	glycine amidinotransferase (L-arginine:glycine amidinotransferase)	0.871127	0.000101
Gpc1	glypican 1	-1.37277	0.000109
Cpe	carboxypeptidase E	-1.1319	0.000124
Cuedc1	CUE domain containing 1	-0.76959	0.000125
Ighv6-3	immunoglobulin heavy variable 6-3	2.69463	0.000126
Clec4a3	C-type lectin domain family 4, member a3	0.778348	0.000129
Adam19	a disintegrin and metallopeptidase domain 19 (meltrin beta)	-2.04014	0.000132
Icam1	intercellular adhesion molecule 1	-0.78524	0.000141
Lox	lysyl oxidase	2.284257	0.000144
Arhgef18	rho/rac guanine nucleotide exchange factor (GEF) 18	1.279522	0.000145
Akr1b8	aldo-keto reductase family 1, member B8	-0.7295	0.000148
Igkv12-44	immunoglobulin kappa variable 12-44	3.64194	0.000172
Ppfibp2	PTPRF interacting protein, binding protein 2 (liprin beta 2)	0.692019	0.000178
Plekhh2	pleckstrin homology domain containing, family H (with MyTH4 domain) member 2	-2.98642	0.000188
Insyn2b	inhibitory synaptic factor family member 2B	2.548138	0.000192
Ralgps2	Ral GEF with PH domain and SH3 binding motif 2	1.017333	0.000199
Igkv10-96	immunoglobulin kappa variable 10-96	3.758385	0.000206
Tppp	tubulin polymerization promoting protein	-2.90759	0.000211
Spsb4	splA/ryanodine receptor domain and SOCS box containing 4	-0.9974	0.000227
Inpp5j	inositol polyphosphate 5-phosphatase J	1.055238	0.000242
Rin2	Ras and Rab interactor 2	-0.49114	0.000248
Map4k1	mitogen-activated protein kinase kinase kinase kinase 1	-1.00843	0.000262
Nod1	nucleotide-binding oligomerization domain containing 1	0.671764	0.000278
Dnah14	dynein, axonemal, heavy chain 14	2.333634	0.000282
Lgalsl	lectin, galactoside binding-like	1.832171	0.000294
Gsta3	glutathione S-transferase, alpha 3	-2.04154	0.000298
Tspan5	tetraspanin 5	-0.66917	0.000319
Sh3bp5	SH3-domain binding protein 5 (BTK-associated)	0.512205	0.000329
Nmd3	NMD3 ribosome export adaptor	0.545703	0.000333
Slc2a6	solute carrier family 2 (facilitated glucose transporter), member 6	-1.137	0.00034
Fcgr4	Fc receptor, IgG, low affinity IV	0.858946	0.00034

doi:10.6342/NTU202403029

Ebi3	Epstein-Barr virus induced gene 3	0.991907	0.000374
Angptl2	angiopoietin-like 2	-0.71613	0.000392
F830016B08Rik	RIKEN cDNA F830016B08 gene	3.53027	0.000408
Slc13a3	solute carrier family 13 (sodium-dependent dicarboxylate transporter), member 3	3.382667	0.000409
Batf2	basic leucine zipper transcription factor, ATF-like 2	0.969473	0.00041
Tle1	transducin-like enhancer of split 1	-0.51156	0.00041
Unc119b	unc-119 lipid binding chaperone B	-0.55198	0.000419
Pou2f2	POU domain, class 2, transcription factor 2	0.997337	0.000424
Aoah	acyloxyacyl hydrolase	0.836738	0.000428
Scarf1	scavenger receptor class F, member 1	0.81692	0.000432
Donson	downstream neighbor of SON	0.912026	0.000436
Igkv6-32	immunoglobulin kappa variable 6-32	2.476234	0.000437
Layn	layilin	-1.1415	0.00044
Pfkfb3	6-phosphofructo-2-kinase/fructose-2,6-biphosphatase 3	0.586336	0.000451

Table 3. DEGs between *Regnase-1*$^{-/-}$ versus wilt-type with IL-4 induction for 4 hours.

SYMBOL	GENENAME	logFC	P.Value
Apol7c	apolipoprotein L 7c	3.155158	5.84E-12
Ighg1	immunoglobulin heavy constant gamma 1 (G1m marker)	5.697535	9.16E-11
Igkv3-4	immunoglobulin kappa variable 3-4	4.984649	1.04E-09
Iglc1	immunoglobulin lambda constant 1	4.694715	1.88E-09
Igkv15-103	immunoglobulin kappa chain variable 15-103	6.331287	2.72E-09
C2	complement component 2 (within H-2S)	3.870704	7.97E-09
Gm8221	apolipoprotein L 7c pseudogene	2.641416	1.02E-08
Ighv1-18	immunoglobulin heavy variable V1-18	4.780037	1.47E-08
Iglv1	immunoglobulin lambda variable 1	5.406479	2.06E-08
Ighv6-3	immunoglobulin heavy variable 6-3	4.63157	2.18E-08
Mmp12	matrix metallopeptidase 12	-1.31223	3.32E-08
Igf2bp3	insulin-like growth factor 2 mRNA binding protein 3	1.814562	7.09E-08
Iigp1	interferon inducible GTPase 1	4.01323	1.37E-07
Gm4951	predicted gene 4951	2.268816	1.87E-07
Gbp6	guanylate binding protein 6	2.490072	2.18E-07

doi:10.6342/NTU202403029

Mb21d2	Mab-21 domain containing 2	1.64702	2.70E-07
Dcstamp	dendrocyte expressed seven transmembrane protein	-3.19421	4.13E-07
Slc24a5	solute carrier family 24, member 5	-1.46391	4.25E-07
Klrb1a	killer cell lectin-like receptor subfamily B member 1A	-3.09157	6.47E-07
Lrrc32	leucine rich repeat containing 32	-1.89601	7.25E-07
Cd209a	CD209a antigen	-4.17217	8.74E-07
Igkv6-32	immunoglobulin kappa variable 6-32	3.846395	1.22E-06
Ighg3	Immunoglobulin heavy constant gamma 3	4.196722	1.46E-06
Ighv1-26	immunoglobulin heavy variable 1-26	3.703088	1.63E-06
Fbln5	fibulin 5	-1.67675	3.02E-06
Pecam1	platelet/endothelial cell adhesion molecule 1	1.161879	3.22E-06
Igkv3-5	immunoglobulin kappa chain variable 3-5	4.234028	3.48E-06
Jchain	immunoglobulin joining chain	8.45141	4.62E-06
Igkv1-117	immunoglobulin kappa variable 1-117	3.806525	4.68E-06
Dpy19l3	dpy-19-like 3 (C. elegans)	1.892009	5.49E-06
Batf2	basic leucine zipper transcription factor, ATF-like 2	1.239437	6.91E-06
Arhgef18	rho/rac guanine nucleotide exchange factor (GEF) 18	1.681858	7.40E-06
Napsa	napsin A aspartic peptidase	-1.02046	9.38E-06
Shisa9	shisa family member 9	-1.55032	9.93E-06
Slc35g1	solute carrier family 35, member G1	1.100396	1.14E-05
Cd209e	CD209e antigen	-3.73725	1.15E-05
Pkp2	plakophilin 2	-1.32993	1.59E-05
Clec4a1	C-type lectin domain family 4, member a1	1.158495	1.96E-05
Igkv4-59	immunoglobulin kappa variable 4-59	5.432072	2.17E-05
Ighv6-6	immunoglobulin heavy variable 6-6	3.664268	2.31E-05
Ptprm	protein tyrosine phosphatase, receptor type, M	1.714368	2.42E-05
Prps1	phosphoribosyl pyrophosphate synthetase 1	0.654777	2.43E-05
H2-M2	histocompatibility 2, M region locus 2	-2.01077	2.46E-05
Maf	avian musculoaponeurotic fibrosarcoma oncogene homolog	0.871717	2.50E-05
Igkv10-96	immunoglobulin kappa variable 10-96	4.378601	2.52E-05
Lifr	LIF receptor alpha	0.854512	2.52E-05
Igkv12-44	immunoglobulin kappa variable 12-44	4.184092	2.53E-05
Nfkbiz	nuclear factor of kappa light polypeptide gene enhancer in B cells inhibitor, zeta	2.445265	2.59E-05
Slco3a1	solute carrier organic anion transporter family, member 3a1	0.987612	2.80E-05
Padi2	peptidyl arginine deiminase, type II	-0.71711	3.48E-05
Fkbp9	FK506 binding protein 9	-0.94829	3.66E-05

doi:10.6342/NTU202403029

Npy	neuropeptide Y	-1.24332	3.87E-05
Me1	malic enzyme 1, NADP(+)-dependent, cytosolic	-1.16654	3.95E-05
Igkv10-94	immunoglobulin kappa variable 10-94	3.405817	4.01E-05
Cd86	CD86 antigen	1.153044	4.19E-05
Ighg2b	immunoglobulin heavy constant gamma 2B	3.931667	4.19E-05
Anxa1	annexin A1	-0.58617	4.26E-05
Gpr68	G protein-coupled receptor 68	-2.11482	4.29E-05
Procr	protein C receptor, endothelial	-1.32316	4.52E-05
Cemip2	cell migration inducing hyaluronidase 2	0.966807	4.72E-05
Adam19	a disintegrin and metallopeptidase domain 19 (meltrin beta)	-1.97412	4.93E-05
Cd300ld	CD300 molecule like family member d	-0.70358	5.11E-05
Nyap2	neuronal tyrosine-phophorylated phosphoinositide 3-kinase adaptor 2	-2.94613	5.29E-05
Ighv1-53	immunoglobulin heavy variable 1-53	3.763264	5.35E-05
Igha	immunoglobulin heavy constant alpha	4.156555	5.96E-05
Scarf1	scavenger receptor class F, member 1	0.939473	6.65E-05
Serpina3g	serine (or cysteine) peptidase inhibitor, clade A, member 3G	1.259113	7.20E-05
Igkv14-111	immunoglobulin kappa variable 14-111	4.176743	7.32E-05
Cuedc1	CUE domain containing 1	-0.85775	7.85E-05
Tmem140	transmembrane protein 140	-0.75531	7.86E-05
Gm17747	predicted gene, 17747	-2.32336	8.15E-05
Gpc1	glypican 1	-1.0084	8.68E-05
Rtn4rl1	reticulon 4 receptor-like 1	-1.72759	0.000106
Dpep2	dipeptidase 2	-0.64369	0.000107
Ptgfrn	prostaglandin F2 receptor negative regulator	-1.31774	0.000111
Amz1	archaelysin family metallopeptidase 1	-0.67504	0.000112
Ighv1-81	immunoglobulin heavy variable 1-81	3.626128	0.000112
Serpina3f	serine (or cysteine) peptidase inhibitor, clade A, member 3F	1.540405	0.000114
Cldn11	claudin 11	-2.00824	0.000115
Nr3c2	nuclear receptor subfamily 3, group C, member 2	1.765961	0.000119
Aoah	acyloxyacyl hydrolase	0.929294	0.000125
Igkc	immunoglobulin kappa constant	8.972697	0.000125
Rin2	Ras and Rab interactor 2	-0.52764	0.000128
Hap1	huntingtin-associated protein 1	-2.56221	0.000134
Bmp2	bone morphogenetic protein 2	1.057704	0.000137
Enpp5	ectonucleotide pyrophosphatase/phosphodiesterase 5	2.918677	0.000146
Nod1	nucleotide-binding oligomerization domain containing 1	0.667202	0.000146

doi:10.6342/NTU202403029

Armcx2	armadillo repeat containing, X-linked 2	-1.80456	0.000153
Snn	stannin	0.546546	0.000156
Chrne	cholinergic receptor, nicotinic, epsilon polypeptide	-2.57001	0.000157
S100a11	S100 calcium binding protein A11	-1.09006	0.000164
Akr1b8	aldo-keto reductase family 1, member B8	-0.75591	0.000165
F2rl2	coagulation factor II (thrombin) receptor-like 2	-2.73109	0.000167
Mzb1	marginal zone B and B1 cell-specific protein 1	3.255224	0.000178
Dnase1l3	deoxyribonuclease 1-like 3	1.551105	0.000199
Ighm	immunoglobulin heavy constant mu	2.571571	0.000203
Sema6d	sema domain, transmembrane domain (TM), and cytoplasmic domain, (semaphorin) 6D	1.225099	0.000204
Rhobtb1	Rho-related BTB domain containing 1	0.664437	0.000208
Il18bp	interleukin 18 binding protein	0.767136	0.000211
Slc13a3	solute carrier family 13 (sodium-dependent dicarboxylate transporter), member 3	3.731425	0.000215
Gnb4	guanine nucleotide binding protein (G protein), beta 4	-0.53991	0.000227

Table 4. DEGs between *Regnase-1*$^{-/-}$ versus wilt-type with IL-4 induction for 24 hours.

SYMBOL	GENENAME	logFC	P.Value
Ighg1	immunoglobulin heavy constant gamma 1 (G1m marker)	6.416545	1.29E-11
Apol7c	apolipoprotein L 7c	2.437617	4.22E-10
Dcstamp	dendrocyte expressed seven transmembrane protein	-2.59609	1.36E-09
C2	complement component 2 (within H-2S)	4.048048	1.88E-09
Iglc1	immunoglobulin lambda constant 1	4.723955	3.90E-09
Iigp1	interferon inducible GTPase 1	5.094974	2.22E-08
Gm8221	apolipoprotein L 7c pseudogene	2.408069	2.26E-08
Igkv15-103	immunoglobulin kappa chain variable 15-103	5.503579	5.31E-08
Igf2bp3	insulin-like growth factor 2 mRNA binding protein 3	1.562009	9.00E-08
Ighv1-18	immunoglobulin heavy variable V1-18	4.44359	1.42E-07
Ighv6-6	immunoglobulin heavy variable 6-6	5.140035	2.02E-07
Iglv1	immunoglobulin lambda variable 1	4.977995	2.24E-07
Igkv3-4	immunoglobulin kappa variable 3-4	3.912074	2.76E-07
Ighg3	Immunoglobulin heavy constant gamma 3	4.794884	2.78E-07
Gbp6	guanylate binding protein 6	2.851218	3.03E-07

doi:10.6342/NTU202403029

Ccl17	chemokine (C-C motif) ligand 17	-3.85935	3.13E-07
Mmp12	matrix metallopeptidase 12	-1.10395	3.70E-07
Klrb1a	killer cell lectin-like receptor subfamily B member 1A	-2.87186	5.88E-07
Igkv6-32	immunoglobulin kappa variable 6-32	4.075467	8.71E-07
Gm4951	predicted gene 4951	2.510868	1.00E-06
Ccl22	chemokine (C-C motif) ligand 22	-2.16464	1.17E-06
Igkv3-5	immunoglobulin kappa chain variable 3-5	4.624826	1.60E-06
Lrrc32	leucine rich repeat containing 32	-1.28622	2.32E-06
Map2	microtubule-associated protein 2	1.125331	3.62E-06
Nfkbiz	nuclear factor of kappa light polypeptide gene enhancer in B cells inhibitor, zeta	2.553832	3.84E-06
Slc24a5	solute carrier family 24, member 5	-1.43338	4.15E-06
Ighv6-3	immunoglobulin heavy variable 6-3	3.568526	4.56E-06
Ighg2b	immunoglobulin heavy constant gamma 2B	4.710587	4.57E-06
H2-M2	histocompatibility 2, M region locus 2	-2.12586	5.07E-06
Arhgef18	rho/rac guanine nucleotide exchange factor (GEF) 18	1.56572	5.47E-06
Tgtp2	T cell specific GTPase 2	2.27128	5.65E-06
Igkv1-117	immunoglobulin kappa variable 1-117	3.895057	6.37E-06
Mzb1	marginal zone B and B1 cell-specific protein 1	4.24717	6.60E-06
Napsa	napsin A aspartic peptidase	-1.04379	7.23E-06
Pkp2	plakophilin 2	-1.09436	1.06E-05
Me1	malic enzyme 1, NADP(+)-dependent, cytosolic	-1.39375	1.23E-05
Dpy19l3	dpy-19-like 3 (C. elegans)	1.396742	1.30E-05
Clec4a1	C-type lectin domain family 4, member a1	1.210211	1.35E-05
Gpr68	G protein-coupled receptor 68	-1.85867	1.52E-05
Ptgir	prostaglandin I receptor (IP)	-0.90595	1.65E-05
C4b	complement component 4B (Chido blood group)	3.494264	2.22E-05
Jchain	immunoglobulin joining chain	7.564774	2.25E-05
Cldn11	claudin 11	-1.58793	2.56E-05
Npy	neuropeptide Y	-1.27636	2.59E-05
Padi2	peptidyl arginine deiminase, type II	-0.72604	3.05E-05
Ocstamp	osteoclast stimulatory transmembrane protein	-1.74157	3.17E-05
Ighv1-26	immunoglobulin heavy variable 1-26	3.098034	3.26E-05
Ccl8	chemokine (C-C motif) ligand 8	2.171594	3.65E-05
Mb21d2	Mab-21 domain containing 2	1.534614	3.74E-05
Amz1	archaelysin family metallopeptidase 1	-0.72483	4.06E-05
Ighm	immunoglobulin heavy constant mu	3.313371	4.08E-05

doi:10.6342/NTU202403029

Prps1	phosphoribosyl pyrophosphate synthetase 1	0.643051	4.13E-05
Gstm2	glutathione S-transferase, mu 2	-1.42632	4.14E-05
Vill	villin-like	-0.81124	4.39E-05
Batf2	basic leucine zipper transcription factor, ATF-like 2	1.023686	5.57E-05
Maf	avian musculoaponeurotic fibrosarcoma oncogene homolog	0.835818	5.66E-05
Large1	LARGE xylosyl- and glucuronyltransferase 1	-0.73463	5.83E-05
Gem	GTP binding protein (gene overexpressed in skeletal muscle)	-2.54672	5.94E-05
Igkv4-59	immunoglobulin kappa variable 4-59	5.212671	6.40E-05
Ighv10-1	immunoglobulin heavy variable 10-1	3.560363	6.84E-05
Spats2l	spermatogenesis associated, serine-rich 2-like	2.454049	7.00E-05
Gipc3	GIPC PDZ domain containing family, member 3	2.65896	7.12E-05
Cuedc1	CUE domain containing 1	-0.80796	7.92E-05
Tnf	tumor necrosis factor	1.12247	8.57E-05
Ighv1-81	immunoglobulin heavy variable 1-81	3.81338	8.93E-05
Ldhb	lactate dehydrogenase B	-1.16285	9.54E-05
Gpc1	glypican 1	-0.87654	0.000101
Arhgef5	Rho guanine nucleotide exchange factor (GEF) 5	2.839395	0.000101
Igkv10-96	immunoglobulin kappa variable 10-96	4.122296	0.000104
Tmem267	transmembrane protein 267	-0.90243	0.00011
Ramp3	receptor (calcitonin) activity modifying protein 3	-2.121	0.000116
Pou2f2	POU domain, class 2, transcription factor 2	1.284198	0.000125
B4galnt1	beta-1,4-N-acetyl-galactosaminyl transferase 1	-0.60637	0.000125
Stac2	SH3 and cysteine rich domain 2	-0.98033	0.000125
Nectin1	nectin cell adhesion molecule 1	-1.55834	0.000129
AW112010	expressed sequence AW112010	1.331579	0.000136

doi:10.6342/NTU202403029

Table 5. Complete blood counts of *Regnase-1*$^{+/+}$ and *Regnase-1*$^{-/-}$ mice.

Complete blood counts of Regnase-1+/+ and Regnase-1-/- mice

Parameter		Regnase-1$^{+/+}$ (n=8)			Regnase-1$^{-/-}$ (n=7)			P-value
RBC	M/uL	9.88	±	0.60	3.31	±	1.84	0.009*
HGB	g/dL	15.09	±	0.77	4.24	±	2.08	<0.001*
HCT	%	52.75	±	4.05	14.60	±	8.32	<0.001*
MCV	fL	53.35	±	1.34	43.63	±	4.08	<0.001*
MCH	pg	15.28	±	0.26	13.41	±	1.77	0.01*
MCHC	g/dL	28.66	±	0.94	31.19	±	6.64	0.3
RET	K/uL	443.25	±	155.81	313.57	±	406.62	0.42
RET	%	4.53	±	1.74	6.87	±	6.67	0.35
PLT	K/uL	637.38	±	141.63	654.43	±	455.99	0.92
WBC	K/uL	2.37	±	1.06	6.98	±	4.60	0.02*
NEUT	K/uL	0.17	±	0.07	1.42	±	1.46	0.03*
LYMPH	K/uL	2.10	±	0.97	3.72	±	3.07	0.18
MONO	K/uL	0.07	±	0.04	1.65	±	1.47	0.009*
EO	K/uL	0.03	±	0.02	0.19	±	0.22	0.06
BASO	K/uL	0.00	±	0.01	0.00	±	0.00	0.08
NEUT	%	7.52	±	1.89	21.79	±	17.04	0.03*
LYMPH	%	88.37	±	2.17	49.38	±	15.74	<0.001*
MONO	%	2.68	±	0.70	26.55	±	15.11	<0.001*
EO	%	1.30	±	0.81	2.30	±	2.65	0.33
BASO	%	0.14	±	0.19	0.00	±	0.00	0.08

Values are presented as mean ± standard deviation. * Statistically significant. RBC, red blood cell. HGB, Hemoglobin. HCT, Hematocrit. MCV, mean corpuscular volume. MCH, mean corpuscular hemoglobin. MCHC, mean corpuscular hemoglobin concentration. RET, reticulocyte. PLT, platelet. WBC, white blood cell. NEUT, neutrophil. LYMPH, lymphocyte. MONO, monocyte. EO, eosinophil. BASO, basophil.

doi:10.6342/NTU202403029

Table 6. Complete blood counts of *Regnase-1*$^{f/f}$ and *Regnase-1*$^{Cre+\ f/f}$ mice.

Complete blood counts of Regnase-1f/f and Regnase-1Cre+ f/f mice

Parameter		Regnase-1f/f (n=11)	Regnase-1Cre+ f/f (n=10)	P-value
RBC	M/uL	9.80 ± 0.62	8.09 ± 1.48	0.009*
HGB	g/dL	14.97 ± 0.96	11.53 ± 2.48	<0.001*
HCT	%	51.83 ± 3.73	40.77 ± 7.85	<0.001*
MCV	fL	52.87 ± 0.91	50.36 ± 2.07	<0.001*
MCH	pg	15.26 ± 0.20	14.20 ± 0.97	0.01*
MCHC	g/dL	28.91 ± 0.48	28.19 ± 1.83	0.3
RET	K/uL	407.80 ± 41.89	1045.39 ± 842.25	0.42
RET	%	4.18 ± 0.56	14.72 ± 14.54	0.35
PLT	K/uL	722.09 ± 200.37	807.90 ± 353.21	0.92
WBC	K/uL	2.72 ± 1.09	3.91 ± 1.96	0.02*
NEUT	K/uL	0.32 ± 0.19	0.40 ± 0.24	0.03*
LYMPH	K/uL	2.31 ± 0.97	2.91 ± 1.46	0.18
MONO	K/uL	0.10 ± 0.06	0.37 ± 0.23	0.009*
EO	K/uL	0.02 ± 0.02	0.23 ± 0.21	0.06
BASO	K/uL	0.00 ± 0.00	0.00 ± 0.01	0.08
NEUT	%	11.18 ± 3.26	10.64 ± 4.58	0.03*
LYMPH	%	83.66 ± 6.06	74.02 ± 6.88	<0.001*
MONO	%	4.27 ± 4.18	10.10 ± 3.59	<0.001*
EO	%	0.84 ± 0.65	5.14 ± 2.88	0.33
BASO	%	0.05 ± 0.10	0.08 ± 0.17	0.08

Values are presented as mean ± standard deviation. * Statistically significant. RBC, red blood cell. HGB, Hemoglobin. HCT, Hematocrit. MCV, mean corpuscular volume. MCH, mean corpuscular haemoglobin.MCHC, mean corpuscular hemoglobin concentration. RET, reticulocyte. PLT, platelet.WBC, white blood cell. NEUT, neutrophil. LYMPH, lymphocyte. MONO, monocyte. EO, eosinophil. BASO, basophil.

doi:10.6342/NTU202403029

References

1. van Furth R, Cohn ZA, Hirsch JG, Humphrey JH, Spector WG, Langevoort HL. The mononuclear phagocyte system: a new classification of macrophages, monocytes, and their precursor cells. *Bull World Health Organ.*46(6):845-852 (1972).

2. Palis J, Robertson S, Kennedy M, Wall C, Keller G. Development of erythroid and myeloid progenitors in the yolk sac and embryo proper of the mouse. *Development.*126(22):5073-5084 (1999).

3. Schulz C, Gomez Perdiguero E, Chorro L, et al. A lineage of myeloid cells independent of Myb and hematopoietic stem cells. *Science.*336(6077):86-90 (2012).

4. Hashimoto D, Chow A, Noizat C, et al. Tissue-resident macrophages self-maintain locally throughout adult life with minimal contribution from circulating monocytes. *Immunity.*38(4):792-804 (2013).

5. Chorro L, Sarde A, Li M, et al. Langerhans cell (LC) proliferation mediates neonatal development, homeostasis, and inflammation-associated expansion of the epidermal LC network. *J Exp Med.*206(13):3089-3100 (2009).

6. Ajami B, Bennett JL, Krieger C, Tetzlaff W, Rossi FM. Local self-renewal can sustain CNS microglia maintenance and function throughout adult life. *Nat Neurosci.*10(12):1538-1543 (2007).

7. Sieweke MH, Allen JE. Beyond stem cells: self-renewal of differentiated macrophages. *Science.*342(6161):1242974 (2013).

8. van Furth R, Cohn ZA. The origin and kinetics of mononuclear phagocytes. *J Exp Med.*128(3):415-435 (1968).

9. Varol C, Mildner A, Jung S. Macrophages: development and tissue specialization. *Annu Rev Immunol.*33:643-675 (2015).

10. Lazarov T, Juarez-Carreno S, Cox N, Geissmann F. Physiology and diseases of tissue-resident macrophages. *Nature.*618(7966):698-707 (2023).

11. Abdelaziz MH, Abdelwahab SF, Wan J, et al. Alternatively activated macrophages; a double-edged sword in allergic asthma. *J Transl Med.*18(1):58 (2020).

12. Liaunardy-Jopeace A, Gay NJ. Molecular and cellular regulation of toll-like receptor-4 activity induced by lipopolysaccharide ligands. *Front Immunol.*5:473 (2014).

13. Ivashkiv LB. IFNgamma: signalling, epigenetics and roles in immunity, metabolism, disease and cancer immunotherapy. *Nat Rev Immunol.*18(9):545-558 (2018).

14. Watanabe S, Kumazawa Y, Inoue J. Liposomal lipopolysaccharide initiates TRIF-dependent signaling pathway independent of CD14. *PLoS One.*8(4):e60078

doi:10.6342/NTU202403029

(2013).

15. Colin S, Chinetti-Gbaguidi G, Staels B. Macrophage phenotypes in atherosclerosis. *Immunol Rev.*262(1):153-166 (2014).

16. Roszer T. Understanding the Mysterious M2 Macrophage through Activation Markers and Effector Mechanisms. *Mediators Inflamm.*2015:816460 (2015).

17. Wang LX, Zhang SX, Wu HJ, Rong XL, Guo J. M2b macrophage polarization and its roles in diseases. *J Leukoc Biol.*106(2):345-358 (2019).

18. Ambarus CA, Krausz S, van Eijk M, et al. Systematic validation of specific phenotypic markers for in vitro polarized human macrophages. *J Immunol Methods.*375(1-2):196-206 (2012).

19. Zizzo G, Hilliard BA, Monestier M, Cohen PL. Efficient clearance of early apoptotic cells by human macrophages requires M2c polarization and MerTK induction. *J Immunol.*189(7):3508-3520 (2012).

20. Lu J, Cao Q, Zheng D, et al. Discrete functions of M2a and M2c macrophage subsets determine their relative efficacy in treating chronic kidney disease. *Kidney Int.*84(4):745-755 (2013).

21. Qian BZ, Pollard JW. Macrophage diversity enhances tumor progression and metastasis. *Cell.*141(1):39-51 (2010).

22. Mantovani A, Sica A. Macrophages, innate immunity and cancer: balance, tolerance, and diversity. *Curr Opin Immunol.*22(2):231-237 (2010).

23. Pittet MJ, Michielin O, Migliorini D. Clinical relevance of tumour-associated macrophages. *Nat Rev Clin Oncol.*19(6):402-421 (2022).

24. Goenka S, Kaplan MH. Transcriptional regulation by STAT6. *Immunol Res.*50(1):87-96 (2011).

25. Li M, Wang M, Wen Y, Zhang H, Zhao GN, Gao Q. Signaling pathways in macrophages: molecular mechanisms and therapeutic targets. *MedComm (2020).*4(5):e349 (2023).

26. Liddiard K, Welch JS, Lozach J, Heinz S, Glass CK, Greaves DR. Interleukin-4 induction of the CC chemokine TARC (CCL17) in murine macrophages is mediated by multiple STAT6 sites in the TARC gene promoter. *BMC Mol Biol.*7:45 (2006).

27. Kimura S, Noguchi H, Nanbu U, Nakayama T. Macrophage CCL22 expression promotes lymphangiogenesis in patients with tongue squamous cell carcinoma via IL-4/STAT6 in the tumor microenvironment. *Oncol Lett.*21(5):383 (2021).

28. Oeckinghaus A, Ghosh S. The NF-kappaB family of transcription factors and its regulation. *Cold Spring Harb Perspect Biol.*1(4):a000034 (2009).

29. Porta C, Rimoldi M, Raes G, et al. Tolerance and M2 (alternative) macrophage polarization are related processes orchestrated by p50 nuclear factor kappaB. *Proc Natl Acad Sci U S A.*106(35):14978-14983 (2009).

doi:10.6342/NTU202403029

30. Lohoff M, Mittrucker HW, Prechtl S, et al. Dysregulated T helper cell differentiation in the absence of interferon regulatory factor 4. *Proc Natl Acad Sci U S A.*99(18):11808-11812 (2002).

31. Satoh T, Takeuchi O, Vandenbon A, et al. The Jmjd3-Irf4 axis regulates M2 macrophage polarization and host responses against helminth infection. *Nat Immunol.*11(10):936-944 (2010).

32. Huang SC, Smith AM, Everts B, et al. Metabolic Reprogramming Mediated by the mTORC2-IRF4 Signaling Axis Is Essential for Macrophage Alternative Activation. *Immunity.*45(4):817-830 (2016).

33. Lee B, Qiao L, Lu M, et al. C/EBPalpha regulates macrophage activation and systemic metabolism. *Am J Physiol Endocrinol Metab.*306(10):E1144-1154 (2014).

34. Ruffell D, Mourkioti F, Gambardella A, et al. A CREB-C/EBPbeta cascade induces M2 macrophage-specific gene expression and promotes muscle injury repair. *Proc Natl Acad Sci U S A.*106(41):17475-17480 (2009).

35. Odegaard JI, Ricardo-Gonzalez RR, Red Eagle A, et al. Alternative M2 activation of Kupffer cells by PPARdelta ameliorates obesity-induced insulin resistance. *Cell Metab.*7(6):496-507 (2008).

36. Christofides A, Konstantinidou E, Jani C, Boussiotis VA. The role of peroxisome proliferator-activated receptors (PPAR) in immune responses. *Metabolism.*114:154338 (2021).

37. Daniel B, Nagy G, Horvath A, et al. The IL-4/STAT6/PPARgamma signaling axis is driving the expansion of the RXR heterodimer cistrome, providing complex ligand responsiveness in macrophages. *Nucleic Acids Res.*46(9):4425-4439 (2018).

38. Lee YJ, Kim BM, Ahn YH, Choi JH, Choi YH, Kang JL. STAT6 Signaling Mediates PPARgamma Activation and Resolution of Acute Sterile Inflammation in Mice. *Cells.*10(3) (2021).

39. Odegaard JI, Ricardo-Gonzalez RR, Goforth MH, et al. Macrophage-specific PPARgamma controls alternative activation and improves insulin resistance. *Nature.*447(7148):1116-1120 (2007).

40. Chawla A. Control of macrophage activation and function by PPARs. *Circ Res.*106(10):1559-1569 (2010).

41. Takahashi K, Tanabe K, Ohnuki M, et al. Induction of pluripotent stem cells from adult human fibroblasts by defined factors. *Cell.*131(5):861-872 (2007).

42. Kapoor N, Niu J, Saad Y, et al. Transcription factors STAT6 and KLF4 implement macrophage polarization via the dual catalytic powers of MCPIP. *J Immunol.*194(12):6011-6023 (2015).

43. Locati M, Curtale G, Mantovani A. Diversity, Mechanisms, and Significance of

doi:10.6342/NTU202403029

Macrophage Plasticity. *Annu Rev Pathol.*15:123-147 (2020).

44. Bi K, He MX, Bakouny Z, et al. Tumor and immune reprogramming during immunotherapy in advanced renal cell carcinoma. *Cancer Cell.*39(5):649-661 e645 (2021).

45. Bassez A, Vos H, Van Dyck L, et al. A single-cell map of intratumoral changes during anti-PD1 treatment of patients with breast cancer. *Nat Med.*27(5):820-832 (2021).

46. Xu J, Peng W, Sun Y, et al. Structural study of MCPIP1 N-terminal conserved domain reveals a PIN-like RNase. *Nucleic Acids Res.*40(14):6957-6965 (2012).

47. Zhou L, Azfer A, Niu J, et al. Monocyte chemoattractant protein-1 induces a novel transcription factor that causes cardiac myocyte apoptosis and ventricular dysfunction. *Circ Res.*98(9):1177-1185 (2006).

48. Akira S. Regnase-1, a ribonuclease involved in the regulation of immune responses. *Cold Spring Harb Symp Quant Biol.*78:51-60 (2013).

49. Matsushita K, Takeuchi O, Standley DM, et al. Zc3h12a is an RNase essential for controlling immune responses by regulating mRNA decay. *Nature.*458(7242):1185-1190 (2009).

50. Uehata T, Iwasaki H, Vandenbon A, et al. Malt1-induced cleavage of regnase-1 in CD4(+) helper T cells regulates immune activation. *Cell.*153(5):1036-1049 (2013).

51. Li Y, Huang X, Huang S, et al. Central role of myeloid MCPIP1 in protecting against LPS-induced inflammation and lung injury. *Signal Transduct Target Ther.*2:17066 (2017).

52. Li M, Cao W, Liu H, et al. MCPIP1 down-regulates IL-2 expression through an ARE-independent pathway. *PLoS One.*7(11):e49841 (2012).

53. Jiang H, Lv X, Lei X, Yang Y, Yang X, Jiao J. Immune Regulator MCPIP1 Modulates TET Expression during Early Neocortical Development. *Stem Cell Reports.*7(3):439-453 (2016).

54. Dobosz E, Wilamowski M, Lech M, et al. MCPIP-1, Alias Regnase-1, Controls Epithelial Inflammation by Posttranscriptional Regulation of IL-8 Production. *J Innate Immun.*8(6):564-578 (2016).

55. Lin CC, Shen YR, Chang CC, et al. Terminal uridyltransferase 7 regulates TLR4-triggered inflammation by controlling Regnase-1 mRNA uridylation and degradation. *Nat Commun.*12(1):3878 (2021).

56. Iwasaki H, Takeuchi O, Teraguchi S, et al. The IkappaB kinase complex regulates the stability of cytokine-encoding mRNA induced by TLR-IL-1R by controlling degradation of regnase-1. *Nat Immunol.*12(12):1167-1175 (2011).

57. Mino T, Murakawa Y, Fukao A, et al. Regnase-1 and Roquin Regulate a Common Element in Inflammatory mRNAs by Spatiotemporally Distinct Mechanisms.

doi:10.6342/NTU202403029

*Cell.*161(5):1058-1073 (2015).

58. Mino T, Iwai N, Endo M, et al. Translation-dependent unwinding of stem-loops by UPF1 licenses Regnase-1 to degrade inflammatory mRNAs. *Nucleic Acids Res.*47(16):8838-8859 (2019).

59. Liang J, Saad Y, Lei T, et al. MCP-induced protein 1 deubiquitinates TRAF proteins and negatively regulates JNK and NF-kappaB signaling. *J Exp Med.*207(13):2959-2973 (2010).

60. Lee RC, Feinbaum RL, Ambros V. The C. elegans heterochronic gene lin-4 encodes small RNAs with antisense complementarity to lin-14. *Cell.*75(5):843-854 (1993).

61. Lai EC. Micro RNAs are complementary to 3' UTR sequence motifs that mediate negative post-transcriptional regulation. *Nat Genet.*30(4):363-364 (2002).

62. Siomi H, Siomi MC. Posttranscriptional regulation of microRNA biogenesis in animals. *Mol Cell.*38(3):323-332 (2010).

63. O'Connell RM, Rao DS, Chaudhuri AA, Baltimore D. Physiological and pathological roles for microRNAs in the immune system. *Nat Rev Immunol.*10(2):111-122 (2010).

64. Davis BN, Hilyard AC, Lagna G, Hata A. SMAD proteins control DROSHA-mediated microRNA maturation. *Nature.*454(7200):56-61 (2008).

65. Sun Y, Oravecz-Wilson K, Bridges S, et al. miR-142 controls metabolic reprogramming that regulates dendritic cell activation. *J Clin Invest.*129(5):2029-2042 (2019).

66. Zhang P, Frederick MI, Heinemann IU. Terminal Uridylyltransferases TUT4/7 Regulate microRNA and mRNA Homeostasis. *Cells.*11(23) (2022).

67. Suzuki HI, Arase M, Matsuyama H, et al. MCPIP1 ribonuclease antagonizes dicer and terminates microRNA biogenesis through precursor microRNA degradation. *Mol Cell.*44(3):424-436 (2011).

68. Roy A, Zhang M, Saad Y, Kolattukudy PE. Antidicer RNAse activity of monocyte chemotactic protein-induced protein-1 is critical for inducing angiogenesis. *Am J Physiol Cell Physiol.*305(10):C1021-1032 (2013).

69. Shao Z, Shen Q, Yao B, et al. Identification and mechanism of G protein-biased ligands for chemokine receptor CCR1. *Nat Chem Biol.*18(3):264-271 (2022).

70. Alferink J, Lieberam I, Reindl W, et al. Compartmentalized production of CCL17 in vivo: strong inducibility in peripheral dendritic cells contrasts selective absence from the spleen. *J Exp Med.*197(5):585-599 (2003).

71. Semmling V, Lukacs-Kornek V, Thaiss CA, et al. Alternative cross-priming through CCL17-CCR4-mediated attraction of CTLs toward NKT cell-licensed DCs. *Nat Immunol.*11(4):313-320 (2010).

72. Greaves DR, Hakkinen T, Lucas AD, et al. Linked chromosome 16q13

doi:10.6342/NTU202403029

chemokines, macrophage-derived chemokine, fractalkine, and thymus- and activation-regulated chemokine, are expressed in human atherosclerotic lesions. *Arterioscler Thromb Vasc Biol.*21(6):923-929 (2001).

73. Zhang Y, Ye Y, Tang X, et al. CCL17 acts as a novel therapeutic target in pathological cardiac hypertrophy and heart failure. *J Exp Med.*219(8) (2022).

74. Amo L, Kole HK, Scott B, Qi CF, Wu J, Bolland S. CCL17-producing cDC2s are essential in end-stage lupus nephritis and averted by a parasitic infection. *J Clin Invest.*131(11) (2021).

75. Chen YT, Hsu H, Lin CC, et al. Inflammatory macrophages switch to CCL17-expressing phenotype and promote peritoneal fibrosis. *J Pathol.*250(1):55-66 (2020).

76. Vulcano M, Albanesi C, Stoppacciaro A, et al. Dendritic cells as a major source of macrophage-derived chemokine/CCL22 in vitro and in vivo. *Eur J Immunol.*31(3):812-822 (2001).

77. Godiska R, Chantry D, Raport CJ, et al. Human macrophage-derived chemokine (MDC), a novel chemoattractant for monocytes, monocyte-derived dendritic cells, and natural killer cells. *J Exp Med.*185(9):1595-1604 (1997).

78. Panina-Bordignon P, Papi A, Mariani M, et al. The C-C chemokine receptors CCR4 and CCR8 identify airway T cells of allergen-challenged atopic asthmatics. *J Clin Invest.*107(11):1357-1364 (2001).

79. Baer C, Kimura S, Rana MS, et al. CCL22 mutations drive natural killer cell lymphoproliferative disease by deregulating microenvironmental crosstalk. *Nat Genet.*54(5):637-648 (2022).

80. Yoshie O, Matsushima K. CCR4 and its ligands: from bench to bedside. *Int Immunol.*27(1):11-20 (2015).

81. Villoslada P, Hauser SL, Bartke I, et al. Human nerve growth factor protects common marmosets against autoimmune encephalomyelitis by switching the balance of T helper cell type 1 and 2 cytokines within the central nervous system. *J Exp Med.*191(10):1799-1806 (2000).

82. Sather BD, Treuting P, Perdue N, et al. Altering the distribution of Foxp3(+) regulatory T cells results in tissue-specific inflammatory disease. *J Exp Med.*204(6):1335-1347 (2007).

83. Mizukami Y, Kono K, Kawaguchi Y, et al. CCL17 and CCL22 chemokines within tumor microenvironment are related to accumulation of Foxp3+ regulatory T cells in gastric cancer. *Int J Cancer.*122(10):2286-2293 (2008).

84. Carbo JM, Leon TE, Font-Diaz J, et al. Pharmacologic Activation of LXR Alters the Expression Profile of Tumor-Associated Macrophages and the Abundance of Regulatory T Cells in the Tumor Microenvironment. *Cancer Res.*81(4):968-985 (2021).

doi:10.6342/NTU202403029

85. Roy S, Guler R, Parihar SP, et al. Batf2/Irf1 induces inflammatory responses in classically activated macrophages, lipopolysaccharides, and mycobacterial infection. *J Immunol.*194(12):6035-6044 (2015).

86. Liu J, Li J, Tuo Z, Hu W, Liu J. BATF2 inhibits PD-L1 expression and regulates CD8+ T-cell infiltration in non-small cell lung cancer. *J Biol Chem.*299(11):105302 (2023).

doi:10.6342/NTU202403029